Lawrence Berkeley National Laboratory
Recent Work

Title
A MODEL FOR PREDICTING THERMAL CONDUCTIVITY OF ROCK-FLUID SYSTEMS

Permalink
https://escholarship.org/uc/item/1cs283s5

Author
Ghaffari, A.

Publication Date
1980-08-01

A MODEL FOR PREDICTING THERMAL CONDUCTIVITY
OF ROCK-FLUID SYSTEMS

Anoushiravan Ghaffari
(Ph.D. thesis)

August 1980

DISCLAIMER

A Model for Predicting Thermal Conductivity
of Rock-fluid Systems

By

Anoushiravan Ghaffari

B.S. (Arya Mehr University of Technology, Tehran,Iran)1973
M.S. (University of Southern California) 1976

Dissertation

Submitted in partial satisfaction of the
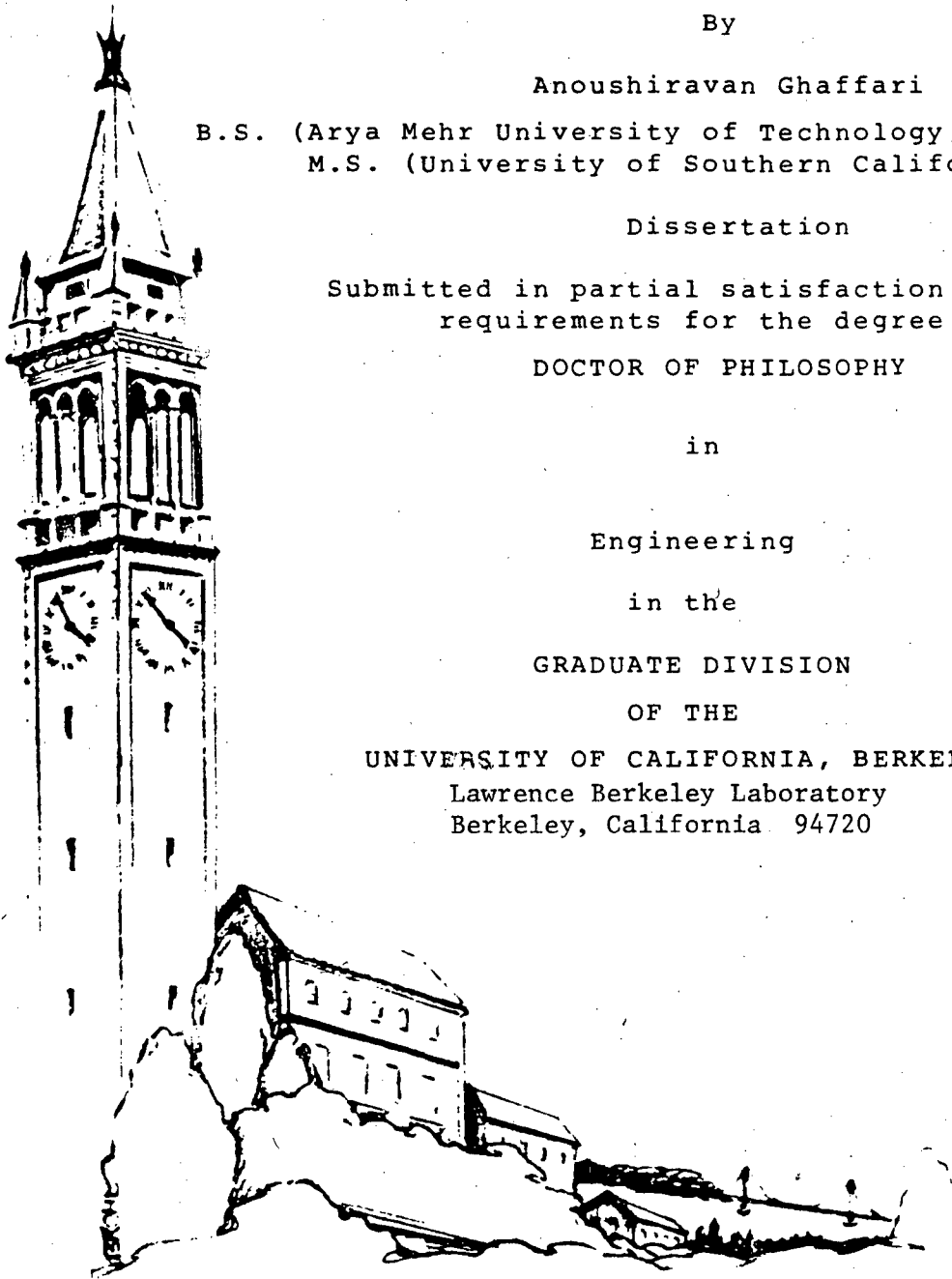requirements for the degree of

DOCTOR OF PHILOSOPHY

in

Engineering

in the

GRADUATE DIVISION

OF THE

UNIVERSITY OF CALIFORNIA, BERKELEY
Lawrence Berkeley Laboratory
Berkeley, California 94720
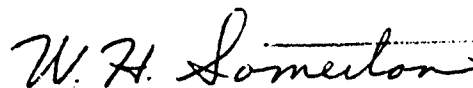
COLLEGE OF ENGINEERING

UNIVERSITY OF CALIFORNIA, Berkeley

A Model for Predicting Thermal Conductivity

of Rock-fluid Systems

Anoushiravan Ghaffari

ABSTRACT

An analytical study is presented for determining the effective

thermal conductivity of partially liquid saturated porous media. A

model made up of normal cubic-packed spheres, flattened at their contacts

is utilized. The relative size of the contacts is determined from the

two easily measurable properties of porosity and electrical formation

resistivity factor. A reasonable fluid distribution in the model is

incorporated by choosing the wetting phase to be a spherical layer of

uniform thickness on the solid grain surfaces. Neglecting the contribu-

tion of any convection of the fluids in the pore channels and heat

transfer by radiation, the heat conduction equation was solved for a

unit cell of the model. The final results are presented in the form

of working graphs using the dimensionless groupings of effective thermal

conductivity divided by fluid or solid conductivity, solid conductivity

divided by fluid conductivity, porosity, saturation of the wetting phase

and dimensionless radius of top-bottom contacts. There is good agree-

ment between values of the effective thermal conductivities of partially

liquid saturated consolidated sandstones and unconsolidated sands calcu-

lated by the model and existing experimental data.

Professor W. H. Somerton
Chairman, Dissertation Committee

ACKNOWLEDGMENTS

Although I often found myself working alone during the course of this investigation, I have also experienced my dependence on others.

I am deeply indebted to all my colleagues and friends, who helped me whenever I needed them. Their camaraderie indeed kept my spirit high in hard moments.

I would like to thank my adviser, Professor Wilbur Somerton, for his help and support, as well as my dissertation committee members, Professor John Newman and Proffesor Chang Lin Tien, for their valuable suggestions and remarks.

Thanks are also due to David White for his help with the laboratory work, Gloria Pelatowski for drawing the figures, and Coral Miller for typing this manuscript.

TABLE OF CONTENTS

LIST OF FIGURES

LIST OF TABLES

1

INTRODUCTION

The subject of thermal properties, especially the thermal conductivity of porous systems, is one of the most challenging problems which has attracted the interest of scientists and engineers for many years. This current great interest is due to the fact that such data have found rather wide usage in a number of industrial branches like thermal recovery processes in the petroleum field, geothermal energy development, thermal insulation in cryogenic applications, and many more.

In general, porous systems have a very complex configuration, solid particles of different shapes and sizes, and pores of even more complicated geometry which may be filled with a single or several fluids. This irregular structure makes the exact theoretical investigation of a problem very difficult or rather impossible for these systems. Therefore, experimental examinations seem to be more logical to analyze a complex phenomenon for these media. However, to obtain reliable experimental results one should undertake very careful procedures, which are usually difficult and time consuming.

Because of these complexities, there have been numerous attempts to model porous systems by analytic studies. In this case one assumes a typical particle shape and size and a typical packing, and analyzes the desired problem for such a model. Although some of these models may not be very realistic, they will help us to gain a better understanding of the problem under investigation.

In the present work a conceptual model has been developed for theoretical study of effective thermal conductivities of porous rocks saturated with one or two stagnant fluids. Distinction is made between unconsolidated particles and consolidated rocks. Studies concerning the effect of some

parameters such as axial and pore pressures, temperature, and grain size on
the thermal conductivity of porous rocks were also made in this investigation.

CHAPTER 1

DEFINITIONS AND LITERATURE REVIEW

1-1 The Effective Thermal Conductivity Coefficient

It is understood in thermodynamics that heat flow is the result of a temperature gradient. A basic relation between the amount of heat conducted per unit time per unit area and the temperature gradient was first defined by the French mathematician Jean Baptiste Fourier and in his honor is called the Fourier law of heat conduction, which is written mathematically as:

$$q = - \lambda \ grad \ T \ . \qquad (1\text{-}1\text{-}1)$$

The quantity λ which serves as a proportionality factor between the heat flux and the temperature gradient is called the coefficient of thermal conductivity.

In general a relation such as Eq. (1-1-1) can be written macroscopically for any system in which there is a flow of heat due to an imposed temperature difference. In this case one may call λ the coefficient of effective thermal conductivity, and calculate it by experimental measurement or theoretical estimation of the heat flux, knowing the temperature gradient .

Experimental measurement of the heat flux q , and therefore effective thermal conductivity, will be discussed later in this chapter. However, for theoretical predictions one should examine the contribution of the three basic modes of heat transfer, namely, conduction, convection and radiation, to the desired problem.

For a porous system without any mass exchange with the outside, free or natural convection is the only participant in the convection mechanism. Natural convection occurs when the density of the saturating fluid phase in pores is not uniform. The most common parameter that

influences the density of the fluid is temperature. However, in some cases other buoyancy effects are also observed, resulting from mass diffusion. By nondimensionalizing the equations of continuity, momentum and energy properly, one could obtain an important dimensionless parameter fundamental to the natural convection heat transfer in porous media which is called the Rayleigh number and defined as:

$$Ra = g.\beta . \frac{\rho C}{\nu} . \frac{K}{\lambda_e} . (\Delta T).D ,$$
(1-1-2)

where β, ρ, C, ν are the volumetric thermal expansion coefficient, the density, the specific heat at constant pressure, and the kinematic viscosity ($\nu = \frac{\mu}{\rho}$) of the fluid in the pores, respectively, K the permeability, λ_e the effective thermal conductivity of the porous system, g the gravitational acceleration, and finally (ΔT) and D are appropriate temperature difference, and length reference quantities.

The main consequence of convective motion is to increase the overall heat transfer. Therefore, when this occurs, the overall effective thermal conductivity is greater than when the fluid in the pores is stagnant. A comprehensive treatment of convection in porous media can be found elsehwere [1]. It is important to note that the criterion for the onset of convective motion in such system is given by:

$$Ra_{cri} = 4\pi^2 \simeq 40 .$$
(1-1-3)

This is obtained theoretically, and observed experimentally by many authors [2], [3].

At high temperatures, radiation between particle surfaces and radiation absorption by the fluid in the pores become important. Radiation contribution to the effective thermal conductivity has been studied by many authors. Chan and Tien [4] analyzed the radiative transfer through a packed bed of microspheres on the basis of a conceptual model, and found qualitative agreement between the predicted and existing

experimental data of some radiative properties such as absorption and scattering parameters. Schotte [5] also analyzed the radiation contribution to the effective thermal conductivity. Schotte considered both the radiation between adjacent particle surfaces and the radiation between particle surfaces seen through more than one void space, giving:

$$(\lambda_e)_{rad.} = \phi(4D_p \epsilon \sigma T^3) + \cfrac{1 - \phi}{\cfrac{1}{\lambda_s} + \cfrac{1}{(4D_p \epsilon \sigma T^3)}} \quad , \quad (1\text{-}1\text{-}4)$$

where $(\lambda_e)_{rad.}$ is the radiation contribution to the effective thermal conductivity, λ_s, D_p, ϵ are the thermal conductivity, the diameter and the emissivity of the solid particle, respectively, ϕ the porosity, T the absolute temperature, and finally σ is the Stefan-Boltzmann constant.

In the absence of any mass exchange with the outside and at Rayleigh numbers below $Ra_{cri.}$, conduction is the only important mechanism to be considered in the theoretical prediction of heat transfer in a porous system at low to moderate temperatures. A considerable amount of theoretical work has been done to study conduction heat transfer in such media. A review of some fundamental, historic, and most practical works in this field is presented in the following section.

1-2 Conductive Heat Transfer in Porous Media.

1-2-1   Two-Component Systems

In general for a two-phase porous system, the effective thermal conductivity in its simplest form depends on the thermal conductivity, volume, and distribution of each phase. Therefore, if the two phases are a single solid component and a single fluid filling the pore space, the above statement is equivalent to:

$$\lambda_e = f(\lambda_s, \lambda_f, V_s, V_f) \quad , \qquad\qquad (1\text{-}2\text{-}1)$$

where λ_e is the effective thermal conductivity, V the volume, and sub-

scripts s and f denote solid and fluid phase, respectively. Notice that the functional relationship represented by f is fixed if one chooses a specific phase distribution.

Using the Buckingham pi theorem, Eq. (1-2-1) in its dimensionless form can be written as:

$$\frac{\lambda_e}{\lambda_f} = F(\frac{\lambda_s}{\lambda_f}, \phi) \quad , \qquad (1-2-2)$$

where ϕ is the fractional porosity, defined as

$$\phi = \frac{V_f}{V_s + V_f} \quad . \qquad (1-2-3)$$

For most cases $\lambda_s > \lambda_f$, and therefore $1 < \frac{\lambda_e}{\lambda_f} < \frac{\lambda_s}{\lambda_f}$. However, closer and much more useful limits can be placed on λ_e by considering two very simple phase distributions. For any two-phase system the effective thermal conductivity is maximum when the phases are presented as plane layers parallel to the direction of heat flow, and minimum, when the phases are separated by planes perpendicular to the direction of heat flow. These simple models are known as parallel and series distributions. The effective thermal conductivity for these limits are given by:

parallel:
$$\frac{\lambda_{max.}}{\lambda_f} = \phi + (1 - \phi) \frac{\lambda_s}{\lambda_f} \quad , \qquad (1-2-4)$$

series:
$$(\frac{\lambda_{min.}}{\lambda_f})^{-1} = \phi + (1 - \phi)(\frac{\lambda_s}{\lambda_f})^{-1} \quad . \qquad (1-2-5)$$

The effective thermal conductivity resulting from parallel and series distributions are also known as weighted arithmetic mean and weighted harmonic mean of the solid and the fluid conductivities. There is also an intermediate value for the thermal conductivity of a composite system, which is called weighted geometric mean conductivity and corresponds to a weighted arithmetic mean of the logarithm of the individual conductivities,

$$\log \lambda_e = \phi \log \lambda_f + (1 - \phi) \log \lambda_s \quad ,$$

or

$$\frac{\lambda_e}{\lambda_f} = \left(\frac{\lambda_s}{\lambda_f}\right)^{1-\phi} \quad , \qquad (1-2-6)$$

It is very interesting to note that for both parallel and series distributions we have:

$$\left(\frac{d(\frac{\lambda_e}{\lambda_f})}{d(\frac{\lambda_s}{\lambda_f})}\right)_{\frac{\lambda_s}{\lambda_f} = 1} = 1 - \phi \quad . \qquad\qquad (1-2-7)$$

In fact it would not be very difficult to prove that the effective thermal conductivity equation for any phase distribution should also satisfy Eq. (1-2-7).

Other than these two fundamental bounds for effective thermal conductivity, Tien and Vafai [6] show that having additional geometric information about the porous media other than porosity leads to a narrower band for this thermal property.

Probably one of the earliest works in the area of conductivity of composite systems is Maxwell's [7] model for the electrical conductivity of a random distribution of spheres of conductivity λ_f embedded in a matrix of conductivity λ_s. Because of the mathematical analogy between the electrostatic field which forms when particles of a dielectric are placed in a uniform electrical field with a different dielectric constant, and the temperature field in the composite systems, Maxwell's result can be written for thermal conductivity as:

$$\frac{\lambda_e}{\lambda_f} = \frac{\lambda_s}{\lambda_f} \frac{2(1 - \phi)\frac{\lambda_s}{\lambda_f} + (1 + 2\phi)}{(2 + \phi)\frac{\lambda_s}{\lambda_f} + (1 - \phi)} \quad . \qquad\qquad (1-2-8)$$

To derive Eq. (1-2-8) it was assumed that the spheres are so far apart that their disturbance to the thermal field is not felt by neighboring spheres. Therefore, because of this assumption Eq. (1-2-8) cannot be used widely. For porous rocks, Beck [8] claims that Maxwell's model is reasonably successful in the case of water saturated rocks ($\frac{\lambda_s}{\lambda_f} < 10$) of relatively low porosities ($\phi < .10$). By using appropriate correction factors obtainable from the existing data in the

literature, he extends the use of Maxwell's model to much wider
ranges of λ_s/λ_f and porosity.

Kunii and Smith [9] developed equations for predicting the ef-
fective thermal conductivity of unconsolidated and consolidated porous
beds. Under the assumption of unidirectional flow of the heat through
models made up of spheres of uniform size in cubic or rhombohedral
arrangement, they arrived at the following equation for the effective
thermal conductivity of unconsolidated particles:

$$\frac{\lambda_e}{\lambda_f} = \phi + \frac{\beta(1 - \phi)}{\alpha + \frac{2}{3}\left(\frac{\lambda_f}{\lambda_s}\right)} \quad , \qquad\qquad (1\text{-}2\text{-}9)$$

where β is a packing parameter (1.0 for cubic and .895 for rhombo-
hedral arrangement) and α a parameter which depends on λ_s/λ_f and the
number of contact points on a semispherical surface of one solid particle.

For beds of consolidated particles, Kunii and Smith extended their
theoretical work by introducing a dimensionless consolidation parameter
in Eq. (1-2-9) and finally obtained the following equation for the
effective thermal conductivity:

$$\frac{\lambda_e}{\lambda_f} = \phi + \frac{(1 - \phi)(1 + \frac{\phi}{\phi_0}\alpha)}{\left(\frac{\lambda_s}{\lambda_f}\right)^{-1} + \frac{(\phi/\phi_0)}{\frac{1}{\alpha} + \frac{D_p h_p}{\lambda_f}}} \quad , \qquad\qquad (1\text{-}2\text{-}10)$$

where the new parameters ϕ, D_p and h_p are, respectively, the porosity
of the original packed bed from which the consolidated porous media
is made, the diameter of particles, and the heat transfer coefficient
representing the heat transfer rate through the contact surface be-
tween solid particles. The authors claim that values of .2 to .3
for the consolidation parameter $\frac{D_p h_p}{\lambda_s}$ give satisfactory results.

Kunii and Smith state that their equations appear to predict with reasonable accuracy the effective thermal conductivities for various types of sandstones filled with stationary fluid, but it seems any agreement with experiment for high values of λ_s/λ_f was probably fortuitous, because heat flow was assumed to be unidirectional in their investigation. However, such models might serve as a guide for correlating their data.

Krupiczka [10] modeled granular materials by solid cylinders and solid spheres of uniform size packed in a normal cubic arrangement, and pores filled with a single fluid phase. By a rigorous mathematical solution of the Laplace equation for the above models, combined with experimental data, he developed a general correlation for effective thermal conductivity as:

$$\frac{\lambda_s}{\lambda_f} = \left(\frac{\lambda_s}{\lambda_f}\right)^{0.28-0.757 \log\phi-0.057 \log (\lambda_s/\lambda_f)} . \qquad (1-2-11)$$

This correlation formula is valid in the region of $.215<\phi<.476$, but it can also be used with some approximation for values going a little beyond this region. Krupiczka's correlation is reasonably successful in most cases of porous rocks but for dry consolidated sandstones (porosities $.23<\phi<.29$) there is a poor agreement between computed and experimental values.

Anand, Somerton and Gomaa [11] developed the following correlation based on experimental data for the effective thermal conductivity of dry and saturated porous rock:

$$\lambda_D = 0.340\rho_D - 3.20\phi + 0.530K^{0.10} + 0.0130F - 0.031 , \qquad (1-2-12)$$

$$\frac{\lambda_{sat.}}{\lambda_D} = 1 + 0.30 \left[(\frac{\lambda_f}{\lambda_a}) - 1 \right]^{0.33} + 4.57 \left[\frac{\phi}{1 - \phi} \frac{\lambda_f}{\lambda_D} \right]^{0.482m} \left[\frac{\rho_{sat}}{\rho_D} \right]^{-0.43}, \quad (1-2-13)$$

where:

λ_D, $\lambda_{sat.}$ = thermal conductivities of dry and fluid saturated

rock, respectively, Btu/hr. ft. °F,

λ_a, λ_f = thermal conductivity of air and saturating fluid

respectively, Btu/hr. ft. °F,

ρ_D, ρ_{sat} = density of dry and fluid saturated rock, respectively,

g /cc ,

K = absolute permeability, md ,

F = electrical formation resistivity factor, and

m = Archie's cementation factor.

Emphasis in these correlations is placed on prediction of thermal

conductivity from more easily measured properties. The authors re-

ported that for the 38 experimental data points which were used to

obtain correlation Eq. (1-2-12), the standard deviation was 0.139

for a thermal conductivity range of 0.4-2.2 Btu/hr. ft. °F, while

for the 52 literature data points used in correlation Eq. (1-2-13),

the standard deviation was found to be 0.179 for the range of λ_s/λ_D

ratio values of 1.2-2.3.

1-2-2 Multi-fluid Saturated Porous Rocks

For petroleum or geothermal reservoirs the situation in which

pores are filled with more than a single fluid phase is more likely.

In petroleum reservoirs, oil, water and gas may exist simultaneously

in the voids, or water and steam could occupy the pores together in

formations around a geothermal well. Therefore, knowledge of thermal

conductivity for these systems is also important. The simple idea of

weighted arithmetic mean, weighted harmonic mean and weighted geometric mean conductivity for a two-phase system could be generalized for a multi-phase composite system as:

$$\lambda_A = \sum_{i=1}^{n} \phi_i \lambda_i \quad , \tag{1-2-14}$$

$$\lambda_H = \left(\sum_{i=1}^{n} \phi_i / \lambda_i\right)^{-1} , \tag{1-2-15}$$

$$\lambda_G = \prod_{i=1}^{n} (\lambda_i^{\phi_i}) \quad , \tag{1-2-16}$$

where subscripts A, H, G represent arithmetic, harmonic and geometric means, respectively, λ_i is the thermal conductivity and ϕ_i the volumetric fraction of each individual component. Above equations are useful when λ_i of the individual components are not very different from each other.

Based on experimental measurements, Somerton, Kesse and Chu [12] obtained the following correlation equation for thermal conductivity of partially brine saturated unconsolidated sands.

$$\lambda_e = 0.735 - 1.30\phi + 0.390\lambda_s S_w^{\frac{1}{2}} , \tag{1-2-17}$$

where S_w is brine saturation (fraction of the pore space occupied by brine), and thermal conductivities are in (Btu/hr-ft-°F). Equation (1-2-17) is reported to be in excellent agreement with thermal conductivity data of oil sands containing original fluids.

Ozbek [13] developed a conceptual model for prediction of thermal conductivity of multi-fluid saturated porous media. Using the model, he obtained the following correlation equation for effective thermal conductivity.

$$\lambda_e = 0.0585e^{-3.31\phi} + 0.0166\, S_w^{0.5} + 0.1939\lambda_s^{0.783} + 0.0197e^{18.13\lambda_w}$$

$$+ 0.0159^{86.36\lambda_{nw}} - 0.0002R_{ws} - 0.0001R_{nws} - 0.067 \qquad (1\text{-}2\text{-}18 \quad,$$

where

λ_e = effective thermal conductivity of two-fluid saturated rock, W/cm-K ,

ϕ = fractional porosity, (0.10 - 0.45),

S_w = fractional wetting fluid saturation, (0-1.0),

λ_s = thermal conductivity of rock solids, (0.03-0.08 W/cm-K),

λ_w = thermal conductivity of the wetting fluid, (0.0004 - 0.010 0.010 W/cm-K),

λ_{nw} = thermal conductivity of the non-wetting fluid, (0.0001 - 0.001) W/cm-K),

R_{ws} = wetting fluid-solid contact resistivity (0-10 $\frac{cm^2-K}{W}$),

R_{nws} = non-wetting fluid-solid contact resistivity, (0-20 $\frac{cm^2-K}{W}$),

Ozbek reported that thermal conductivity predictions by the model equation and the experimental results are generally in good agreement with standard deviations of 0.0014, 0.0017, 0.0027, 0.0033 W/cm-K for brine-decane saturated Ottawa sand, Boise sandstone, and Bandera sandstone, respectively.

A comparison of the values of λ_e/λ_f calculated with some of the formulas proposed by different authors was made for different values of porosity and for two different values of λ_s/λ_f, namely, 10 and 200 which are typical for porous rocks fully saturated with water and with air, respectively. Figure 1 shows that for high values of λ_s/λ_f the effective thermal conductivity of a porous system for a given porosity is greatly influenced by the model which represents the system and the
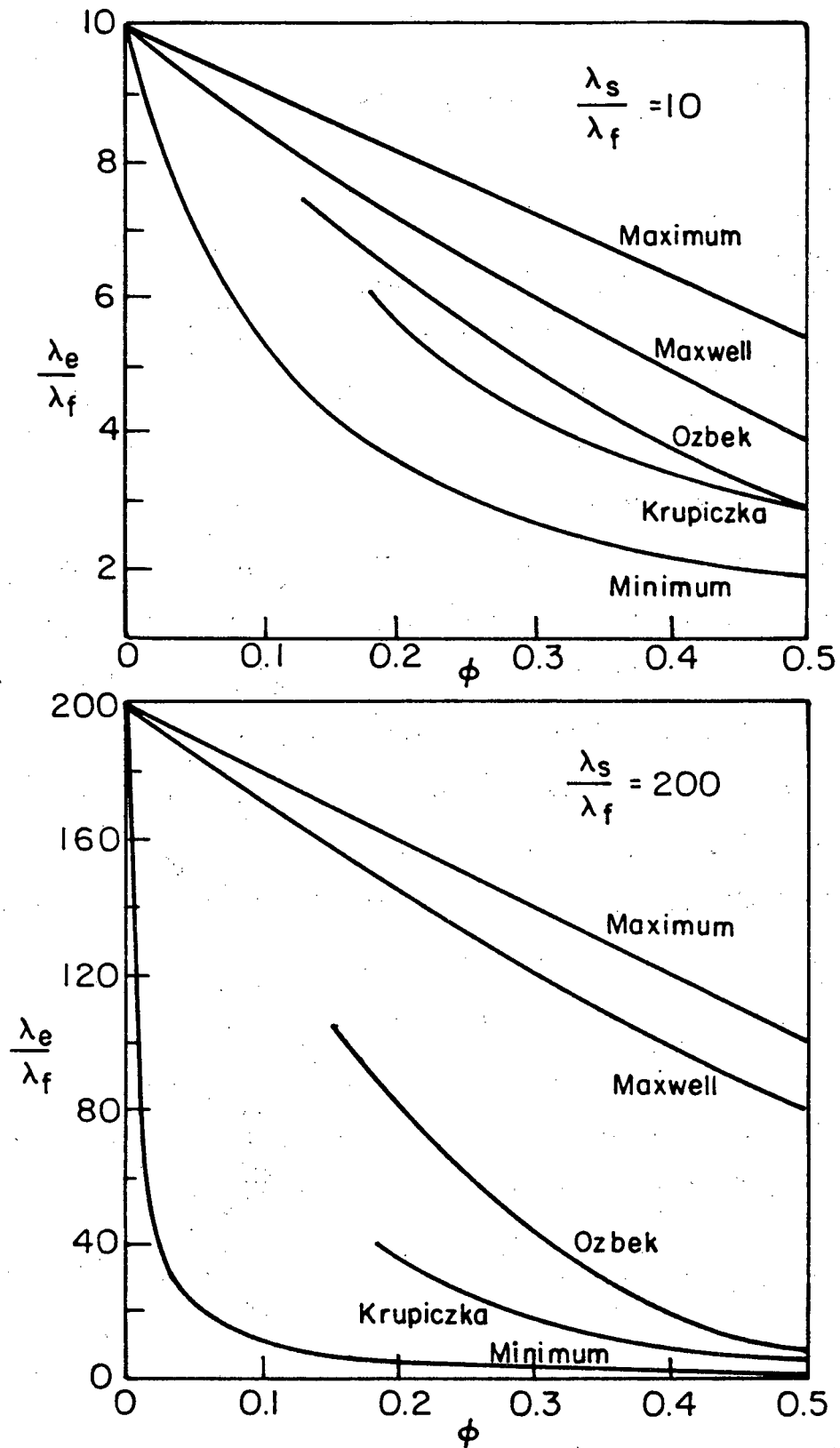
Fig. 1 Comparison of equations relating $\frac{\lambda_e}{\lambda_f}$ and ϕ for values of $\lambda_s/\lambda_f = 10$ and 200

method of calculation, while for low values of λ_s/λ_f, these are of lesser importance.

1-3   Effect of Temperature, Pressure and Grain Size on Effective Thermal Conductivity

1-3-1   Effect of Temperature

At low to moderate temperatures and in the absence of any convective motion inside the pores, temperature dependence of the effective thermal conductivity is mostly due to the fact that thermal conductivities of solid matrix and fluids filling the pore channels may be temperature dependent.

The solid matrix of porous rocks consists of many different minerals of which quartz or feldspar predominates with thermal conductivities of 7.7 W/m-K and 2.2 W/m-K, respectively. It has been shown by Tikhominov [14] that in low to moderate temperature range, thermal conductivity of highly conductive consolidated rocks decreases with increase in temperature, while for poorly conductive rocks this trend is reversed. This corresponds to the behavior of well-crystallized materials which show a decreasing trend with temperature, and poorly crystallized or amorphous materials which show increasing thermal conductivity with temperature. Based on experimental measurements, Tikhominov obtained the following correlation equation for the effect of temperature on thermal conductivity of porous dry rocks.

$$\lambda_T = 0.047 \, \lambda_{20} \cdot T^{\,4.98 \, (0.171 \log T - 1.61 \log \lambda_{20} + 0.12)} \quad , \quad (1\text{-}3\text{-}1)$$

where

λ_T = thermal conductivity of dry rock at temperature T (cal/sec-cm-°C) $\cdot 10^{-3}$,

λ_{20} = thermal conductivity of dry rock at temperature 20°C (cal/sec-cm-°C)$.10^{-3}$,

T = temperature (K).

Anand, Somerton and Gomaa [11] found that Eq. (1-3-1) does not predict the effect of temperature on thermal conductivity of porous rocks satisfactorily. Based on their own experimental data, the above authors arrived at the following correlation equation which is applicable to both dry and fluid saturated rocks.

$$\lambda_T = \lambda_{20} - 1.047 \times 10^{-3} (T - 293)(\lambda_{20} - 1.385) \left[\lambda_{20} (1.8T\ 10^{-3})^{-\lambda_{20}/3.176} + 1.277 \right] \lambda_{20}^{-0.64} . \tag{1-3-2}$$

In Eq. (1-3-2), temperature T is in K, thermal conductivities in W/m-K and subscript 20 refers to temperature of 20 °C.

The above correlations were not tested in the present work. However, it is recommended that the model be used to estimate thermal conductivities at a base temperature (20°C) and that the correlating equation (1-3-2) be used to estimate values at higher temperatures.

1-3-2 Effect of Pressure

In subsurface porous rock formations, pressure could either be referred to the hydrostatic pressure of the fluids filling the pores, or to the effective stress which is defined as the difference between the overburden pressure and the pore pressure.

Increasing the effective stress on the porous rock improves the contact between adjacent grains and therefore increases the overall thermal conductivity. In partially liquid saturated porous rocks, when the wetting phase is a good thermal conductor, the effective stress might not affect the overall thermal conductivity appreciably.

This is due to the fact that the wetting phase occupies the interstices between the grain contacts and reduces the thermal contact resistance at these areas. However, the increase of overall thermal conductivity with increasing effective stress could be significant when the wetting fluid is a poor conductor. Woodside and Messmer [15] have reported a 30% increase in overall thermal conductivity of air saturated Berea sandstone when the axial stress on the test sample was increased from zero to 2000 psi (pore pressure was 1 atm.). Only 5% increase in effective thermal conductivity has been measured by the above authors when the axial stress was increased from 2000 psi to 4000 psi. The effect of axial stress on the overall thermal conductivity of porous rocks has also been studied by Edmondson [16], Anand, Somerton and Gomaa [11]. Edmondson's experimental results show that the overall thermal conductivities of dry Berea, Bandera and Boise sandstones increase by 7.8%, 9.5% and 12.3%/1000 psi, respectively, in the axial pressure range of 900–3600 psi. However, work of Anand, Somerton and Gomaa shows that for dry Berea and Boise sandstones, effective thermal conductivities increased by only 1.25 and 2 percent/1000 psi respectively, above 500 psi axial stress.

Keeping the effective stress constant, the pore pressure affects the overall thermal conductivity through affecting the thermal conductivity of the fluids filling the pores. In general an increase or decrease in conductivities of the pore fluids would be expected to increase or decrease the overall thermal conductivity of the porous rocks, respectively. For liquids the increase in pressure increases the molecular contact and consequently the thermal conductivity. Bridgman [17] shows that the thermal conductivity of liquids may increase by a factor of two in the pressure range of 0 to 12000 kg/cm^2.

For gases the thermal conductivity is essentially independent of
pressure in moderate pressure ranges, but increases with increasing
pressure at high pressures. As an example, at temperature of 100°C
the thermal conductivity of air increases by a factor of 1.3 in the
pressure range of 1-200 kg/cm^2 [18].

1-3-3 Effect of Grain Size

In a porous system if the arrangement of the solid grains is
kept the same, enlargement or reduction of their size to any degree
may affect the overall thermal conductivity. The total surface area
of the grains exposed to the pores per unit total volume, or the
total surface area of the grain-to-grain contacts per unit total
volume is inversely proportional to a characteristic dimension of
the grains such as median grain diameter. One would expect that for
a fixed porosity and packing arrangement, packs of smaller grains
would have larger total surface area and larger number of grain-to-
grain contacts for a given volume. There may exist a contact thermal
resistance due to surface roughness between the grains at their
contacts, or a film resistance due to surface contamination at the
surface of the grains exposed to the pores. In this case, for a
fixed porosity and packing arrangement, porous systems with smaller
grains would offer a larger resistance to the heat flow compared to
systems with larger grains, and consequently would have lower effective
thermal conductivity.

Other than the absolute size of the grains forming a porous rock,
the non-uniformity of their size might also be of importance with
respect to the value of the effective thermal conductivity.

Based on experimental thermal conductivities for a large variety
of unconsolidated sands and consolidated sandstones fully saturated

with brine, Cruze [19] obtained the following correlation equation
which gives some measure of the effect of grain size and grain size
distribution on the effective thermal conductivity:

$$\lambda_e/\lambda_f = (\lambda_s/\lambda_f)^E \; , \qquad\qquad\qquad (1\text{-}3\text{-}3)$$

$$E = 0.961 - 0.347 \; \log\phi - 0.431 \; \log\,(\lambda_s/\lambda_f) + 0.121 \; \log\,(D_{50})$$
$$-0.869 \; \log\,(D_{90}/D_{10}) \; ,$$

where

λ_e = effective thermal conductivity,

λ_s = thermal conductivity of rock solids,

λ_f = thermal conductivity of saturating fluid,

ϕ = fractional porosity,

D_{90}/D_{10} = grain size distribution function,

D_{50} = median grain size (mm),

D_{90} = grain size at which 90% of the grains by weight are coarser,

D_{10} = grain size at which 10% of the grains by weight are coarser.

Equation (1-3-3) does indeed show a decrease in effective thermal
conductivity when the grains are reduced in size. It also shows that
the broader the distribution of grain sizes (low values of D_{90}/D_{10})
the higher is the thermal conductivity. Note that $D_{90}/D_{10} = 1.$ for
single grain size.

1-4   Experimental Measurement of Thermal Conductivity

Because of the very complex geometry of porous rocks, an exact
theoretical investigation of a heat transfer problem for these systems
is very difficult.   Therefore, an accurate experimental study of the
problem cannot be avoided by one who is interested in examining the
matter precisely.   However, these experimental procedures are difficult

and time consuming and usually require great skill and much patience.

In determining thermal conductivity, any experimental measurement usually simulates a solution of the governing differential equation, expressing the conduction of heat in a homogenous media, that is

$$\nabla^2 T = \frac{\rho c}{\lambda} \frac{\partial T}{\partial t} \quad , \tag{1-4-1}$$

where ρ, c, λ are the density, the specific heat at constant pressure, and the thermal conductivity of the material, respectively. A comprehensive examination of such solutions that may be simulated experimentally with little difficulty, along with an extensive study on the measurement of thermal conductivity can be found in the text of Tye [20]. Therefore, detailed descriptions of different experimental procedures are not given here and only the comparative method of thermal conductivity measurement will be discussed briefly.

For a cylindrical test sample, the steady state solution of Eq. (1-4-1) with undirectional flow of heat and no radial heat loss, can be written as:

$$Q = \frac{\lambda A}{L} (\Delta T) \quad , \tag{1-4-2}$$

where:

A = cross section-sectional area of the sample normal to heat flow direction,

L = length of the sample,

ΔT = temperature difference across length L,

Q = heat flow through the sample,

λ = thermal conductivity of the sample.

Measuring Q, A, L and (ΔT), thermal conductivity can be obtained from Eq. (1-4-2). Depending on whether the heat flow is measured directly by potentiometric means, or by use of "standards" of known thermal conductivity, the method is called absolute or comparative, respectively.

A schematic diagram of an apparatus used to measure thermal conductivity by the steady state comparative method is shown in Fig. 2. The essential principles of the method together with detailed technical information about this system are discussed elsewhere by Anand [21] and Somerton [22]. Therefore, just some important technical points will be given here.

This system consists of a cylindrical test sample, 32 mm thick and 51 mm in diameter, which is placed in a holder, 38.5 mm thick, and having an outer diameter of 102 mm. The holder is made of polyimide resin (Vespel SP-1 by Du Pont) which has low thermal conductivity (0.433 W/m-K), good mechanical strength, and is also thermally stable up to 300°C. The holder is fitted at each end by a circular stainless steel plate, 3.2 mm thick and 76.2 mm in diameter, with a copper-constantan thermocouple embedded in its center. Each thermocouple plate is seated on a Vitron O-ring placed in a groove in the holder, which provides a good seal to maintain the inside pore fluid pressure. Pore pressure can be controlled through a line connected to a fluid extraction or injection system. The sample holder is located between two other holders of the same material but only 22.4 mm thick, and containing standards of known thermal conductivity not very different from the test sample. These holders are also closed at their ends with thermocouple plates. The stack of holders is bounded by heat source

1. Temp. controllers
for heat source and
heat sink
2. Voltage regula-
tors for guard
heating
3. Temp. recorder
4. Absol., Diff.
temp. selector
5. Pore press.
recorder
6. Injection
pump
7. Heat ex-

changer
8. Axial loading
system
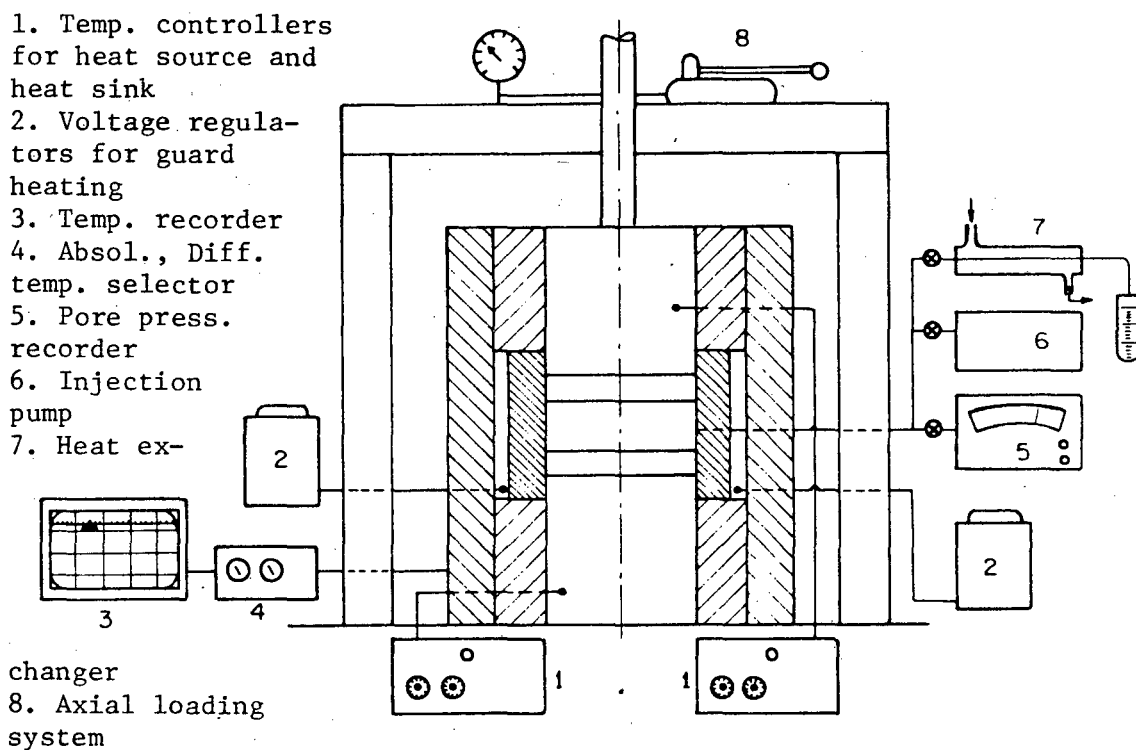
Fig. 2 Schematic diagram of thermal conductivity apparatus

electric heater

upper standard

test sample

pore pressure
fitting

lower standard

temperature sensor

thermocouples

vespel holders
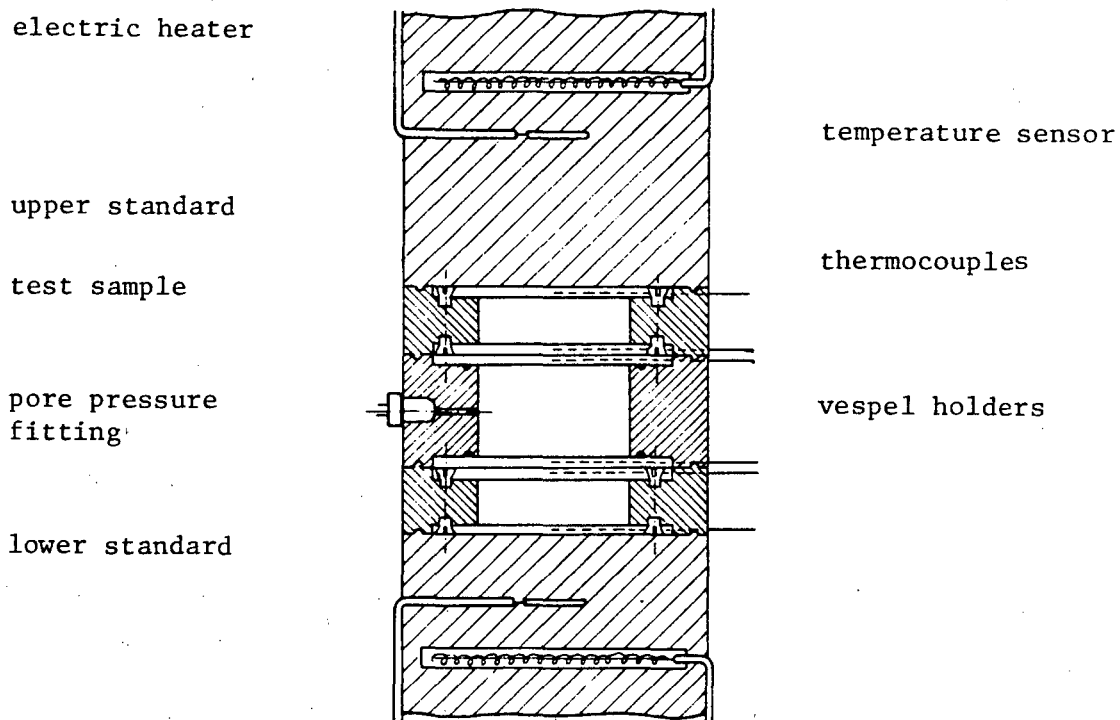
Fig. 3 Details of the
test section

and sink on the top and bottom which are copper cylinders, 200 mm long and 102 mm in diameter, with built-in electric heaters and temperature sensors. Temperature controllers are used to maintain the desired high and low temperature levels. The assembly of the holders and the copper heaters are surrounded by separate semi-annular pieces of insulation. Electric guard heaters are built into the insulators around the holders in order to minimize radial heat flow.

One of the interesting features of this apparatus is that the liquid saturation of the test sample can be changed without removing it from the test section. Detailed discussion on this matter is made elsewhere by Ozbek [13]. It is important to note that lowering the pore pressure, by opening the exit valve, to a value below the vapor pressure at the existing test temperature, causes the pore liquid to vaporize. The vapor pressure drives the evaporated liquid through a cooling system which condenses the vapor. Measuring the volume of the condensate, and knowing the previous volume of the pore liquid, one can easily calculate the new liquid saturation for the test sample.

CHAPTER 2

DEVELOPMENT OF THE MODEL AND

CALCULATION TECHNIQUES

2-1 Porous System Model.

For many years a number of authors have been examining various

means of predicting the highly important properties of composite sys-

tems including porous rocks. In general a precise solution to any

problem in porous media requires a knowledge of the shape, size,

location and physical properties of each component in the system, to-

gether with a set of appropriate fundamental equations governing the

desired phenomenon. Because of the complex nature of porous systems

it has been a tradition to model them by choosing a typical particle

shape and size, and a typical packing.

The subject of arrangement of units in space which might serve

as a model to represent porous systems has by this time been thoroughly

explored and one would expect a sound and complete set of principles

would now be available for use in any specific applications that might

arise. Most of the authors tend to consider porous materials as

spheres of uniform size in cubic or rhombohedral packing arrangements.

The effective porosity (fraction of the total volume which is occu-

pied by the connected voids) of the most densely packed arrangement

is 26.0 percent, which belongs to a rhombohedral arrangement charater-

ized by a unit cell of six planes passed through eight sphere centers

located at the corner of a regular rhombohedron, each edge of which

is twice the radius of the spheres. Simple cubic packing gives the

loosest or the most open textured packing with a porosity of 47.6

percent. In this case the unit is a cube, the eight corners of which

are centers of spheres tangent to each other. Other packings give porosities between these two limits. Therefore, the choice of a packing sets its porosity. However, it is not practical to develop a different model for each packing because this would yield discrete variations of porosity, and rather complex pore geometries in some cases.

Gomaa [23] modeled porous rock with uniform spheres packed in a normal cubic arrangement. Spheres were flattened at their side contacts while keeping their radii constant. In this manner the flattening causes a continuous reduction in porosity. Assuming that the heat flow is in the same direction and parallel to the contacts at every point, he arrives at an expression for thermal conductivity of fully fluid saturated porous media. This model is reasonably good for the case of fully water saturated rocks (λ_s/λ_f <10). However, there is poor agreement between the computed and experimental values for dry rocks (λ_s/λ_f>100). In general the experimental values for effective thermal conductivity are mostly greater than his analytical results.

Ozbek [13] modified Gomaa's work by adding an equal amount of flattening on the top and bottom contacts. He also assumes that the heat flow is unidirectional, and finally arrives at his own equation for the effective thermal conductivity of partially saturated porous systems. Comparison of the experimental data with the results calculated by Ozbek's model show a reasonable agreement for fully brine saturated sandstones, but significant differences have been detected when λ_s/λ_f is large (λ_s/λ_f >10). His prediction of thermal conductivity is usually lower than the observed experimental values.

The reasonable agreement of the above two models with the experimental results for water saturated rocks indicates that when λ_s/λ_f is

small the effective thermal conductivity of porous systems is not greatly influenced by the model which represents their structure or by the method used to calculate the effective thermal conductivity. However, for large values of λ_s/λ_f (dry rocks), the choice of a proper model for porous systems and a correct method for calculating thermal conductivity is of great importance.

The unidirectional heat flow assumption considered in the above two models neglects the distortion of heat flow lines. Accounting for the distortion is more realistic and would result in an increase in heat flow and consequently a higher thermal conductivity. This argument suggests that the proper accounting of heat flow lines in the model used by Gomaa would permit a correction to thermal conductivities of dry and liquid saturated rocks calculated by his analysis. But because only point contacts in the direction of the heat flow were considered in this model, one anticipates a zero effective thermal conductivity for such a system when the pores are evacuated. However, experimental results for evacuated sandstones show finite values for the effective thermal conductivity, even though it is small for packs of unconsolidated grains. Therefore, it would be more realistic to introduce finite grain-to-grain contact areas in the direction of the heat flow lines as well. Ozbek did consider such finite areas of contact when he modified the earlier model of Gomaa. However, because in Ozbek's work the relative size of these contact areas are dictated just by porosity, one would end up with large areas of contact for unconsolidated grains as well as for consolidated rocks. This causes such a large increase in effective thermal conductivity, that the calculated values of this property will be higher than their experimental counterparts.

In the present work a model made up of normal cubic-packed spheres, flattened at their contacts, is considered. As shown in Fig. 4 side flattenings are the same for all contacts, and all top and bottom flattenings are chosen to be the same but smaller than those on the sides. The proper choice for the relative size of these contacts is dictated by porosity and the degree of consolidation of the rocks, which will be investigated later. Motion of the heat is also considered to be two dimensional in the calculation of the effective thermal conductivity. This is more realistic when λ_s/λ_f is large, and allows another correction over the previous works of Gomaa and Ozbek. Furthermore this model is extended to multi-fluid saturated porous systems, by choosing a reasonable distribution of wetting and non-wetting phase fluids in the pore space.

2.2 Porosity Calculation

The porosity of the sphere pack shown in Fig. 4 is continuously variable as a function of the top-bottom and side flattenings. A rectangular parallelepiped with dimensions $2(r_0^2 - r_{c1}^2)^{\frac{1}{2}}$, $2(r_0^2 - r_{c1}^2)^{\frac{1}{2}}$, $2(r_0^2 - r_{c2}^2)^{\frac{1}{2}}$, containing a spherical solid of radius r_0, and flattened on the sides, top and the bottom is taken as a unit cell as shown in Fig. 5. Let V_T be the total volume, and V_s, the volume of the solid phase of the unit cell, then V_s, V_T and therefore, porosity, can be calculated as follows:

$$V_T = 8 \, r_0^3 m_1^2 m_2 \, , \qquad (2\text{-}2\text{-}1)$$
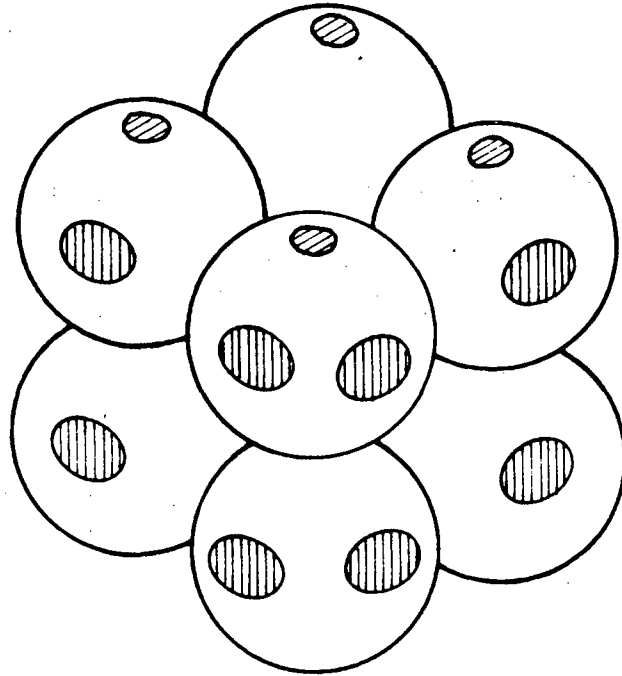
Fig. 4 Normal cubic packing of spheres flattened at their contacts
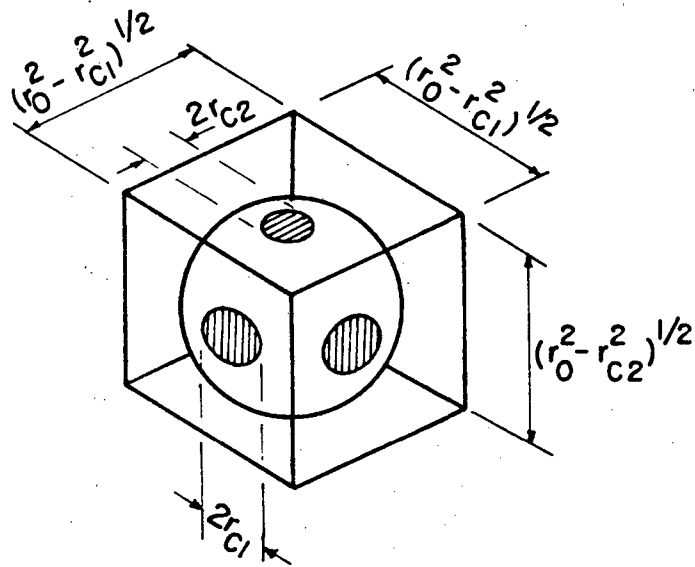
Fig. 5 A unit cell for porosity calculation
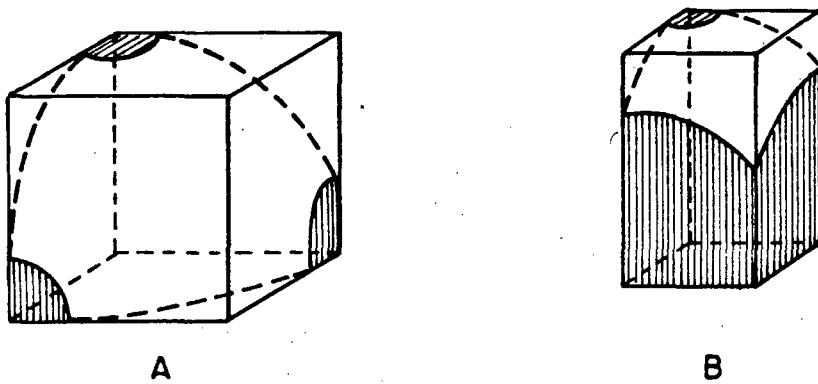
Fig. 6 One-eighth of a unit cell. A for $r_{cl}/r_o < 0.701$,
B for $r_{cl}/r_o > 0.701$
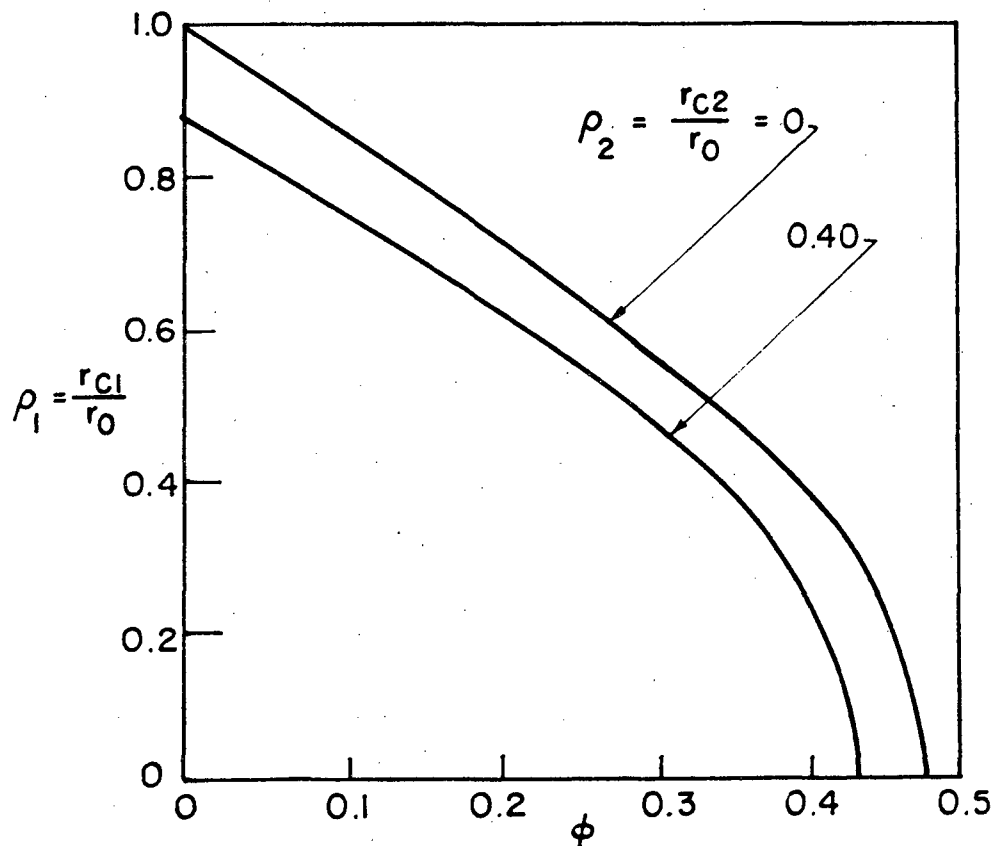
Fig. 7 Dimensionless radius of side contacts as a
function of porosity, for different values
of dimensionless radius of top-bottom contacts

$$V_s = \frac{4}{3}\pi r_0^3 \left\{ 1 - (1 - m_1)^2(2 + m_1) - \frac{1}{2}(1 - m_2)^2(2 + m_2) \right\} , \quad (2\text{-}2\text{-}2)$$

$$\phi = 1 - V_s/V_T = 1 - \frac{\pi}{12}\left\{ \frac{6m_1 - 2m_1^3 + 3m_2 - m_2^3 - 4}{m_1^2 m_2} \right\} , \quad (2\text{-}2\text{-}3)$$

where

$$m_1 = (1 - \rho_1^2)^{\frac{1}{2}} , \quad \rho_1 = \frac{r_{c1}}{r_0} ,$$

$$m_2 = (1 - \rho_2^2)^{\frac{1}{2}} , \quad \rho_2 = \frac{r_{c2}}{r_0} .$$

The above expressions for V_s, and porosity ϕ, are valid up to $\rho_1 = \sqrt{2}/2 = 0.701$, where the contact areas on the sides touch each other. Thereafter by referring to Fig.6B, V_s and porosity must be calculated from the following equations:

$$V_s = \frac{\pi r_0^3}{6}\left\{ 1 - (1 - m_1)^2(2 + m_1) - \frac{1}{2}(1 - m_2)^2(2 + m_2) \right\} + \frac{r_0^3}{6}\left\{ 2m_1^2 \times \right.$$

$$\left. (1 - 2m_1^2)^{\frac{1}{2}} - 2m_1(3 - m_1^2) \sin^{-1}(\frac{1 - 2m_1^2}{1 - m_1^2})^{\frac{1}{2}} + 4 \tan^{-1}(1 - 2m_1^2)^{\frac{1}{2}} \right\} , \quad (2\text{-}2\text{-}4)$$

$$\phi = 1 - \frac{V_s}{V_T} = 1 - \frac{f_1(m_1)}{m_2} + \frac{f_2(m_2)}{m_1^2} , \quad (2\text{-}2\text{-}5)$$

where

$$f_1(m_1) = \frac{\pi\left\{ 1 - (1 - m_1)^2(2 + m_1) \right\} + \left\{ 2m_1^2(1 - 2m_1^2)^{\frac{1}{2}} - 2m_1(3 - m_1^2) \times \right.}{}$$

$$\frac{\left. \sin^{-1}(\frac{1 - 2m_1^2}{1 - m_1^2})^{\frac{1}{2}} + 4 \tan^{-1}(1 - 2m_1^2)^{\frac{1}{2}} \right\}}{6m_1^2} ,$$

$$f_2(m_2) = \frac{\pi}{12}(1 - m_2)^2(2 + m_2)/m_2 .$$

In this case, the expression for $f_1(m_1)$ can be well approximated by a much simpler function as:

$$f_1(m_1) = 1 - \frac{2}{3}\left\{1 - (1 - m_1^2)^{\frac{1}{2}}\right\} \ .$$

Equation (2-2-4) for V_s, and (2-2-5) for ϕ are obtained with consideration that the contacts on the top and bottom never touch the side ones, i.e. $\rho_2 < (1 - \rho_1^2)^{\frac{1}{2}}$. Later developments showed that in fact ρ_2 is not very large, and therefore regions for which $\rho_2 > (1 - \rho_1^2)^{\frac{1}{2}}$ were not examined.

Detailed analysis leading to Eqs. (2-2-1) to (2-2-4) are developed in Appendix A. Fig. 7 is obtained by calculations using Eqs. (2-2-3) and (2-2-5) and gives porosity as a function of dimensionless radius $\rho_1 = \dfrac{r_{c1}}{r_0}$ of side contacts, for different values of dimensionless radius $\rho_1 = \dfrac{r_{c2}}{r_0}$ of top and bottom contacts.

2-3 Effective Thermal Conductivity Calcuation

In the present work the contribution of convection and radiation to heat transfer in the model are neglected. Therefore, the final results are applicable for porous rocks in which the Rayleigh number characterizing the natural convection is below its critical limit for that system, and for low to moderate temperatures. Of course there will be no forced convection since there will be no flow of fluids through the pores.

Taking into consideration the symmetry of the model, as well as appropriate boundary conditions, one could consider that the effective thermal conductivity of the model and that of the unit cell are equal. Therefore, it is sufficient to obtain the effective thermal conductivity of a unit cell. In order to do so, the temperature distribution due to imposed boundary conditions on this unit cell must first

be calculated. The temperature distribution would be symmetrical about both the horizontal plane containing the sphere's center and the vertical axis, if constant uniform temperatures are imposed on the horizontal boundaries. Thus, because of this symmetry, it is sufficient to obtain the temperature distribution in a one-eighth segment of a unit cell. All further discussions will refer only to this unit, which is called an elementary cell as shown in Fig. 8.

Assuming that conduction is the only mode of heat transfer, the governing equation for steady state temperature distribution in the elementary cell is:

$$\nabla \cdot (\lambda \nabla T) = 0 \ , \qquad (2\text{-}3\text{-}1)$$

with boundary conditions:

$$T = T_1 \text{ at } z = 0 \qquad , \ T = T_2 \text{ at } z = (r_0^2 - r_{c2}^2)^{\frac{1}{2}} \ , \qquad (2\text{-}3\text{-}2)$$

$$\frac{\partial T}{\partial x} = 0 \text{ at } x = 0 \qquad \text{and } x = (r_0^2 - r_{c1}^2)^{\frac{1}{2}} \ , \qquad (2\text{-}3\text{-}3)$$

$$\frac{\partial T}{\partial y} = 0 \text{ at } y = 0 \qquad \text{and } y = (r_0^2 - r_{c1}^2)^{\frac{1}{2}} \ . \qquad (2\text{-}3\text{-}4)$$

The conditions (2-3-3) and (2-3-4) arise from the fact that the lateral boundaries are adiabatic due to the symmetry of the temperature distribution.

A solution to equation (2-3-1) for the elementary cell, with boundary conditions as described, would yield a three dimensional temperature field which could be used to calculate the total heat flow passing through the elementary cell as:

$$Q = \int_A \lambda_s (\frac{\partial T}{\partial z})_{z=0} \ dA \ , \qquad (2\text{-}3\text{-}5)$$
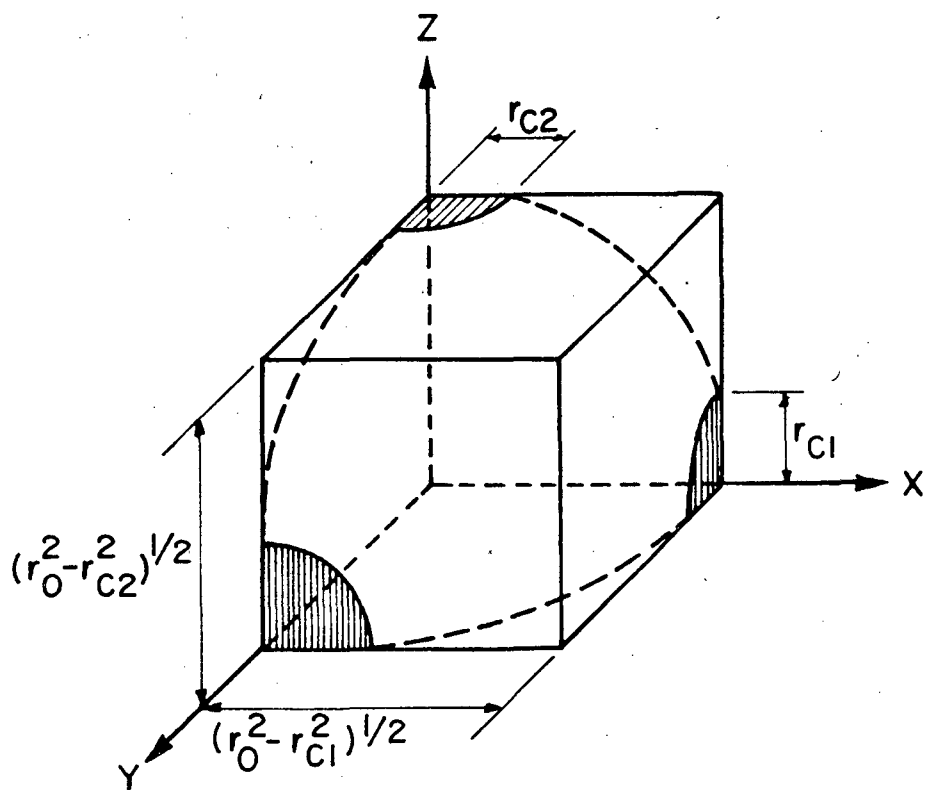
Fig. 8 An elementary cell for the effective thermal conductivity calculation
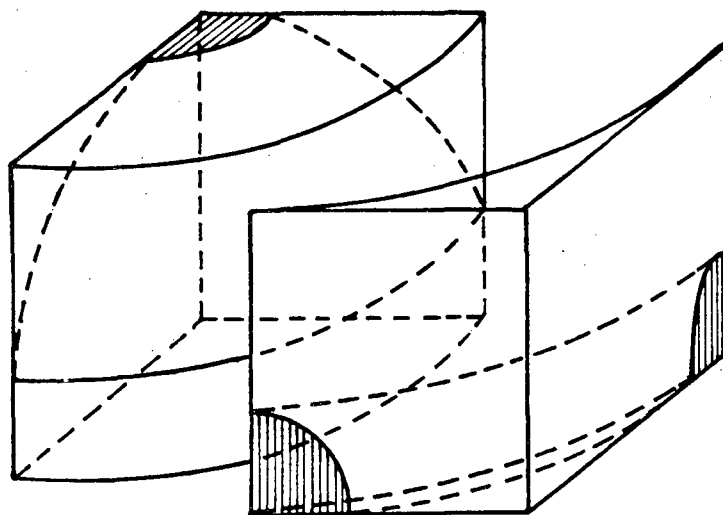
Fig. 9 Elementary cell divided by an adiabatic surface

where A is the area normal to the direction of heat flow. This heat flow value can then be used to determine the effective thermal conductivity of the elementary cell, which is defined by

$$\lambda_e = \frac{Q \cdot L}{A \cdot (T_2 - T_1)} \quad . \qquad (2\text{-}3\text{-}5)$$

It is not very difficult to show that this effective thermal conductivity is equal to that of a unit cell, or of the model.

Before starting to solve the problem, the elementary cell was divided into two regions by a cylindrical surface of radius $(r_0^2 - r_{cl}^2)^{\frac{1}{2}}$, having the Z coordinate as its axis (Fig. 9), and it was assumed that the total heat flow Q could be divided into two independent flows, namely Q_I and Q_{II}, each passing one of the separated regions. This could be justified as follows: For $\lambda_s/\lambda_f = 1$ it is obvious that the heat flow lines are parallel with each other everywhere and perpendicular to the xy plane, and therefore heat flows Q_I and Q_{II} are indeed independent of each other. It is easy to show that in this case $Q_{II}/Q = 1 - \frac{\pi}{4} = .215$, in other words only 21.5 percent of the total heat will flow as Q_{II}. The matter will be similar for λ_s/λ_f values not very far from unity. However, for large values of λ_s/λ_f most of the total heat flows as Q_I and Q_{II} will be even less than 21.5 percent of the total heat. Thus there is a weak interaction between the heat flow lines passing through region II and the boundary which separates this region from the rest of the elementary cell.

As a consequence of the above consideration, the cylindrical surface which divides the elementary cell into two regions can be safely approximated as an adiabatic boundary. This enables us to determine the thermal resistance of each region separately, and because these resistances are parallel with each other, the total thermal resistance is

given by
$$\frac{1}{R_T} = \frac{1}{R_I} + \frac{1}{R_{II}} \quad, \tag{2-3-6}$$

and the effective thermal conductivity would be:

$$\lambda_e = \frac{L}{A \cdot R_T} \quad, \tag{2-3-7}$$

where

$$L = (r_0^2 - r_{c2}^2)^{\frac{1}{2}} \quad,$$

$$A = (r_0^2 - r_{c1}^2) \quad.$$

Therefore our original problem has been reduced to the calculation of the thermal resistances R_I and R_{II}.

2-4 Determination of the Thermal Resistance of Region I

The thermal resistance of this region can be determined in terms of the heat flow Q_I as follows:

$$R_I = \frac{(T_1 - T_2)}{Q_I} \quad. \tag{2-4-1}$$

In order to evaluate Q_I, the temperature distribution in the cylindrical region I, as shown in Fig.10, must first be calculated. With the temperature distribution calculated, the heat flow Q_I can be evaluated from the temperature gradients at either the lower or upper boundary. Agreement of the heat flows calculated at these two boundaries gives a check on the accuracy of the temperature distribution.

Calculation of temperature distribution in region I is possible by solving the steady state heat conduction equation in the solid and in the fluid. In the system of cylindrical coordinates this has the form

$$\frac{\partial^2 T}{\partial r^2} + \frac{1}{r}\frac{\partial T}{\partial r} + \frac{1}{r^2}\frac{\partial^2 T}{\partial \theta^2} + \frac{\partial^2 T}{\partial z^2} = 0 \quad. \tag{2-4-2}$$
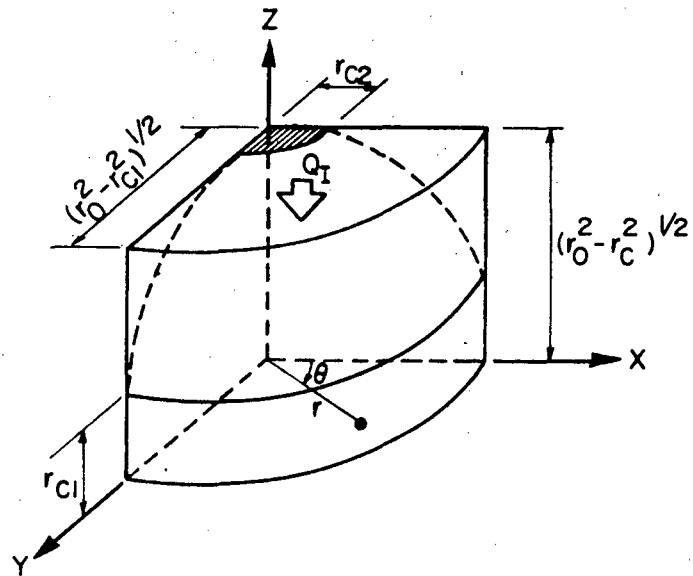
Fig. 10 Region I
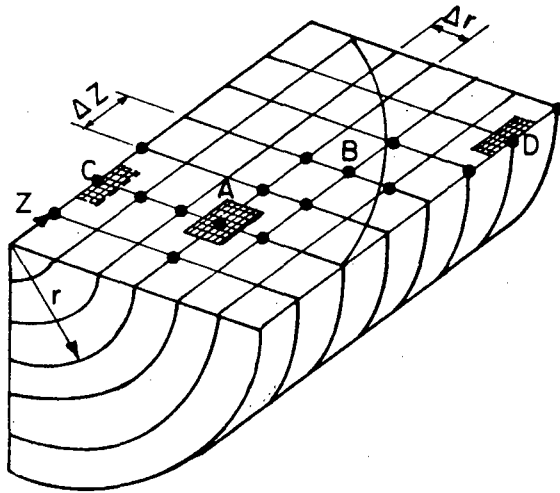
Fig. 11A Region I subdivided into finite difference elements
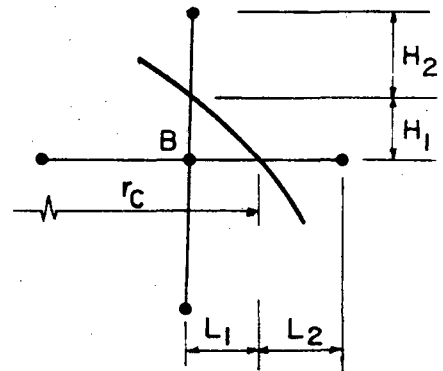
Fig. 11B An interior node near the solid-fluid interface

Because the geometry and the boundary conditions for this region are
independent of the coordinate Θ, the temperature will be a function
of r and z coordinates only, and Eq. (4-4-2) reduces to

$$\frac{\partial^2 T}{\partial r^2} + \frac{1}{r} \frac{\partial T}{\partial r} + \frac{\partial^2 T}{\partial z^2} = 0 \quad . \qquad (2\text{-}4\text{-}3)$$

In this case the flow of heat takes place in planes passing through
the z axis.

The temperature distribution T_s of the solid phase and T_f of the
fluid phase are both governed by Eq. (2-4-3) so the problem reduces
to solution of the following systems of equations:

$$\frac{\partial^2 T_s}{\partial r^2} + \frac{1}{r} \frac{\partial T_s}{\partial r} + \frac{\partial^2 T_s}{\partial z^2} = 0 \quad , \qquad (2\text{-}4\text{-}4)$$

$$\frac{\partial^2 T_f}{\partial r^2} + \frac{1}{r} \frac{\partial T_f}{\partial r} + \frac{\partial^2 T_f}{\partial z^2} = 0 \quad , \qquad (2\text{-}4\text{-}5)$$

and the boundary conditions are:

$$T_s = T_1 \text{ at } z = 0, \qquad 0 < r < (r_0^2 - r_{c1}^2)^{\frac{1}{2}} ,$$

$$\frac{\partial T_s}{\partial r} = 0 \text{ at } r = 0, \qquad 0 < z < (r_0 - r_{c2})^{\frac{1}{2}} ,$$

$$\frac{\partial T_s}{\partial r} = 0 \text{ at } r = (r_0^2 - r_{c1}^2)^{\frac{1}{2}} , \qquad 0 < z < r_{c1} ,$$

$$T_s = T_2 \text{ at } z = (r_0^2 - r_{c2}^2)^{\frac{1}{2}} , \qquad 0 < r < r_{c2} ,$$

$$T_f = T_2 \qquad \text{at } z = (r_0^2 - r_{c2}^2)^{\frac{1}{2}}, \; r_{c2} < r < (r_0^2 - r_{c1}^2)^{\frac{1}{2}} ,$$

$$\frac{\partial T_f}{\partial r} = 0 \qquad \text{at } r = (r_0^2 - r_{c1}^2)^{\frac{1}{2}}, \; r_{c1} < z < (r_0^2 - r_{c2}^2)^{\frac{1}{2}} \quad .$$

In addition to the above boundary conditions, at the common boundary
of the phases, continuity relations for temperature and heat flux
must be satisfied, i.e.:

$$T_s = T_f \ ,$$

$$\lambda_s (\nabla . T_s).\vec{n} = \lambda_f (\nabla T_f).\vec{n} \ ,$$

where $\vec{n}$ is a unit vector perpendicular to the interface.

An exact analytical solution to the system of Eqs. (2-4-4) and (2-4-5), which satisfies the above boundary and interface conditions, is difficult and may be impossible. This is due to the fact that analytical methods can be applied most effectively to homogeneous problems of simple geometry. A comprehensive study of such solutions can be found in the famous work of Carslaw and Jaeger [24]. However, there is another important method for obtaining solutions to these problems, namely, numerical analysis. Although the basic fundamentals of numerical techniques have long been known in mathematics, it has only been since the development of large scale digital computers that these methods have been used widely in scientific and engineering fields.

A numerical solution to a boundary value problem such as Eq. (2-4-3) can be obtained by finite difference methods which have been the subject of many texts [25, 26, 27]. The basic idea of these methods is to replace derivatives at a point by ratios of the changes in appropriate variables over a small but finite interval. Adopting the the notation of subscripts i,j to denote the positions (r,z), and notation

$$T_{i,j} = T (r = i \, \Delta r, \ Z = j \, \Delta Z) \ , \qquad (2-4-6)$$

where we have specified a mesh size (Δr, ΔZ), the finite difference approximation of Eq. (2-4-3) is:

$$\frac{T_{i-1,j} - 2T_{i,j} + T_{i+1,j}}{(\Delta r)^2} + \frac{T_{i+1,j} - T_{i-1,j}}{2(\Delta r)r_{i,j}} +$$

$$\frac{T_{i,j-1} - 2T_{i,j} + T_{i,j+1}}{(\Delta z)^2} = 0 \ . \qquad (2-4-7)$$

This equation can also be obtained making an energy balance for the node (i, j), i.e., equating the sum of thermal currents directed toward this node to zero. This can be expressed mathematically as:

$$\lambda(\frac{\Delta z}{\Delta r})\ (r_{i,j} - \frac{\Delta r}{2})(T_{i,j} - T_{i-1,j}) + \lambda(\frac{\Delta z}{\Delta r})\ (r_{i,j} + \frac{\Delta r}{2})(T_{i,j} - T_{i+i,j})$$

$$+ \lambda(r_{i,j}\frac{\Delta r}{\Delta z})(T_{i,j} - T_{i,j-1}) + \lambda(r_{i,j}\frac{\Delta r}{\Delta z})\ (T_{i,j} - T_{i,j+1}) = 0 \cdot \quad (2\text{-}4\text{-}8)$$

Rearranging terms in Eq. (2-4-8), yields Eq. (2-4-7).

In general the method of making an energy balance for an individual node m and its adjacent n nodes can be represented as:

$$\sum_n k_{mn}(T_n - T_m) = 0 \ , \qquad\qquad (2\text{-}4\text{-}9)$$

where K_{mn} is the thermal conductance between the node m and adjacent n nodes, and is defined as:

$$k_{mn} = \lambda\,(\frac{A_{mn}}{L_{mn}}) \ , \qquad\qquad (2\text{-}4\text{-}10)$$

where λ is the thermal conductivity, A_{mn} the average surface area perpendicular to the direction of heat flow, and L_{mn} the distance between the nodes. If the line connecting the two adjacent nodes is located entirely in the interior of the solid or of the fluid phase, then λ in Eq. (2-4-10) would be considered λ_s or λ_f, respectively. Otherwise, when the element connecting the two adjacent nodes is partly located in the solid and partly in the fluid phase, the overall thermal conductance between the nodes is calculated using the following relation:

$$\frac{1}{K_{mn}} = \frac{1}{K_1} + \frac{1}{K_2} \ , \qquad\qquad (2\text{-}4\text{-}11)$$

where K_1 and K_2 are the thermal conductances of the parts located entirely in the solid and in the fluid phase. This relation is obtained based on the fact that K_1 and K_2 are thermally in series with respect to the direction of heat flow.

Using the method of energy balance, for a node near the boundary between the solid and fluid like node B in Fig. 11B, one would obtain a nodal equation such as

node B

$$\frac{1}{\dfrac{L_1}{\lambda_s(r_c - \frac{L_1}{2})(\Delta z)} + \dfrac{L_2}{\lambda_f(r_c + \frac{L_2}{2})(\Delta z)}}(T_{i,j} - T_{i+1,j}) + \lambda_f(r_{i,j}\frac{\Delta r}{\Delta z}) \times$$

$$(T_{i,j} - T_{i,j-1}) + \frac{1}{\dfrac{H_1}{\lambda_s(\Delta r)r_{i,j}} + \dfrac{H_2}{\lambda_f(\Delta r)r_{i,j}}}(T_{i,j} - T_{i,j+1}) + \lambda_s \times$$

$$(\frac{\Delta z}{\Delta r})(r_{i,j} - \frac{\Delta r}{2})(T_{i,j} - T_{i-1,j}) = 0 \quad . \tag{2-4-12}$$

By the same token, for a node on the left boundary such as C and one on the right boundary such as D shown in Fig.11A, the nodal equation would be, respectively, as following:

node C

$$(T_{i,j} - T_{i+1,j})(\Delta z) + \frac{1}{4}\left\{(T_{i,j} - T_{i,j-1}) + (T_{i,j} - T_{i,j+1})\right\}\frac{(\Delta r)^2}{(\Delta z)} = 0 \quad , \tag{2-4-13}$$

node D

$$2(T_{i,j} - T_{i-1,j})(r_{i,j} - \frac{\Delta r}{2})(\frac{\Delta z}{\Delta r}) + (T_{i,j} - T_{i,j+1})(r_{i,j} - \frac{\Delta r}{4})(\frac{\Delta r}{\Delta z})$$

$$+ (T_{i,j} - T_{i,j-1})(r_{i,j} - \frac{\Delta r}{4})(\frac{\Delta r}{\Delta z}) = 0 \quad . \tag{2-4-14}$$

The nodal equations given by (2-3-12), (2-3-13) and (2-3-14) can also be obtained by using the original governing equation, that is, Eq. (2-4-3), and existing boundary conditions for the problem. This approach, together with an investigation of the errors involved in the difference formulation of the problem, are discussed in Appendix B.

To evaluate the temperature at each nodal point in the field, equations such as (2-4-8), (2-4-2) for interior nodes and (2-4-13),

(2-14-14) for boundary nodes should be written, and the resulting

set of equations must be solved simultaneously.

2-5   Solution of the Difference Equations.

The system of difference equations can be written in matrix

notation as:

$$A.T = B \quad , \qquad (2-5-1)$$

where T and B are column matrices containing the unknown values of

temperature and known values connected to the boundary conditions,

respectively, while A is a square matrix containing the coefficients

of unknown temperatures in the difference equations.

Solutions to such a set of algebraic equations are usually

considered in two general categories, direct and iterative methods.

The direct methods, of which Gaussian elimination is a well known

example, yield the exact solution of a system of difference equations

using a finite number of operations, while iterative methods consist

of the repeated application of a simple algorithm, and usually

yield the exact solution only as a limit of a sequence of trials.

Direct methods are ideally suited for the solution of a small

set of equations or system of equations which have been generated

in approximating parabolic equations. Thomas algorithm, which

plays an essential role in such problems, is perhaps one of the most

efficient methods in direct approaches.

The iterative methods, on the other hand, are usually pre-

ferred for solving large spares, that is when the coefficient

matrices associated with the finite difference solution of the

differential equations contain a large number of zero elements.

These methods take full advantage of these numerous zeros, both

in storage and operation. There are many different iterative methods, among which successive over-relaxation (SOR) is a very efficient and effective device to reduce the time required to obtain a desired accuracy. This technique along with some generalized concepts underlying direct and iterative methods are discussed in Appendix C.

Because the number of simultaneous equations, the solution of which yields the temperature field, can become very large for this problem, and also due to the fact that the coefficient matrix A contains a large number of zero elements, the successive over-relaxation technique is used in the present work to solve the resulting set of algebraic equations.

Solving a large set of equations with the S.O.R. method may require many iterations over many nodes, thus it is very important, even with a modern digital computer, to optimize the iteration procedure. For this problem a method described by Carré [28] is used to estimate the optimum acceleration factor for the successive iterations.

2-6 Determination of the Thermal Resistance of Region II.

As explained earlier in Section (2-3), when λ_s/λ_f is large, only a small fraction of the total heat will flow through region II. Thus the effective thermal conductivity of the model and that of the region I are very close. Therefore the method of calculation of the heat flow Q_{II} does not have a real effect on our final result. For this reason the thermal resistance of this region is calculated with the assumption of undirectional motion of the heat, which of course yields satisfactory results for small values of λ_s/λ_f as well.

Region II is divided into five sections as shown in Fig. 12A
The thermal resistance of each section is calculated separately and
a network of these resistances is constructed to evaluate the total
thermal resistance of this region. Determination of the thermal
resistance of each individual section is given as follows:

Section 1

This section contains fluid only. Therefore:

$$R_1 = \frac{(\Delta T)_1}{Q_I} = \frac{L_1}{A_1 \lambda_f} = \frac{(r_0^2 - r_{c2}^2)^{\frac{1}{2}} - r_{c1}}{(1 - \frac{\pi}{4})(r_0^2 - r_{c1}^2)\lambda_f} \quad . \qquad (2\text{-}6\text{-}1)$$

Section 2

This section contains both solid and fluid. To determine the
thermal resistance of this section, first the heat flow through the
infinitesimal cylindrical element of thickness dr, shown in Fig. 13,
is calculated as:

$$dQ_2 = \frac{(\Delta T)_2}{\dfrac{L_s}{\lambda_s dA_2} + \dfrac{L_f}{\lambda_f dA_2}} \quad , \qquad (2\text{-}6\text{-}2)$$

but

$$dA_2 = \Theta r \, dr \qquad , \quad \Theta = \frac{\pi}{2} - 2 \sin^{-1}(\frac{r_{c1}}{r_0}) \quad ,$$

$$L_s = (r_0^2 - r^2)^{\frac{1}{2}} \quad ,$$

$$L_f = r_{c1} - L_s = r_{c1} - (r_0^2 - r^2)^{\frac{1}{2}} \quad ,$$

therefore Equa. (2-6-2) becomes:

$$dQ_2 = \frac{(\Delta T)_2 . \Theta . r . dr}{\dfrac{(r_0^2 - r^2)^{\frac{1}{2}}}{\lambda_s} + \dfrac{r_{c1} - (r_0^2 - r^2)^{\frac{1}{2}}}{\lambda_f}} \quad .$$

43
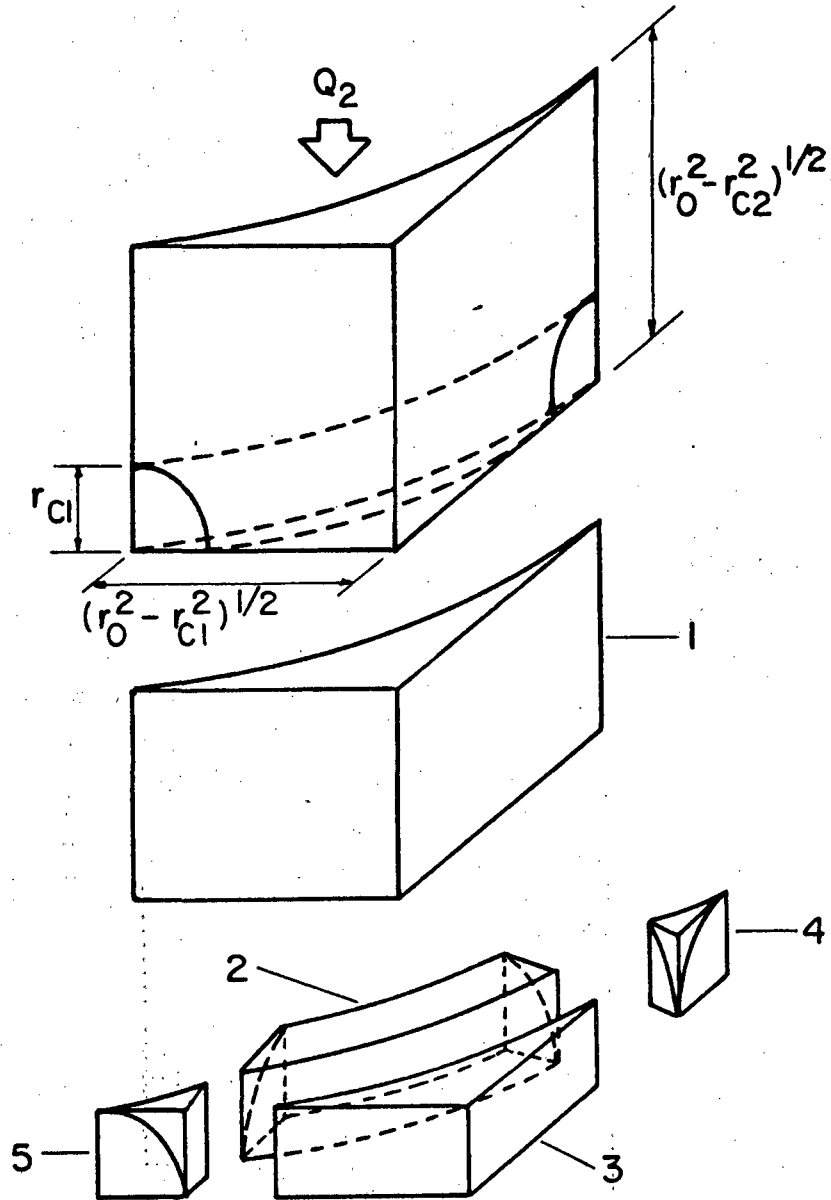
Fig. 12A Region II subdivided into 5 individual sections
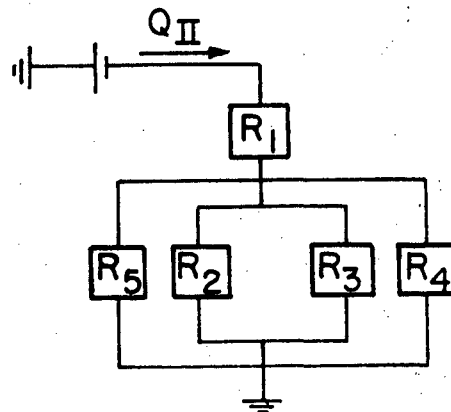
Fig. 12B Electrical analog of region II
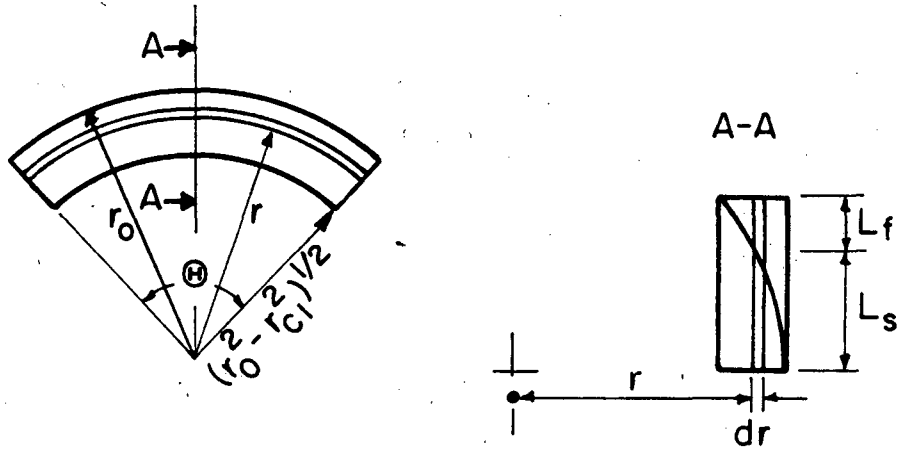
Fig. 13 Top view of section 2 and its side cross-section
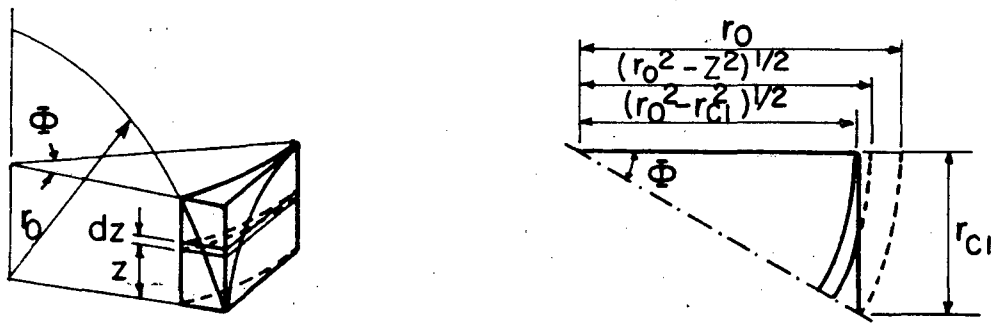
Fig. 14 Section 4 and its top view
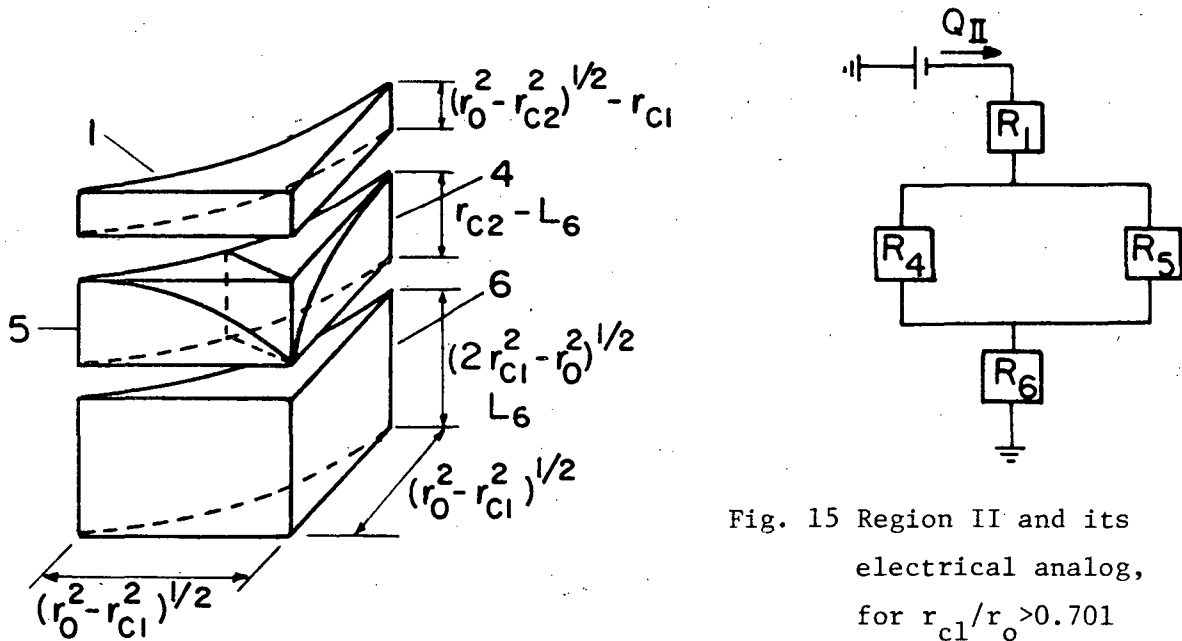
Fig. 15 Region II and its

electrical analog,

for $r_{c1}/r_o > 0.701$

The total heat flow passing through section 2 is

$$Q_2 = \Theta \cdot (\Delta T)_2 \int\limits_{(r_0^2 - r_{cl}^2)^{1/2}}^{r_0} \frac{r\,dr}{\left(\frac{1}{\lambda_s} - \frac{1}{\lambda_f}\right)(r_0^2 - r^2)^{1/2} + \frac{r_{cl}}{\lambda_f}} \quad ,$$

Carrying out the integration yields:

$$R_2 = \frac{Q_2}{(\Delta T)_2} = \frac{\left(\frac{\lambda_s}{\lambda_f} - 1\right)}{\left\{\frac{(\lambda_s/\lambda_f)}{\frac{\lambda_s}{\lambda_f} - 1}\ln\left(\frac{\lambda_s}{\lambda_f}\right) - 1\right\}} \cdot \frac{1}{\Theta \cdot r_{cl} \cdot \lambda_s} \quad . \qquad (2\text{-}6\text{-}3)$$

Section 3

This section also contains fluid only. Thus:

$$R_3 = \frac{(\Delta T)_3}{Q_3} = \frac{L_3}{A_3 \lambda_f} = \frac{r_{cl}}{\left\{(r_0^2 - r_{cl}^2) - \frac{\Theta r_0^2}{2} - r_{cl}(r_0^2 - r_{cl}^2)^{1/2}\right\}\lambda_f} \cdot (2\text{-}6\text{-}4)$$

Sections 4 and 5

These two sections contain both solid and fluid and are also identical. Therefore, it is sufficient to determine the thermal resistance of only one of these components. An infinitesimal element of thickness dz in section 4 is considered (Fig. 14), and the heat flow through this element is calculated as:

$$Q_4 = \frac{(\Delta T)_4}{\int\limits_0^{r_{cl}} \frac{dz}{\lambda_s A_1 + \lambda_f A_2}} \quad , \qquad (2\text{-}6\text{-}5)$$

where A_1 and A_2 are the areas of the infinitesimal solid and fluid phase perpendicular to the direction of heat flow, respectively.

These areas can be expressed as following:

$$A_1 = \frac{1}{2} (r_{cl}^2 - z^2) \Phi - \frac{1}{2} (r_0^2 - z^2) \tan^{-1}(\frac{r_{cl}^2 - z^2}{r_0^2 - r_{cl}^2})^{\frac{1}{2}}$$

$$+ \frac{1}{2} (r_0^2 - r_{cl}^2)^{\frac{1}{2}}(r_{cl}^2 - z^2)^{\frac{1}{2}} \quad ,$$

$$A_2 = \frac{1}{2} r_0 (r_0^2 - r_{cl}^2)^{\frac{1}{2}} \sin \Phi - \frac{1}{2} (r_0^2 - r_{cl}^2)\Phi - A_1, \quad \Phi = \sin^{-1}(\frac{r_{cl}}{r_0}) \quad .$$

Substitution of A_1 and A_2 into Equa. (2-6-5) yields the following for the thermal resistance of this section:

$$R_4 = \frac{(\Delta T)_4}{Q_4} = \int_0^{r_{cl}} \frac{dz}{C_1 + C_2 (r_{cl}^2 - z^2)^{\frac{1}{2}} + C_3 (r_{cl}^2 - z^2) - C_4 (r_0^2 - z^2) \times \tan^{-1} \left(\frac{r_{cl}^2 - z^2}{r_0^2 - r_{cl}^2}\right)^{\frac{1}{2}}} \quad , \qquad (2-6-6)$$

where

$$C_1 = \lambda_f \left\{ r_0 (r_0^2 - r_{cl}^2)^{\frac{1}{2}} \sin \Phi - (r_0^2 - r_{cl}^2) \Phi \right\} /2 \quad ,$$

$$C_2 = (\lambda_s - \lambda_f)(r_0^2 - r_{cl}^2)^{\frac{1}{2}} /2 \quad ,$$

$$C_3 = (\lambda_s - \lambda_f) \cdot \Phi /2 \quad ,$$

$$C_4 = (\lambda_s - \lambda_f) /2 \quad .$$

Analytical evaluation of the integral involved in Equa. (2-6-6) is very difficult and cannot be found. Therefore, this integral is evaluated numerically.

The electrical analog for the heat conducted through region II is shown in Fig. 12B, which gives a total thermal resistance as:

$$R_{II} = R_1 + \cfrac{1}{\cfrac{1}{R_2} + \cfrac{1}{R_3} + \cfrac{2}{R_4}} \quad . \qquad (2\text{-}6\text{-}7)$$

When the contact areas on the sides touch each other, thereafter resistances R_2 and R_3 vanish, but another section, which is completely solid, appears as shown in Fig. 15. Its thermal resistance is given by

$$R_6 = \frac{(\Delta T)_6}{Q_{II}} = \frac{L_6}{A_6 \lambda_s} = \frac{(2r_{c1}^2 - r_0^2)^{\frac{1}{2}}}{(r_0^2 - r_{c1}^2)(1 - \frac{\pi}{4})\lambda_s} \quad . \qquad (2\text{-}6\text{-}8)$$

The total thermal resistance for region II in this case is:

$$R_{II} = R_1 + 1/2 \; R_4 + R_6 \quad . \qquad (2\text{-}6\text{-}9)$$

2-7 Thermal Conductivity of Multi-Fluid Saturated Rocks.

The single fluid saturated systems for which the calculation of the effective thermal conductivity was considered above in detail are very rare in petroleum reservoirs. However, having developed a model for a simpler case, it is easy to extend it to a more complicated one.

Pore spaces in an oil reservoir are usually filled with two or more fluid phases. Oil, water, and gas may exist simultaneously in the voids, each occupying a fraction of the pore volume. This fraction is referred to as the saturation of that phase and is denoted by the symbol S_i, where subscript i identifies each individual fluid component.

In general, if the pore spaces contain fluids of thermal conductivities λ_1, λ_2,....λ_n, and corresponding saturations S_1, S_2,.... .S_n, then the effective thermal conductivity of the system in its

dimensionless form can be written as:

$$\frac{\lambda_e}{\lambda_s} = F\ (\frac{\lambda_s}{\lambda_1},\ \frac{\lambda_s}{\lambda_2},\cdots\cdots\frac{\lambda_s}{\lambda_n},\ \phi,\ S_1,\ S_2,\cdots\cdots S_{n-1})\ . \qquad (2\text{-}7\text{-}1)$$

The functional relationship represented by F depends on the texture (i.e. size, shape, and arrangement) of the solid components as well as on the distribution of each individual fluid within the pore space.

To make the problem less complicated, it was thought that a two-fluid saturated system would be a simple and rather practical case to examine, since oil-water or gas-oil systems are relatively common in petroleum reservoirs. Using the present model to represent the porous rock where the size, shape and arrangement of the solid grains are fixed, it remains to specify phase distribution of the fluids within the pores for calculation of the effective thermal conductivity. Distribution of the fluids in the porous network of a reservoir rock is a function of the saturation as well as the wetting characteristic of the rock solids and the fluids. For example, for an oil-water system, the reservoir rock could be either water wet, which means water preferentially adheres to the reservoir rock surface, or oil wet. From the geometry point of view, the distribution of two immiscible fluids within the pore space can be considered as the following widely accepted model. When the porous medium has the lowest possible saturation of the wetting phase, this phase forms pendular rings around the grain contact points. These rings are not connected with each other except perhaps through a molecular thickness on the solid surface. If the wetting phase saturation is increased beyond this minimum, the pendular rings expand and finally become large enough to merge and form continuous channels while the non-wetting fluids stays in the middle forming

also a continuous network. Further increase in saturation of the wetting-fluid causes the non-wetting fluid to break into individual droplets. Fig.16 represents the above possible regimes for an oil-water system where grains are considered to be water wet.

To incorporate a reasonable fluid distribution into the existing model, the wetting phase is chosen to be a spherical layer of uniform thickness next to the solid grain surfaces (Fig. 17). Even though this choice may not be very realistic for very low and high saturations of the wetting phase where the wetting and non-wetting fluids become discontinuous, it would be a good approximation for the intermediate saturations, and is also convenient from the analysis point of view.

The relation between the wetting phase saturation S_w and radius to the interface of the fluids r_w is needed. As mentioned before, the wetting phase saturation is the fraction of the pore space occupied by this phase; thus:

$$S_w = \text{volume of wetting phase/pore volume} \qquad (2\text{-}7\text{-}2)$$

By referring to Fig. 17, the volume of wetting phase and pore volume can be expressed as follows:

$$V_w = \frac{\pi r_0^3}{6} \left\{ \rho_w^3 - (\rho_w - m_1)^2(2\rho_w + m_1) - \frac{1}{2}(\rho_w - m_2)^2(2\rho_w + m_2) - \right.$$
$$\left. \frac{6}{\pi}(1 - \phi)m_1^2 m_2 \right\} , \qquad (2\text{-}7\text{-}3)$$

$$V_v = r_0^3 \, \phi m_1^2 m_2 , \qquad (2\text{-}7\text{-}4)$$

where

$$\rho_w = r_w/r_0 .$$

The above relation for V_w is valid until $r_w \leqslant \sqrt{2} \, (r_0^2 - r_{c1}^2)^{\frac{1}{2}}$. For the region where $\sqrt{2} \, (r_0^2 - r_{c1}^2)^{\frac{1}{2}} < r_w < (2r_0^2 - r_{c1}^2 - r_{c2}^2)^{\frac{1}{2}}$, Eq. (2-7-3) should be modified as:

Low water saturation   Intermediate water   High water saturation
                           saturation
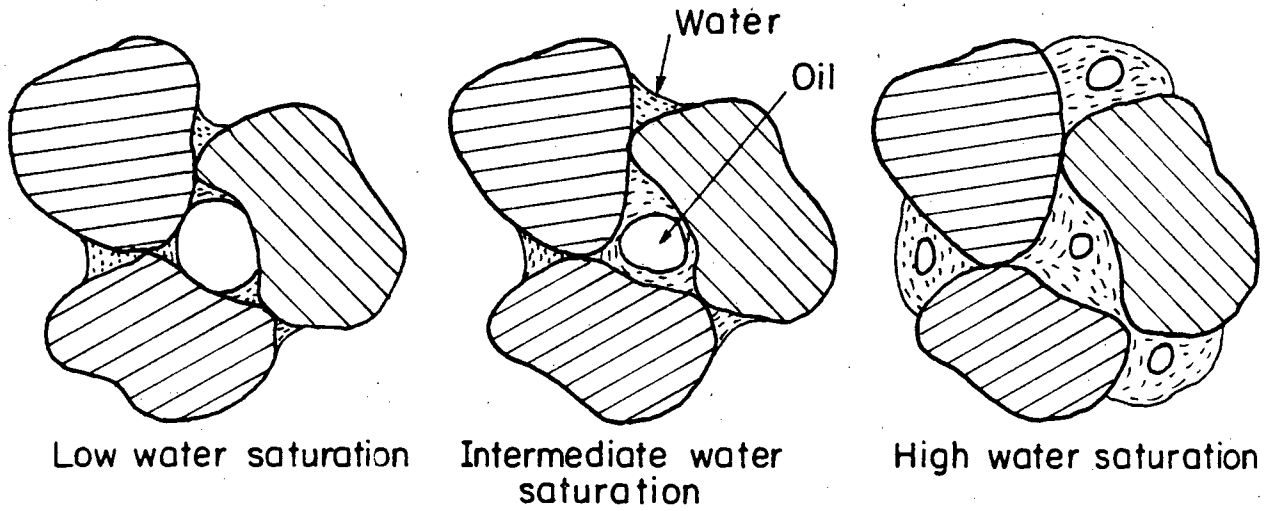
Fig. 16 Three possible regions for an oil-water system where water
is the wetting phase
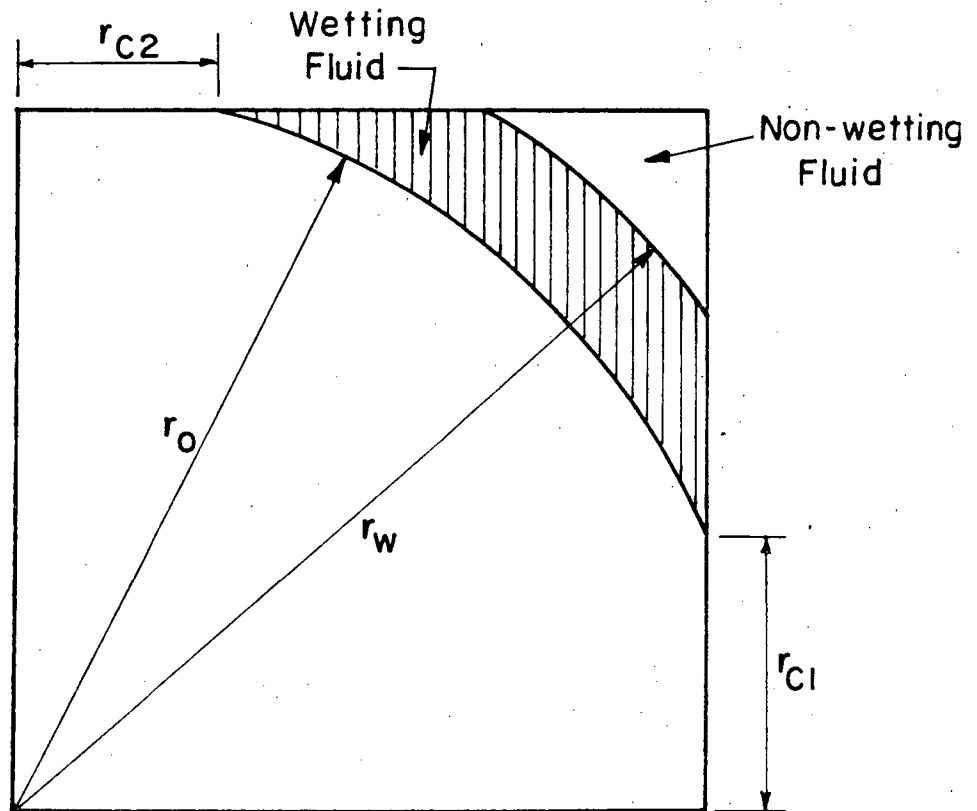
Fig. 17 Distribution of the wetting and the
non-wetting fluids in the pore space

$$V_w = \frac{\pi r_0^3}{6} \left\{ \rho_w^3 - (\rho_w - m_1)^2 (2\rho_w + m_1) - \frac{1}{2}(\rho_w - m_2)^2(2\rho_w + m_2) + V_0 \right.$$
$$\left. - \frac{6}{\pi}(1 - \phi) m_1^2 m_2 \right\} \quad , \qquad (2\text{-}7\text{-}5)$$

where

$$V_0 = \frac{\rho_w^3}{\pi} \left\{ 2(2\rho^2 - 1)^{\frac{1}{2}}(1 - \rho^2) - 2(\rho^2 + 2)(1 - \rho^2)^{\frac{1}{2}} \sin^{-1}\left(\frac{2\rho^2 - 1}{\rho^2}\right)^{\frac{1}{2}} \right.$$

$$\left. + 4 \tan^{-1}(2\rho^2 - 1)^{\frac{1}{2}} \right\} \qquad (2\text{-}7\text{-}6)$$

$$\rho = \frac{(\rho_w^2 - m_1^2)^{\frac{1}{2}}}{\rho_w} \quad .$$

There is another region where $r_w > (2r_0^2 - r_{c1}^2 - r_{c2}^2)^{\frac{1}{2}}$, for which the functional form of V_w becomes very complicated. This region is not examined, because $r_0 \leqslant r_w \leqslant (2r_0^2 - r_{c1}^2 - r_{c2}^2)^{\frac{1}{2}}$ itself covers a wide range of the wetting phase saturation.

Figure 18 is plotted using the appropriate relation for the volume of wetting phase in Eq. (2-7-2), and gives saturation as a function of dimensionless radius to the wetting fluid-non-wetting fluid interface, for different porosities and no flattening on the top and bottom contacts. It is very interesting to note that these curves are not very sensitive to changes in ρ_2 for a fixed porosity. Therefore these curves can also be used for the other values of ρ_2 with an error less than one percent. Only at very low porosities (less than 0.10) does this error increase, and different curves should be considered for different values of ρ_2.

The existing knowledge developed earlier for a single fluid saturated model can be used with some modifications for the calculation of the effective thermal conductivity of the proposed two-fluid phase system. Referring to Fig. 17 the thermal resistance of
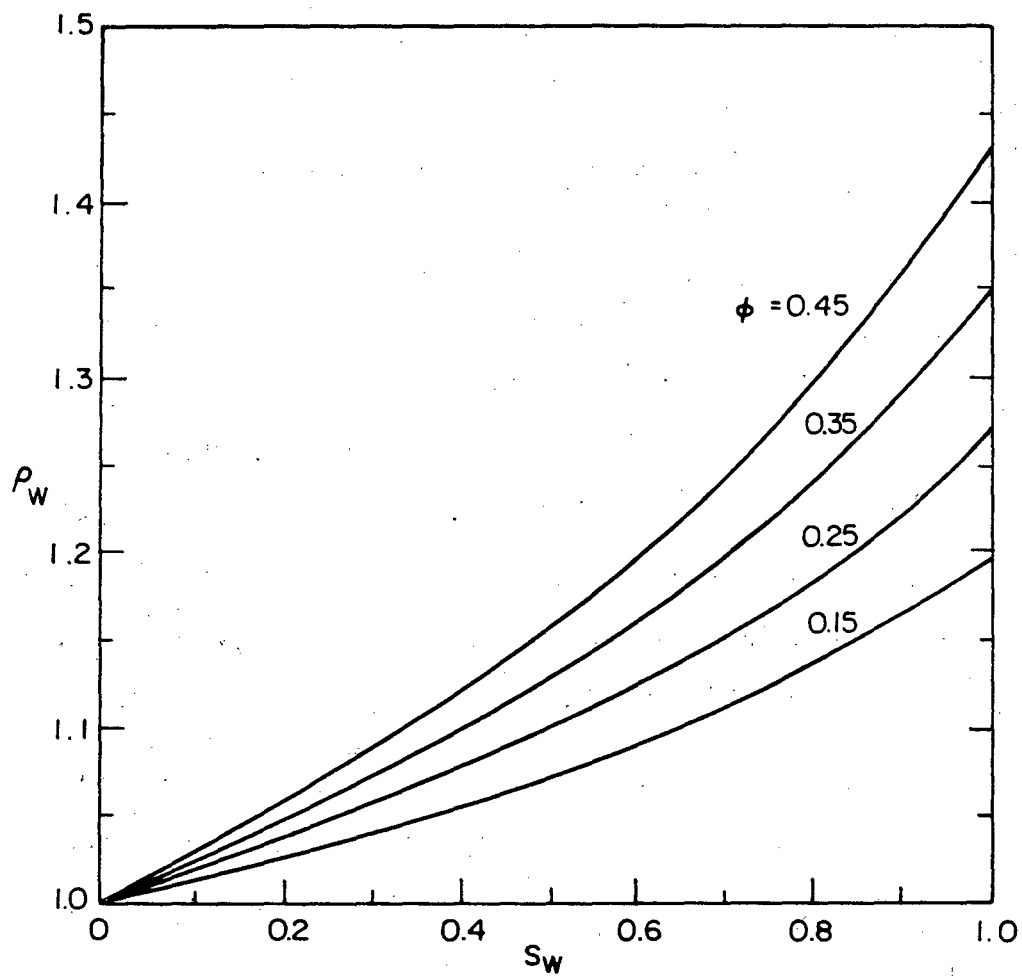
Fig. 18 Dimensionless radius to the wetting-non-wetting fluid
interface as a function of saturation of the wetting
phase, for different porosities and $r_{c2} = 0$

region I can be easily determined following the same procedures described earlier to solve the steady state heat conduction equation for this region by the method of finite difference.

Thermal resistance of region II can be calculated as before making the assumption of undirectional flow of heat. However, because of the complex geometry of the two phase system, a weighted geometric mean of the conductivity of these phases is assigned for the thermal conductivity of this region, given by:

$$\lambda_{II} = \lambda_s^{(\frac{V_s}{V_T})_{II}} \cdot \lambda_w^{(\frac{V_w}{V_T})_{II}} \cdot \lambda_{nw}^{(\frac{V_{nw}}{V_T})_{II}} \text{ ,} \qquad (2\text{-}7\text{-}7)$$

where V_s, V_w, V_{nw} are the volume of solid, wetting, and non-wetting phase in region II, respectively, and V_T is the total volume of this region, given by:

$$V_s = r_0^3 \left\{ (1 - \phi)(1 - \rho_1^2)(1 - \rho_2^2)^{\frac{1}{2}} - \frac{\pi}{12}\left[(1 - \rho_2^2)^{\frac{1}{2}}(2 + \rho_2^2) - 3\rho_1 + \rho_1^3\right] \right.$$

$$\left. - \frac{\pi}{4}(1 - \rho_1^2)\rho_1 \right\} \text{ ,} \qquad (2\text{-}7\text{-}8)$$

$$V_w = r_0^3 \left\{ \phi S_w(1 - \rho_1^2)(1 - \rho_1^2)(1 - \rho_2^2)^{\frac{1}{2}} + \frac{\pi}{12}\left[(1 - \rho_2^2)^{\frac{1}{2}}(2 + \rho_2^2)\right.\right.$$

$$\left. - 3\rho_1 + \rho_1^3\right] + \frac{\pi}{4}(1 - \rho_1^2)\rho_1 - \frac{\pi}{4}(1 - \rho_1^2)(\rho_w^2 + \rho_1^2 - 1)^{\frac{1}{2}}$$

$$- \frac{\pi}{12}\left[3\rho_w^2(1 - \rho_2^2)^{\frac{1}{2}} - 3\rho_w^2(\rho_w^2 + \rho_1^2 - 1)^{\frac{1}{2}} - (1 - \rho_2^2)^{3/2} + \right.$$

$$\left.\left. (\rho_w^2 + \rho_1^2 - 1)^{3/2}\right]\right\} \text{ ,} \qquad (2\text{-}7\text{-}9)$$

$$V_T = r_0^3(1 - \frac{\pi}{4})(1 - \rho_1^2)(1 - \rho_2^2)^{\frac{1}{2}} \text{ ,} \qquad (2\text{-}7\text{-}10)$$

$$V_{nw} = V_T - V_s - V_w \text{ .} \qquad (2\text{-}7\text{-}11)$$

As argued before, any reasonable method to evaluate the thermal conductivity of this region will be satisfactory and does not have an important effect on the value of the overall thermal conductivity. Having assigned a thermal conductivity as in Eq. (2-7-7) for region II, its thermal resistance can be given by

$$R_{II} = \frac{L_{II}}{\lambda_{II} A_{II}} = \frac{(r_0^2 - r_{c2}^2)^{\frac{1}{2}}}{(1 - \frac{\pi}{4})(r_0^2 - r_{c1}^2)\lambda_{II}} \quad . \qquad (2\text{-}7\text{-}12)$$

2-8 Determination of the Relative Size of Grain to Grain Contacts.

The equations obtained for porosity of the proposed model reveals the fact that knowledge of porosity alone is not enough to define a unique configuration for the system, and some argument should be made about the relative size of grain-to-grain contacts to fix the geometry for a given porosity.

In general a complete understanding of the relation between the grains, such as the number and type of contacts, requires a comprehensive study of the size, shape and arrangement of these particles. Also required is knowledge of the processes which are responsible for reduction of the pore space, namely compaction under which gravitational stress over geological ages causes closer packing, crushing and deformation of the grains, and cementation in which minerals serve as cement to hold together the individual grains. Such studies have been made elsewhere in texts on sedimentary rocks [29, 30]. However, a sound and precise relationship among these properties and the relative size of the contact between the grains is very difficult to obtain. Taylor [31] classifies the sand grain contacts as they appear in the plane of a random thin-section and considers that three

types of contacts, namely tangential, long, and concave-convex, as shown in Fig. 19 , can occur between the grains. Taylor finally concludes that the number of contacts per grain and the types of them due to stress increase with depth. In connection with the mutual spatial relationship among the grains, Kahn [32] introduces two numerical parameters, namely the packing proximity, and the packing density. The former is a qualitative measure of grain-to-grain contacts, and is expressed as the ratio of the number of grain-to-grain contacts in a traverse across the thin-section, to the total number of contacts of all kinds in the same traverse. When this parameter is small, most of the contacts are those between a grain and cement, and the grains have only a small area of contact with each other. Conversely a large packing proximity means that most of the contacts are grain-to-grain, with less mutual relation between the grains and cementing minerals, which suggests that the rock has been under compaction without the introduction of much cementing agents. The second parameter introduced by Khan, i.e. the packing density, is a measure of aggregation of the packing and is defined as the ratio of the sum of the length of grain intercepts to the total length of the traverse across the thin section.

Although the above authors have examined types and the number of grain-to-grain contacts, they have not made any quantitative statement about their relative size, which is of course a difficult parameter to investigate from thin-section analysis. However, for porous rocks there exists a physical property, namely, the effective thermal conductivity, which can be used as a guide for estimation of some average size of the grain-to-grain contacts.
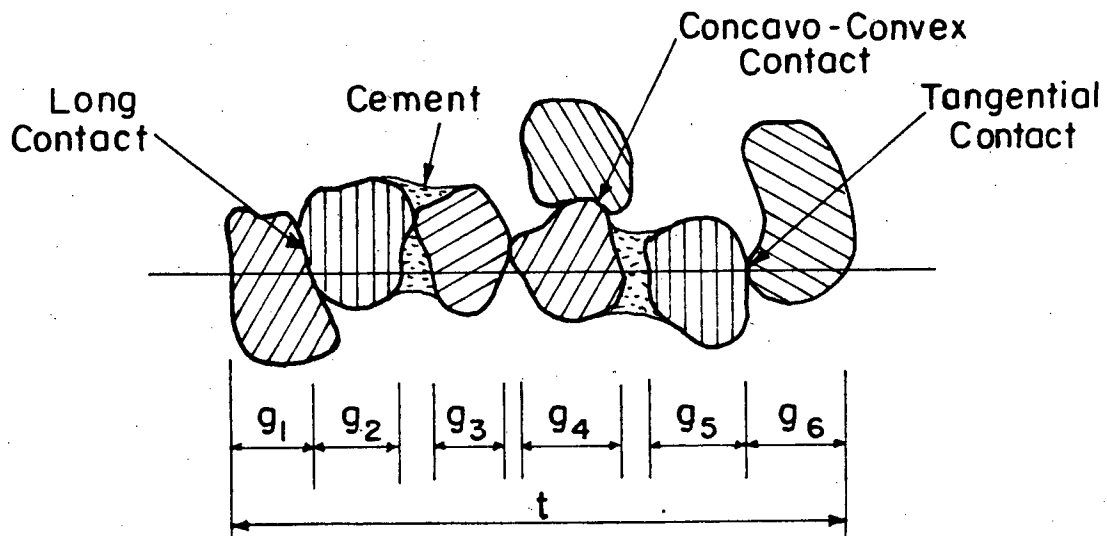
Fig. 19 Mutual spatial relationship among the grains in a typical
    sedimentary rock (after Taylor [31])

    The total number of grains in the traverse is six and there
    are only two grain-to-grain contacts in the traverse. Packing
    proximity is therefore, $\frac{2}{6}$ .100 = 33.3%. Packing density is
    the ratio of the sum of the intersept-size values for the
    six grains to the length of the traverse. Therefore, packing
    density = $\sum_{i=1}^{6} g_i/t$.

In a porous system if the interconnected pores are evacuated, in the absence of radiation energy transfer, heat can only be conducted by the solid components through their finite contact areas present in the direction of heat flow. Therefore, the effective thermal conductivity in this case will be a function of the size, shape, arrangement, and thermal conductivity of the grains as well as the number and size of their contacts.

The influence of the thermal conductivity of the solid components, λ_s, on the effective thermal conductivity of a porous system under the vacuum condition, λ_{e0}, is very easy to investigate. In fact because the interconnected pores are non-conductive, the conductivity of the system is entirely due to the solid grains and their finite areas of contact. Consequently, one can conclude that λ_{e0} is proportional to λ_s. This can be expressed as:

$$F = \frac{\lambda_s}{\lambda_{e0}} \ .$$
(2-8-1)

It is obvious from Equa. (2-8-1) that the factor F, which serves as a proportionality constant, fully embodies the influence of the geometry of the grains and their mutual relationship.

Similar to the above factor, there exists a widely used parameter in the oil industry to characterize the pore structure of sedimentary rocks and sands. This parameter, which is called the electrical formation resistivity factor, F, is defined as the ratio of the electrical resistivity of a fully saturated porous rock, R_e, to the electrical resistivity of the saturant fluid, R_f. This can be shown as:

$$F_{electrical} = \frac{R_e}{R_f} . \qquad (2-8-2)$$

In terms of electrical conductivities, **Eq.** (2-8-2) becomes:

$$F_{electrical} = \frac{\gamma_f}{\gamma_e} . \qquad (2-8-3)$$

The fact that the rock forming minerals are usually poor electrical conductors reveals the striking similarity between the two Eqs. (2-8-1) and (2-8-3). Therefore, it will be appropriate to call the factor F in Eq. (2-8-1), the thermal formation resistivity, and denote it by $F_{thermal}$.

Many attempts have been made to find analytical or empirical relations that can express the influence of the geometry and packing of the grains on the thermal formation resistivity factor. Chan and Tien [33] studied the heat transfer through the solid phase of three different packed beds of uniform size spheres, namely, simple cubic, body-centered cubic, and face-centered cubic, as shown in Fig. 20. In each case heat can be transferred through the circular patches which are formed at the contact points of the spheres, due to an axial load on the system. Based on the assumption that the contact areas are very small, these authors obtained an analytic solution, for the temperature field within a single sphere, which has a uniform heat flux on the two diametrically opposite contacts, while the rest of its surface is insulated. This basic solution together with some geometrical parameters provides the necessary information for the calculation of the effective thermal conductivity of each packing. Chan and Tien's final results can be expressed as follows:
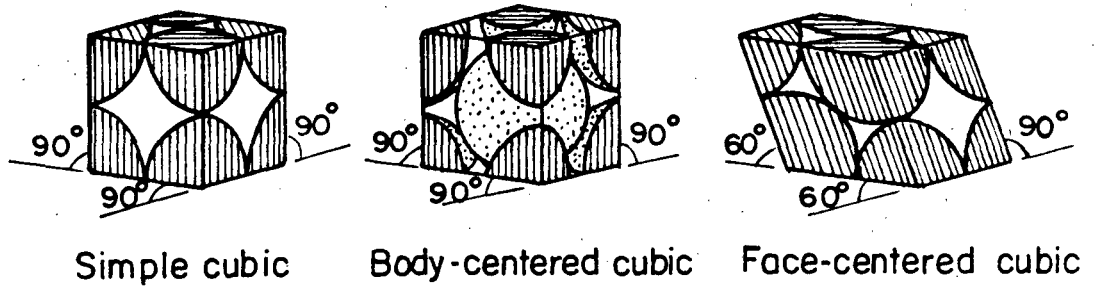
Simple cubic   Body-centered cubic   Face-centered cubic

Fig. 20 Unit cell of three different regularly packed spheres

Table 1 Basic Parameters for different packing patterns

	ϕ	N_t	N_a
Simple cubic	0.476	$1/2r_o$	$1/4r_o^2$
Body-centered cubic	0.320	$\sqrt{3}/2r_o$	$3/16r_o^2$
Face-centered cubic	0.260	$\sqrt{6}/4r_o$	$\sqrt{3}/6r_o^2$
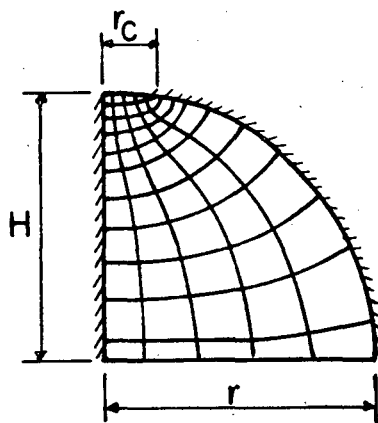
Fig. 21 Curvilinear square
network for a
spherical element
with circular con-
tacts
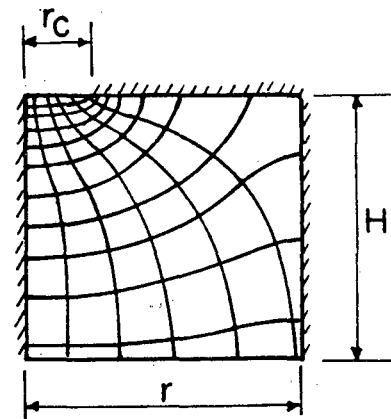
Fig. 22 Curvilinear square
network for a cy-
lindrical element
with circular con-
tacts

$$F_{thermal} = \frac{\lambda_s}{\lambda_{e0}} = (\frac{N_t}{N_a} \cdot S_j \cdot S_r)(\frac{0.64}{r_c}) \quad , \qquad (2\text{-}8\text{-}4)$$

where N_t and N_a are the number of particles per unit length and per unit area, respectively, and are presented in Table (1) for the three regular packing patterns, r_c is the radius of the circular contact area, S_j a packing parameter which is equal to 1, 1/4, 1/3 for simple cubic, body-centered cubic and face-centered cubic, respectively, and finally S_r a parameter which depends on the ratio of the radius of the contact r_c to the radius of spherical grain r_0, its numerical values given as:

$\frac{r_c}{r_0}$	0.001	0.002	0.004	0.006	0.008	0.010
S_r	0.8252	0.8193	0.8207	0.8334	0.8280	0.8331

Because of the assumption that the contact areas are not very large, the application of Equa. (2-8-4) is limited to small values of r_c/r_0. In fact Chan and Tien suggest that the ratio of r_c/r_0 should be smaller than 0.10. For larger values of r_c/r_0, the analytical solution of the conduction equation for the propagation of heat through the solid phase of the foregoing packed beds becomes rather difficult. Therefore, approximation methods are usually used to obtain the effective thermal conductivity of such systems.

Kaganer [34] used the method of curvilinear squares to determine the thermal resistance of a single spherical particle, which has uniform temperatures on the two diametrically opposite contact patches, while the rest of its surface is insulated. For a particular case of $r_c/r_0 = 0.2$, for which in Fig. 21 a network of isotherms and constant flow paths are shown on the cross-section of a quarter sphere Kaganer

calculated the thermal resistance of the whole spherical grain as:

$$R_T = \frac{0.55}{r_c \lambda_s} \quad , \quad r_c/r_0 = 0.2 \; . \qquad (2-8-5)$$

The thermal resistance given by Eq. (2-8-5) can be used to evaluate the thermal formation resistivity factor of a normal cubic packing arrangement of uniform spheres which are just flattened at their top and bottom contacts as follows:

$$F_{thermal} = \frac{\lambda_s}{\lambda_{e0}} = \frac{\lambda_s}{\frac{L}{A} \cdot \frac{1}{R_T}} = \frac{\lambda_s}{\frac{2(r_0^2 - r_c^2)^{\frac{1}{2}}}{4r_o^2} (\frac{r_c \lambda_s}{0.55})} = 5.61 \quad , \qquad (2-8-6)$$

$$\frac{r_c}{r_0} = 0.2 \quad , \quad \phi = 0.466 \quad .$$

Note that for the same packing, a ratio of $\frac{r_c}{r_0} = 0.001$ in Eq. (2-8-4) yields:

$$F_{thermal} = \frac{\lambda_s}{\lambda_{e0}} = 1056 \quad , \qquad (2-8-7)$$

$$\frac{r_c}{r_0} = 0.001 \quad , \quad \phi = 0.47 \quad .$$

In connection with porous rocks, it is very interesting to observe that the unconsolidated aggregates of rock grains usually have thermal formation resistivity factors in the range of the values given by Eq. (2-8-4) for very small ratios of $\frac{r_c}{r_0}$, while systems of consolidated rocks possess much lower values of $F_{thermal}$ which are of the order of the numerical value of this parameter given by Eq. (2-8-6). These can be seen from the experimental investigations of Woodside and Messmer [15,35], who measured the effective thermal conductivity in vacuum of three quartz sand packs and five consolidated sandstones. The three unconsolidated sand packs which had

porosities of 19, 36 and 59 percent possessed values of 645 and

higher for the thermal formation resistivity factor, while values of

this parameter for the five consolidated sandstones with porosities

ranging from 3 to 29 percent ranged between 3 to 5.

The foregoing discussion about the thermal formation resistivity

factor of some regularly packed spheres and their comparison with

the experimentally obtained values of this parameter for the porous

rocks show that once a reasonable model is proposed to represent the

latter, the thermal formation resistivity factor can be used to

establish a relation between the relative size of the grain-to-grain

contacts, although this task might be difficult. For example, in

the original model of normal cubic-packed spheres, flattened at their

points of contact, this can be written as:

$$F_{thermal} = \frac{\lambda_s}{\lambda_{e0}} = f \; (\rho_1 = \frac{r_{c1}}{r_0} \;, \; \rho_2 = \frac{r_{c2}}{r_0}) \cdot \qquad (2\text{-}8\text{-}8)$$

Recalling that the porosity of this system can also provide another

relation between ρ_1 and ρ_2 which is indeed independent of an equation

such as (2-8-8), one can conclude that the porosity and the thermal

formation resistivity factor of a porous rock together will furnish

the necessary equations needed to fix the geometry of the model

representing it.

To find how the thermal formation resistivity factor of the

proposed model depends on the dimensionless radii ρ_1 and ρ_2, efforts

should be made to find the thermal resistance of a single solid

grain which has uniform temperature on top and bottom flattenings,

while the rest of its surface, including the lateral flattenings,

is insulated. As stated before, because of the complex geometry of

such a unit, an exact analytical solution to the problem is difficult.

On the other hand one might think of this situation as a limiting

case of the single-fluid saturated model when λ_f tends to zero.

Therefore, the knowledge developed in the earlier sections of this

chapter can be used to provide an approximate solution of the problem.

However, the limiting case for which thermal conductivity of the

fluid is zero should be examined carefully. Setting $\lambda_f = 0$ in the

finite difference treatment of the problem also makes the thermal con-

ductance of some elements connecting the nodal points equal to

zero, and provides a difficulty for the iterative method of solution

of the system of difference equations. This problem can be overcome

either by choosing a finite but very small value for λ_f, or by some

modification of the solution procedures to avoid the iteration for

the nodes which are surrounded by the elements having zero thermal

conductance. Both alternatives were examined, and as one would

expect, the values of $F_{thermal} = \dfrac{\lambda_s}{\lambda_{e0}}$ obtained by each treatment were

almost the same.

It is important to note that equating λ_f to zero eliminates

the passage of any heat through region II, and makes the effective

thermal conductivity of the model and that of region I equal. Thus,

instead of the former case, attention could be focused on the latter.

The propagation of heat through the solid phase of region I is very

similar to the propagation of heat through a cylindrical element

which has uniform temperature on one base, a circular patch of

another uniform temperature on the other base, and insulation on

the rest of its surface, as shown in Fig. 22. Therefore, it would

be appropriate to assume that the thermal resistance of this element

and that of the solid part of region I are equal, if both possess the same dimensions. Veziroglu [36] gives a closed form solution for the thermal resistance of the above cylindrical element, which can be written as follows:

$$R_T = \frac{\tan^{-1}(\frac{r}{r_c} - 1)}{2\pi r_c \lambda_s} + \frac{H}{\pi r^2 \lambda_s} \quad , \qquad (2\text{-}8\text{-}9)$$

where r and H are the radius and the height of the cylinder, and r_c is the radius of the circular patch on one of the bases. Using Eq. (2-8-9) for the thermal resistance of the solid grain in region I, one can obtain its thermal formation resistivity factor as:

$$F_{thermal} = \frac{\lambda_s}{\lambda_{e0}} = \frac{\lambda_s}{\frac{L}{A} \cdot \frac{1}{R_T}} = \frac{4}{\pi}\left\{1 + \frac{(1 - \rho_1^2)}{2\rho_2(1 - \rho_2^2)^{\frac{1}{2}}} \tan^{-1}\left[(\frac{1 - \rho_1^2}{\rho_2^2})^{\frac{1}{2}} - 1\right]\right\}, (2\text{-}8\text{-}10)$$

$$\rho_1 = \frac{r_{c1}}{r_0} \quad , \quad \rho_2 = \frac{r_{c2}}{r_0} \quad .$$

Notice that for $\rho_1 = 0$ and $\rho_2 = 0.2$ the original model is similar to the one examined by Kaganer. Therefore, a comparison can be made between Eq. (2-8-10), Kaganer's graphical approach, and the present finite difference treatment of the problem. The results are given as follows:

Graphical approach	Eq. (2-8-10)	Finite difference technique
$\frac{\lambda_s}{\lambda_{e0}} = 5.61$	$\frac{\lambda_s}{\lambda_{e0}} = 5.58$	$\frac{\lambda_s}{\lambda_e} = 5.80$

The above figures show that the thermal formation resistivity factor of the present model with $\rho_1 = 0$ and $\rho_2 = 0.2$, calculated by finite difference technique, is only 4% higher than the value of this parameter as determined from Eq. (2-8-10). For cases in which $\rho_1 > 0$,

this difference was found to be even smaller. Thus, Eq. (2-8-10) is indeed a good representation of the present numerical work when $\lambda_f = 0$, and can serve as a second equation in conjunction with the equation for porosity to obtain the relative size of the contacts. In Fig. 23 curves of constant porosity and constant thermal formation resistivity factor are plotted, using Eqs. (2-2-3) and (2-8-10). Knowledge of these two parameters for a porous system defines a pair of these curves, the intersection of which gives the appropriate choice of ρ_1 and ρ_2 for that system.

Although the thermal formation resistivity factor of porous rocks can be used for estimation of average relative size of the grain-to-grain contacts, its knowledge requires laboratory measurement of effective thermal conductivity of the porous rock in vacuum. Therefore, a measurement which in nature is similar to the measurement of effective thermal conductivity cannot be avoided. Another point which should be noted is that the experimental value of the effective thermal conductivity of a porous rock in vacuum contains not only information about the size of the grain-to-grain contacts, but it also embodies information about the thermal contact resistance which exists between the areas of contact. Thus by using the experimental value of λ_{eo} in Eq. (2-8-10), which does not consider any thermal contact resistance, one would underestimate r_{c2}.

As stated before, there exists another physical property of the porous rocks, namely, electrical formation resistivity factor, which is also a representation of the geometry of the pores. Because the electrical formation resistivity factor is easy to measure and does not include any contact resistance contribution, it would be
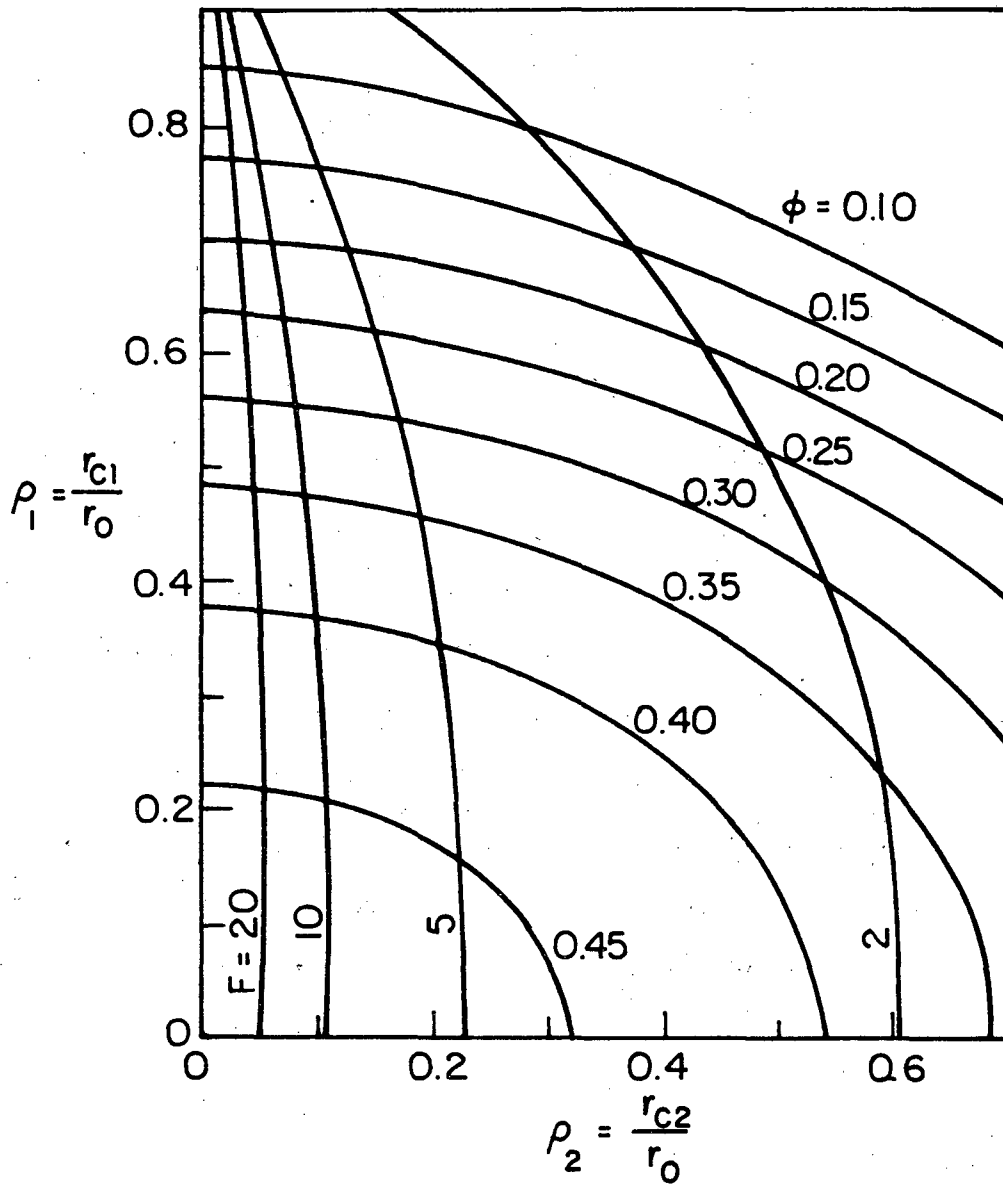
Fig. 23 Curves of constant porosities and constant
thermal formation resistivity factors

a logical substitute for its thermal counterpart. Therefore, it remains to be found an expression which relates the electrical formation resistivity factor to the geometrical parameters of porous rocks. Many attempts have been made to find such an expression, both analytically and experimentally, among which only the following empirical formula proposed by Archie [37] has survived the test of usefulness.

$$F_{electrical} = \frac{1}{\phi^m} \quad , \qquad (2-8-11)$$

where ϕ is porosity, and m a constant called "cementation factor" which depends on the degree of consolidation of the rock. The numerical values of the cementation factor m, given by Archie, are indicated in the following table.

Rock Description	Cementation Factor
Unconsolidated rocks	1.3
Very slightly consolidated	1.4 - 1.5
Slightly cemented (porosities of 0.20 or more)	1.6 - 1.7
Moderately cemented (highly consolidated rocks of 0.15 porosity or less)	1.8 - 1.9
Highly cemented (very low porosity rocks)	2.0 - 2.2

To obtain the electrical formation resistivity factor for the existing model, the Laplace equation for conduction of electricity should be solved in the pore region. The electric potential distribution in the pore space is in general a three-dimensional field, which thus makes the calculation of the electrical formation resistivity factor difficult. One might think that setting $\lambda_s = 0$ in the existing computer program, which calculates the effective thermal conductivity, would provide the solution to this new problem. However, this is not

the case, since it should be noted that in the region of the elementary cell at $z = r_{cl}$ (Fig.10), there is no area available for the flow of electricity. Therefore, this region will have an infinite resistance and make no contribution to the electrical conductance.

Under the assumption of unidirectional flow of electricity through the pore space, approximate values of the electrical formation resistivity factor of the model can be calculated by a simple integration. Referring to Fig. 8, the flow of electricity I passing through any cross-section of the pore volume perpendicular to the Z axis is

$$I = \gamma_f \, A \, \frac{dV}{dz} \quad , \qquad (2\text{-}8\text{-}2)$$

where

γ_f = electrical conductivity of the electrolyte in the pore,

A = cross-sectional area of the pore space perpendicular to the

Z axis,

dV = voltage drop across length dz.

To obtain the total voltage drop ΔV across the elementary cell, Equa. (2-8-12) is integrated as:

$$\Delta V = \int_0^{(r_0^2 - r_{c_2}^2)^{\frac{1}{2}}} \frac{I}{\gamma_f} \frac{dz}{A} = \frac{I}{\gamma_f} \int_0^{(r_0^2 - r_{c2}^2)^{\frac{1}{2}}} \frac{dz}{A} \quad . \qquad (2\text{-}8\text{-}13)$$

The area A in Eq. (2-8-13) can be expressed as a function of r_0, r_{cl}, r_{c2} and z as follows:

$$A(z) = A_1(z) = (r_0^2 - r_{cl}^2) - (r_0^2 - r_{cl}^2)^{\frac{1}{2}} (r_{cl}^2 - z^2)^{\frac{1}{2}} - \frac{1}{2} (r_0^2 - z^2) \left[\frac{\pi}{2} - 2 \cos^{-1} \left(\frac{r_0^2 - r_{cl}^2}{r_0^2 - z^2} \right)^{\frac{1}{2}} \right] , \quad \text{for } 0 < z < r_{cl} \quad ,$$

$$A(z) = A_2(z) = (r_0^2 - r_{c1}^2) - \frac{\pi}{4}(r_0^2 - z^2) \quad , \quad \text{for } r_{c1} < z < (r_0^2 - r_{c2}^2)^{\frac{1}{2}} \quad .$$

Therefore Eq. (2-8-13) becomes:

$$\frac{(\Delta V)\gamma_f}{I} = \int_0^{r_{c1}} \frac{dz}{A_1(z)} + \int_{r_{c1}}^{(r_0^2 - r_{c2}^2)^{\frac{1}{2}}} \frac{dz}{(r_0^2 - r_{c1}^2) - \frac{\pi}{4}(r_0^2 - z^2)} \quad .$$

$$(2\text{-}8\text{-}14)$$

The first integral on the right hand side of Eq. (2-8-14) should be calculated numerically, but the second integral has a closed form value as:

$$\int_{r_{c1}}^{(r_0^2 - r_{c2}^2)^{\frac{1}{2}}} \frac{dz}{A_2(z)} = f_1(\rho_1, \rho_2) \quad , \quad \rho_1 = \frac{r_{c1}}{r_0} \quad , \quad \rho_2 = \frac{r_{c2}}{r_0} \quad ,$$

where:

$$f_1(\rho_1, \rho_2) = \frac{2a}{\sqrt{\pi}} \left(\tan^{-1} \frac{b}{a} - \tan^{-1} \frac{c}{a} \right) \quad \text{for } \rho_1^2 < 1 - \frac{\pi}{4} \quad ,$$

$$f_1(\rho_1, \rho_2) = \frac{a}{\sqrt{\pi}} \ln \left[\frac{(b - a)(c + a)}{(b + a)(c - a)} \right] \quad \text{for } \rho_1^2 > 1 - \frac{\pi}{4} \quad .$$

where $a = \left[(1 - \rho_1^2) - \frac{\pi}{4} \right]^{\frac{1}{2}}$, $b = \frac{\sqrt{\pi}}{2}(1 - \rho_2^2)^{\frac{1}{2}}$, $c = \frac{\rho_1 \sqrt{\pi}}{2}$.

The electrical formation resistivity factor is defined as:

$$F_{electrial} = \frac{I_0}{I} \quad , \tag{2-8-15}$$

where I_0 is the total flow of electricity passing through the elementary cell, when it consists of a single phase of conductivity γ_f. I_0 may be written as:

$$I_0 = \frac{\gamma_f (r_0^2 - r_{c1}^2)(\Delta V)}{(r_0^2 - r_{c2}^2)^{\frac{1}{2}}} \quad . \tag{2-8-16}$$

Substituting I_0 from Eq. (2-8-16) and ΔV from Eq. (2-8-14) into Eq. (2-8-15) yields:

$$F_{electrical} = \frac{f_0(\rho_1, \rho_2)}{\left[f_1(\rho_1,\rho_2) + f_2(\rho_1)\right]^{-1}} \quad , \qquad (2\text{-}8\text{-}17)$$

where $\quad f_0(\rho_1,\rho_2) = \dfrac{1 - \rho_1^2}{(1 - \rho_2^2)^{\frac{1}{2}}} \quad , \quad f_2(\rho_1) = \dfrac{1}{r_0}\displaystyle\int_0^{r_{cl}} \dfrac{dz}{A_1(z)} \quad .$

Using Eq. (2-8-17), $F_{electrial}$ was calculated for different pairs of ρ_1 and ρ_2, which correspond to a fixed value of porosity. Figure 24 represents the results of such calculations and gives $F_{electrical}$ as a function of ρ_2, for different porosities.

For $\rho_1 = \rho_2 = 0$ ($\phi = 0.476$), Eq. (2-8-17) gives $F_{electrical}$ = 2.65, which is the smallest electrical formation resistivity factor that one would obtain for the model with unidirectional assumption of electricity flow through the pores. It is also important to note that for $\rho_1 \geqslant 0.707$, where the contact areas on the sides touch each other, the pores are no longer connected in the Z direction. Therefore, the electrical formation resistivity factor of the model in the Z direction will be infinity for $\rho_1 \geqslant 0.707$. The porosity of the model for $\rho_1 = 0.707$ and $\rho_2 = 0$ is 19 percent. Thus in order to maintain the electrical formation resistivity factor finite for low porosities, ρ_1 must be kept below the critical value of 0.707. In such cases ρ_2 becomes the significant parameter for controlling the porosity.

For unconsolidated sands with porosities ranging from 30 to 45 percent Kesse [38] reports that the experimentally measured values of the electrical formation resistivity factor range from 6 to 3. Kesse's
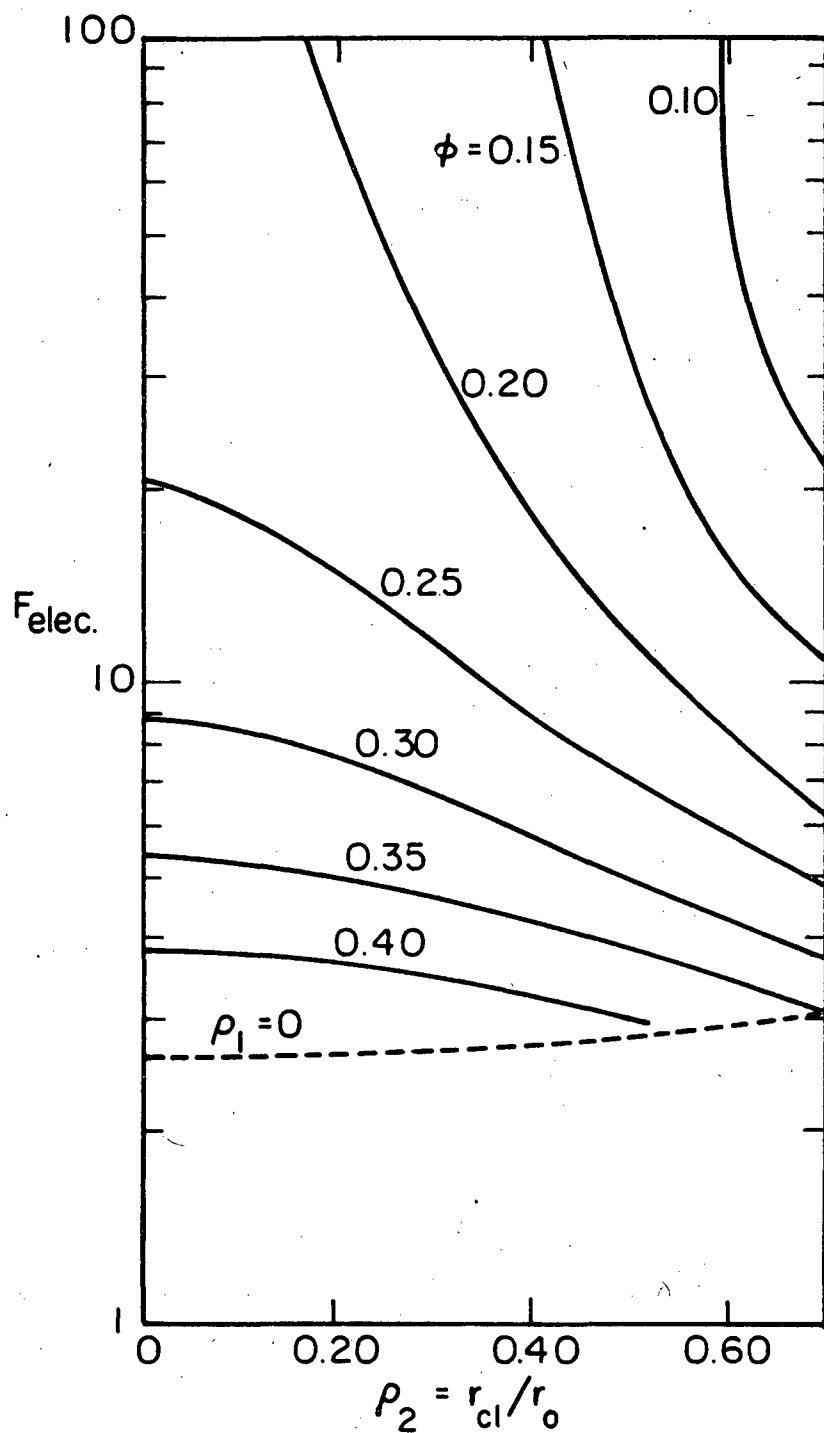
Fig. 24 Electrical formation resistivity factor
of the model as a function of dimension-
less radius of top-bottom contacts, for
different porosities

experimental values for $F_{electrical}$ were compared with the values of this parameter given by Eq. (2-8-17), for $\rho_2 = 0$. Except for a few sands with porosities between 37 to 45 percent, the predicted values of $F_{electrical}$ from Eq. (2-8-17) were much higher than the experimental values. This would be expected, since for $\rho_2 = 0$ or even for small values of ρ_2, the electricity flow lines passing through the pores are so distorted that a unidirectional treatment of the problem would not be realistic. A two-or three-dimensional solution to this problem would result in an increase in electricity flow and consequently a smaller electrical formation resistivity factor. On the other hand as ρ_2 increases, pore channels in the model become less convergent-divergent, and therefore the assumption that the flow lines are parallel becomes relatively valid.

To conclude the discussion on the relative size of the grain-to-grain contacts, a very small value of ρ_2 ($\rho_2 < 0.1$) should be used for unconsolidated sands. In fact $\rho_2 = 0$ will be satisfactory for most unconsolidated sands. For consolidated sandstones, knowing their porosity and electrical formation resistivity factor, Fig. 24 can be used for estimating ρ_2. It should be noted that Fig. 24 in general might overestimate ρ_2.

2-9 Results

A computer program written in FORTRAN IV was developed to calculate the effective thermal conductivity from the model based on the earlier theoretical considerations. The features of this program are given in detail in Appendix D.

The parameters necessary to calculate the effective thermal conductivity λ_e of the model are porosity, ϕ, dimensionless radius

of the top-bottom contacts, ρ_2, saturation of the wetting phase, S_w, thermal conductivity of the rock matrix, λ_s, thermal conductivity of the wetting phase, λ_f, and thermal conductivity of the non-wetting phase, λ_{nw}. However, the dimensionless effective thermal conductivity defined as λ_e/λ_f (or λ_e/λ_s) depends only on five dimensionless parameters, ϕ, ρ_2, S_w, λ_s/λ_f and λ_s/λ_{nw}. Therefore, keeping any four of these parameters constant, the effects of the remaining variable can be studied on λ_e/λ_f. Such a study was made and the final results are presented in form of graphs in Figs. 25 through 30.

Figures 25 through 28 show the effect of λ_s/λ_f on λ_e/λ_f for single fluid saturated systems. Figures 25 and 26 are plotted for $\rho_2 = 0$ and $\rho_2 = 0.05$, respectively, and porosities ranging from 30 to 45 percent. These graphs are suitable for unconsolidated sands. Figures 27 and 28 are for $\rho_2 = 0.2$ and $\rho_2 = 0.3$ respectively and both cover porosities in the range of 30 to 10 percent. Thus they are useful for consolidated rocks. Figures 29 and 30 are plotted for two-fluid saturated unconsolidated and consolidated systems, respectively, with $\lambda_s/\lambda_w = 10$ (a typical value for cases in which grains are quartz and the wetting phase is water). They show the effect of S_w on λ_e/λ_s for two different values of λ_s/λ_{nw}, namely 50 (solid curves) and 200 (broken curves), which are typical for the systems with $\lambda_s/\lambda_f = 10$ and with oil and air the non-wetting phase, respectively.

Examination of Figs. 25 through 28 shows that, for a fixed porosity, λ_s/λ_f increases with increasing ρ_2. This increase is very small when $\lambda_s/\lambda_f < 10$, but becomes significant for large values of λ_s/λ_f. This would be expected since increasing the size of the

grain-to-grain contacts in the direction of heat flow enhances the heat transfer and consequently increases the effective thermal conductivity. However, this increase would not be appreciable when λ_f is not very different from λ_s. As it can be seen from Figs. 25-28, keeping ρ_2 constant, λ_e/λ_f increases with decreasing porosity. This is a logical trend, since the lower the porosity, the higher would be the volume of the solid grains which have a higher thermal conductivity than the fluid filling the pores, and therefore the higher would be the effective thermal conductivity. These figures also show that the rate of change of λ_e/λ_f with ϕ is very small for small values of λ_s/λ_f, but more noticeable in the region of high λ_s/λ_f.

As it appears in Figs. 29 and 30, the effective thermal conductivity of the model increases with increasing S_w. This increase is greater when porosity is higher. The effect of thermal conductivity of the non-wetting phase can also be seen in Figs. 29 and 30. As one would expect, the higher the thermal conductivity of the non-wetting phase, the higher would be the effective thermal conductivity. However, this effect is not very strong at high wetting fluid saturations.
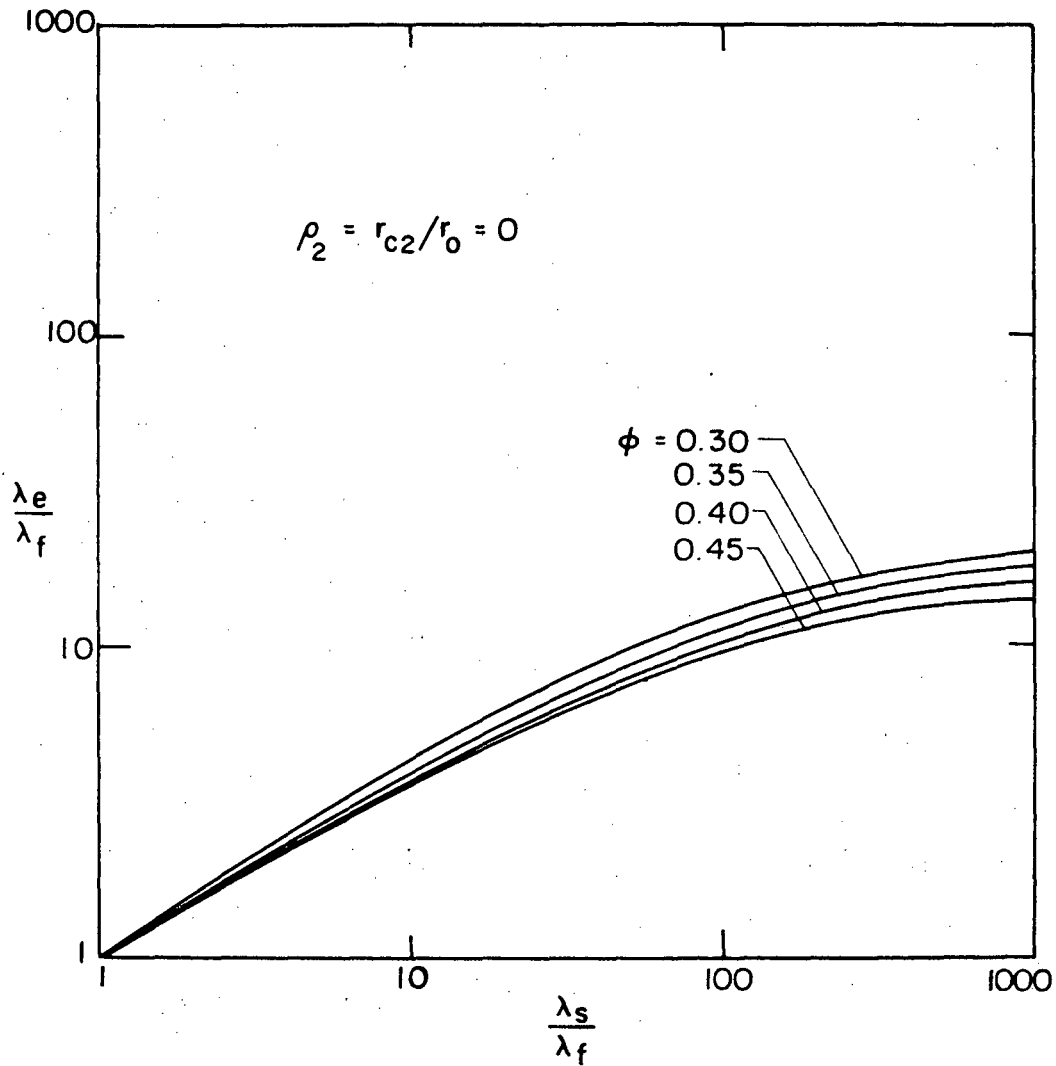
Fig. 25 Dependence of λ_e/λ_f on λ_s/λ_f, predicted by model for $\rho_2=0$ and porosities in the range of unconsolidated sands
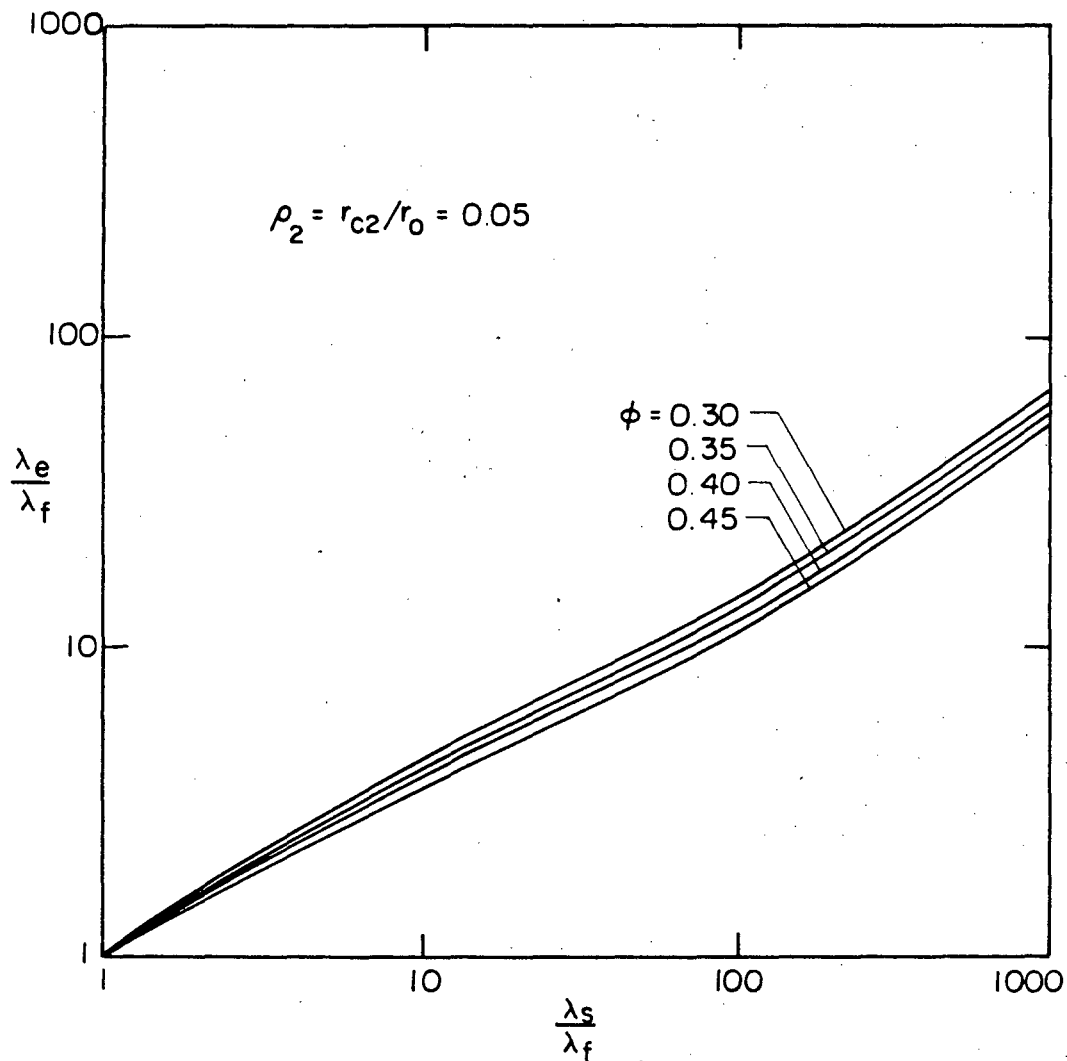
Fig. 26 Dependence of λ_e/λ_f on λ_s/λ_f, predicted by model for ρ_2=0.05 and porosities in the range of uncon- solidated sands
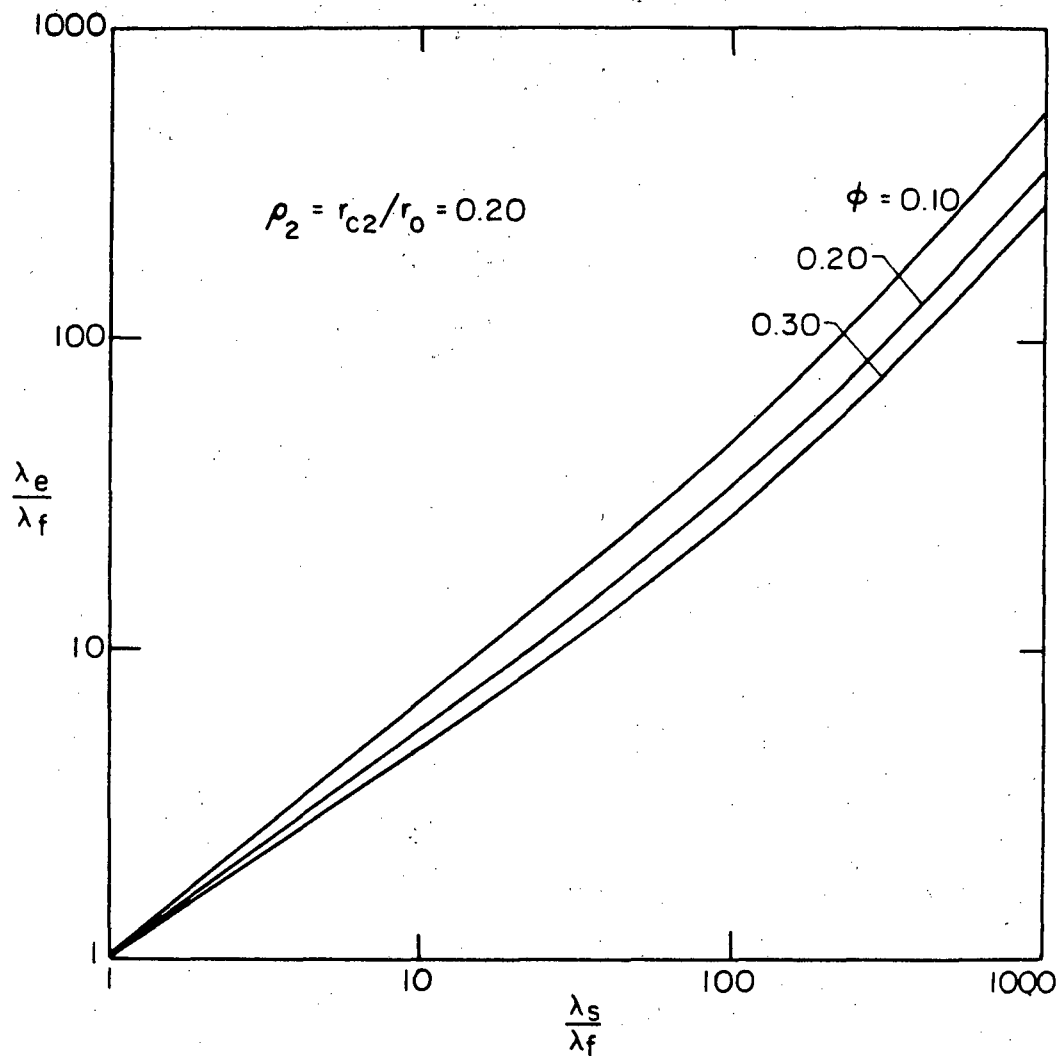
Fig. 27 Dependence of λ_e/λ_f on λ_s/λ_f, predicted by model for $\rho_2=0.20$ and porosities in the range of consolidated rocks
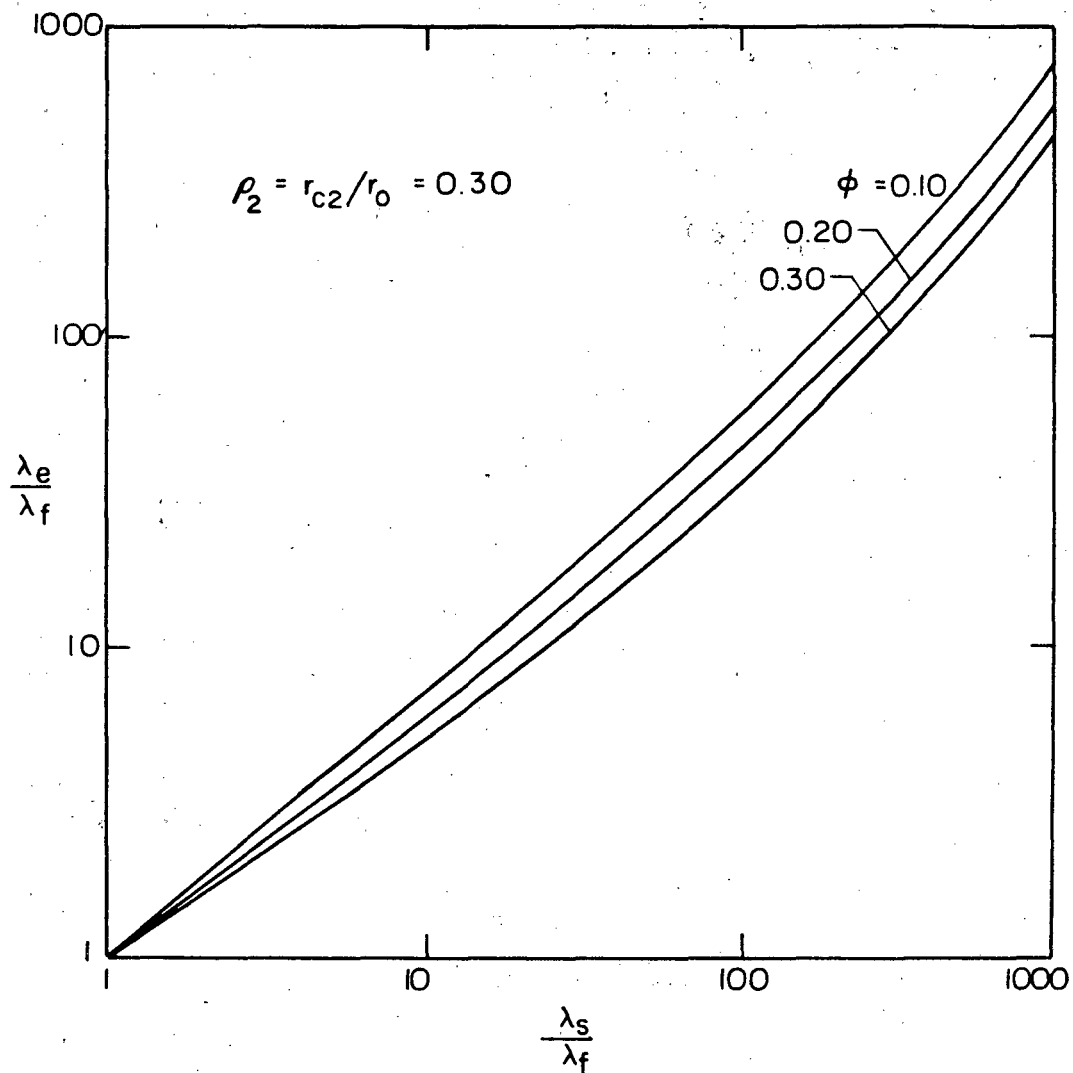
Fig. 28. Dependence of λ_e/λ_f on λ_s/λ_f, predicted by model for $\rho_2 = 0.30$ and porosities in the range of consolidated rocks
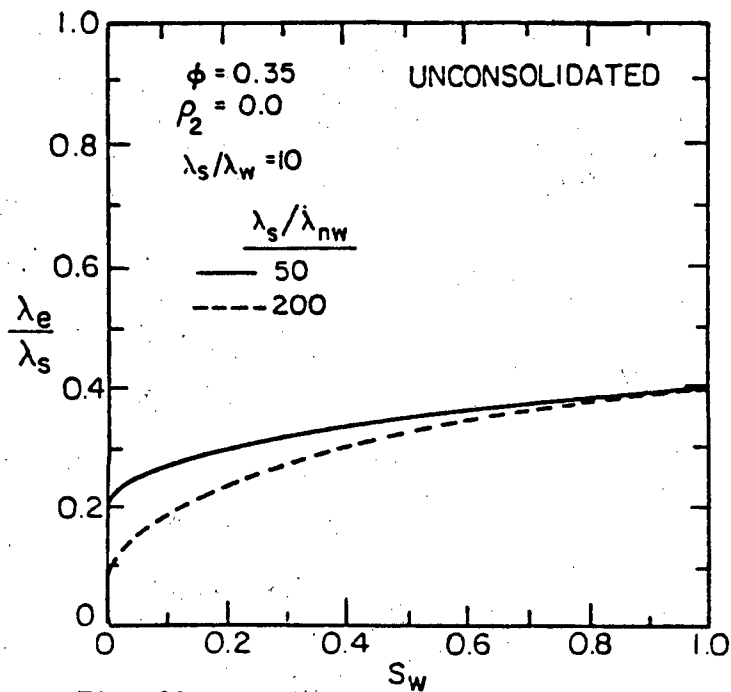
Fig. 29 Dependence of λ_e/λ_s on S_w predicted by model
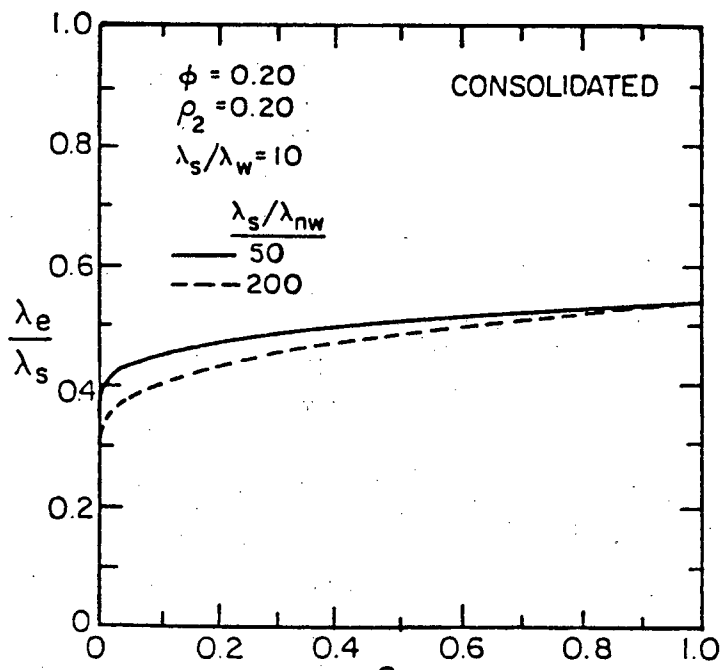
Fig. 30 Dependence of λ_e/λ_s on S_w , predicted by model

CHAPTER 3

COMPARISON OF MODEL RESULTS WITH EXPERIMENTAL DATA

The effective thermal conductivities of four consolidated sand-

stones and one unconsolidated sand pack were calculated by use of the

model for the cases in which the pore channels are filled with brine-air

or brine-decane mixtures, and results are compared with the existing

experimental data. Three of the consolidated samples are Boise, Berea,

and Bandera sandstones, the thermal conductivity of which were experi-

mentally measured by Ozbek [13] and Gomaa [23]. The fourth consolidated

sample is a low porosity, high quartz content sandstone, selected from a

group of cores which were sent to the Petroleum Engineering Laboratories

of the University of California at Berkeley for measurement of their

thermal conductivities. The unconsolidated sand pack consists of Ottawa

sand grains. The effective thermal conductivity of Ottawa sand pack was

measured by both Ozbek and Gomaa.

3-1   Collection of Data For Analysis

The porosities and electrical formation resistivity factors for

Boise, Berea, Bandera and the Ottawa sand pack determined by Gomaa and

Ozbek are given in Table 2. It should be noted that since the electrical

formation resistivity factors of the samples tested by Ozbek were not

reported, the values given in Table 2 for Ozbek's cores were estimated as

follows. The values of porosity and electrical formation resistivity

factor determined by Gomaa were used in Archie's formula, i.e. Eq.

(2-8-11), to obtain the cementation factor for each sample. These

cementation factors, together with the porosities determined by Ozbek,

were substituted back into Eq. (2-8-11) to calculate the electrical

formation resistivity factors. For the low porosity core, the porosity

and electrical formation resistivity factor were measured by Sahnine [39] and are given in Table 2.

Knowing the porosity and the electrical formation resistivity factor, the dimensionless radii of top-bottom contacts, ρ_2, were estimated from Fig. 22. The results are given in Table 2.

The thermal conductivity of the solid matrix and the fluids filling the pores are needed for prediction of the effective thermal conductivity. The solid matrix of the rocks is usually composed of many different minerals. Therefore, its overall thermal conductivity is a function of the volume fraction and the thermal conductivity of each individual mineral. Among the minerals making up the solid matrix of Boise, Berea, and Bandera sandstones, quartz, calcite and feldspar predominate. Clark [40], Somerton [41], Ozbek [13] and Greenwald [42] have reported mineral analysis for Boise, Berea, and Bandera sandstones. From their analysis, the volumetric quartz, calcite, and feldspar contents are given in Table 3. As it appears from this Table, there are inconsistencies between the mineral contents reported by the above authors. The fact that the mineral content may vary within a sample, or from one sample to another (for the same rock), could possibly be responsible for these differences. The low porosity consolidated core belongs to a group of samples for which the quartz contents were reported to be between 80 to 90 percent. Therefore, an average quartz content of 85% was chosen for this sample. The solid grains of unconsolidated Ottawa sand packs are pure quartz.

Table 2 Porosity, electrical formation resistivity factor and dimen-
sionless radius of top-bottom contacts for the samples
tested.

Ref.	Sample	ϕ	$F_{ele.}$	ρ_2
	Boise	0.290	7.90	0.251
[23]	Berea	0.220	14.00	0.365
	Bandera	0.200	14.00	0.451
	Ottawa sand pack	0.355	4.20	0.472
	Boise	0.290	7.90	0.251
[13]	Berea	0.230	12.95	0.360
	Bandera	0.225	11.55	0.410
	Ottawa sand pack	0.360	3.82	0.435
[39]	Low porosity sandstone	0.097	21.90	0.700

Table 3 Quartz, calcite and feldspar content of Boise, Berea and
Bandera sandstones (volumetric percentage).

Ref.	Sample	quartz	calcite	feldspar
	Boise	45.0	neg.	45.0
[40]	Berea	85.0	1.0	5.0
	Bandera	60.0	13.0	20.0
	Boise	33.7	neg.	53.0
[13]	Berea	74.8	3.5	9.1
	Bandera	37.7	32.3	10.6
	Boise	38.7	neg.	39.8
[41]	Berea	67.8	9.4	3.0
	Bandera	55.5	16.6	3.8
	Boise	64.0	neg.	36.0
[42]	Berea	88.0	5.0	7.0
	Bandera	70.0	21.0	9.0

Ki-iti Horai [43] has determined thermal conductivity of 166 rock-forming minerals, of which the important ones are given in Table 4. This table shows that quartz has significantly larger thermal conductivity than the other minerals. Since quartz is the predominant mineral in most sandstones, knowledge of its thermal conductivity at different temperatures would be important for calculation of the overall rock solid thermal conductivity. For a single quartz crystal, depending on whether the direction of heat flow is parallel or perpendicular to the major axis of the crystal, the thermal conductivity would have its maximum and minimum value, respectively. The National Bureau of Standards [44] has given these maximum and minimum values of thermal conductivity as a function of temperature in the form of curves, which are reproduced in Fig. 31. However, because of the probable random orientation of the quartz crystals in the rocks, the direction of heat flow would not necessarily be parallel or perpendicular to the major axis of the crystal. Therefore, neither curve for the maximum or minimum conductivities in Fig. 31 can be used. An intermediate curve was constructed (Fig. 31) based on geometric averaging of the maximum and the minimum conductivity curves (weighted equally). This curve is considered appropriate for obtaining the thermal conductivity of quartz as a function of temperature. It is interesting to note that the value of thermal conductivity obtained from the intermediate curve in Fig. 31 is only 4% higher than the value given by Horai [43] in Table 4.

Even though the volume fraction and thermal conductivity of each mineral is known, the problem still remains to decide on the method of calculation of the overall thermal conductivity of the rock. In this regard one can simply apply the idea of weighted arithmetic, weighted

harmonic, or weighted geometric mean calculations (Eqs. (1-2-14)-

(1-2-16)), to obtain an overall thermal conductivity. Since the weighted

geometric averaging provides an intermediate total thermal conductivity,

it was used for calculation of the overall thermal conductivity of the

rock solids. Table 5 shows the results of such calculations for Boise,

Berea, Bandera, and the low porosity sandstones based on mineral analysis

of Clark and Ozbek. In preparation of this table, the thermal conduc-

tivity of the quartz mineral at the test temperature for each sample was

obtained from Fig. 31 (using the intermediate curve), and the thermal

conductivities of the remaining minerals were assumed to be 3.0 W/m-K.

The saturating fluids used are brine, decane, and air. The

thermal conductivity of brine and decane were taken to be those of water

and light oil. Kreith [45] has reported thermal conductivities of air,

water, and light oil at different temperatures. Using his reported

values, Fig. 32 is prepared which gives thermal conductivities of the

above fluids as a function of temperature.

3-2 Comparison of Results

Figures 33 through 41 show the comparison between predicted

values of the effective thermal conductivity λ_e by use of the model,

and their experimental counterparts. Since four sets of mineral analyses

with different values of quartz content were available for Boise, Berea,

and Bandera sandstones, the predicted values of λ_e for each sample

were calculated by using at least two different mineral analyses, i.e.

those reported by Clark and Ozbek.

Figures 33, 34 and 35 show the predicted curves of effective

thermal conductivities, λ_e, and the experimental values of Ozbek for

Boise, Berea, and Bandera sandstones, respectively, partially saturated

Table 4 Thermal conductivities of some rock-forming
minerals at temperature of 23°C, Horai [43]

Mineral	Chemical composition	Thermal conduc. W/m-K
Quartz	SiO_2	7.70
Plagioclase	$NaAl_2Si_3O_8-CaAlSi_3O_8$	2.15
Orthoclase	$K\ Al_2Si_3O_8$	2.30
Muscovite	$(K,Na)Al_2(OH)_2(AlSi_3O_{10})$	2.20
Calcite	$CaCO_3$	3.60
Chlorite	$(Mg,Fe,Al)_6(OH)_8[(Al,Si)_4O_{10}]$	4.34
Biotite	$K(Mg,Fe)_3(OH)_2(Al,Si_3O_{10})$	2.34
Hornblende	$Na\ Ca_2(Mg,Fe,Al)_5(OH)_2(SiAl)_8O_{22}$	3.10
Magnesite	$MgCO_3$	5.85
Epidote	$Ca_2(Al,Fe)_3(OH)(SiO_4)_3$	2.34
Sphene	$Ca\ Si\ Ti\ O_5$	2.34
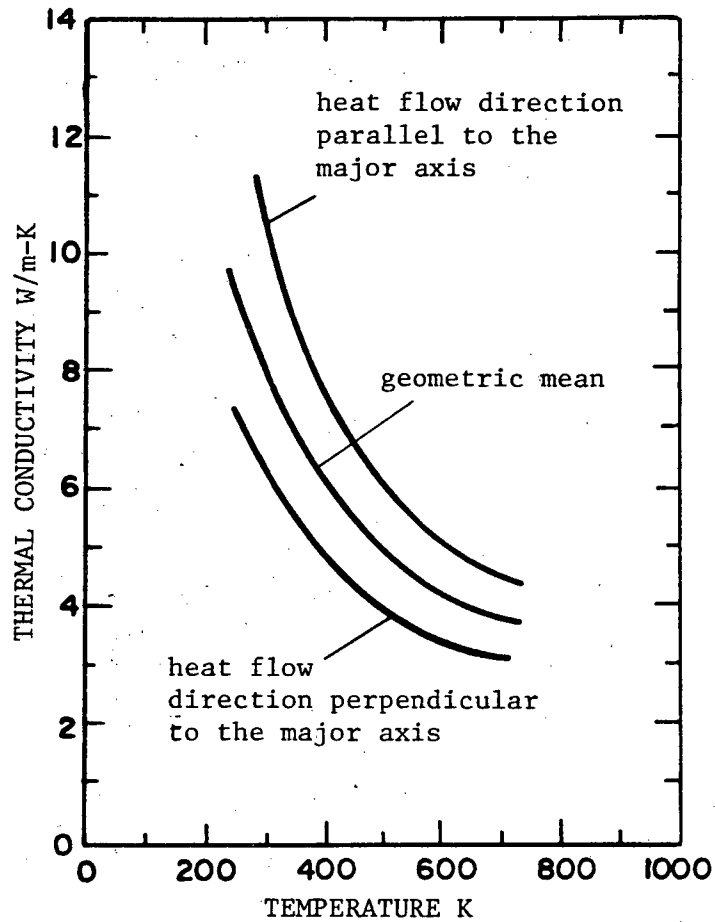
Fig. 31 Recommended thermal conductivity of
quartz for high-purity single crystal
[44]
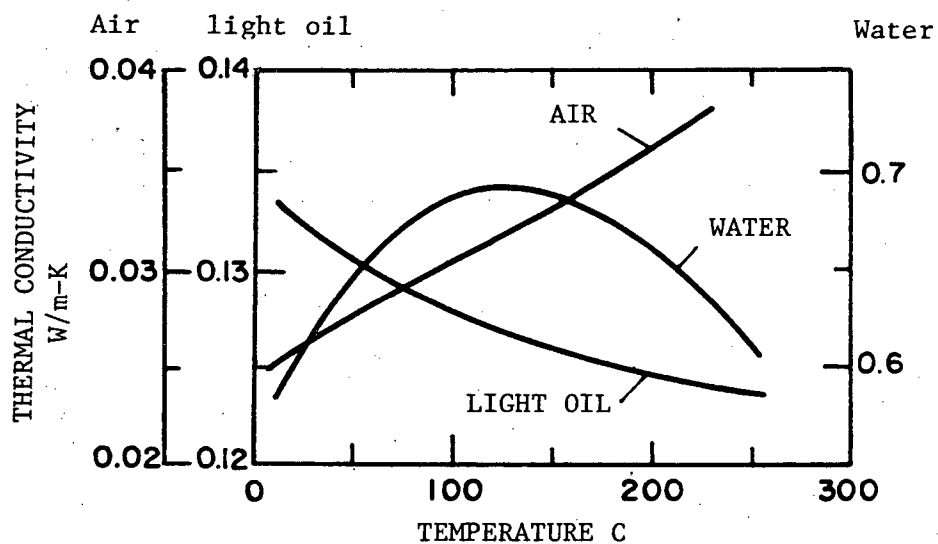
Fig. 32 Thermal conductivities of saturated
water, atmospheric air and light oil
as a function of temperature [45]

87

Table 5 Thermal conductivity of the solid matrix for the
samples tested, based on mineral analysis of Clark [40]
and Ozbek [13]

(W/m-K)

Gomaa's samples

	Boise	Berea	Bandera	Ottawa sand
Test temperature °C	90	58	90	58
mineral analysis of Clark	4.30	6.45	4.85	7.50
mineral analysis of Ozbek	3.90	5.90	4.05	7.50

Ozbek's samples

	Boise	Berea	Bandera	Ottawa sand
Test temperature °C	135	135	135	135
mineral analysis of Clark	4.50	5.40	4.55	6.00
mineral analysis of Ozbek	3.80	5.05	3.90	6.00

Low porosity sample

Test temperature °C	130
Thermal conductivity	5.45

with brine, and with decane as the non-wetting phase. In general the predicted curves based on the higher quartz contents are closer to the experimental values and approximate them with an error of less than $\pm 5\%$ for Boise and Bandera sandstones. In the case of the Berea sample, this error is less than 15%.

In Fig. 36 through 38, the predicted values of λ_e for brine-air saturated Boise, Berea, and Bandera sandstones are compared with the experimental measurements of Gomaa. For Boise sandstone there is good agreement between the experimental values and the predicted values calculated based on the higher quartz content. In the case of Berea sandstone, the calculated values of λ_e by the model based on the higher quartz content agree with the experimental data, with an error less than 15%. The model values are somewhat higher (except the fully air saturated case for which the model calculated values is 16% higher). For Bandera sandstone the experimental values of λ_e lie between the predicted curves for which solid conductivities are 4.85 W/m-K and 4.05 W/m-K. In general except for the air-dry case, the differences between the predicted values and the experimental results are less than $\pm 15\%$. The calculated values of λ_e by model for the air-dry case, with λ_s values of 4.85 W/m-K and 4.05 W/m-K, are 50% and 20% higher than the test value, respectively.

Figure 39 compares the model predicted values of λ_e with the experimental measurements for the brine-air saturated low porosity sandstone. For $0.40 < S_w < 1.0$ the model approximates the experimental data with an error of less than 10% (predicted values are lower). When the sample is fully saturated with air, the effective thermal conductivity given by model is 45% higher than its experimental

counterpart.

Figures 40 and 41 represent the comparison between the calcu-
lated curves of the effective thermal conductivity by use of the model,
and the experimental data for unconsolidated Ottawa sand pack, satur-
ated with brine-decane and brine-air, respectively. When the pore
channels are saturated with brine-decane, except for low values of
brine saturation, there exists good agreement between the predicted
values of λ_e and the experimental measurements of Ozbek. For the
brine-air saturated case, the predicted values of λ_e are higher
than the experimental results of Gomaa.

3-3 Discussion of Results

The foregoing comparisons between predicted values of effective
thermal conductivity, λ_e, by the model and the experimental data,
show that the present model is reasonable for calculation of effective
thermal conductivities of partially liquid saturated sandstones and
unconsolidated sands. The difference between the experimental and the
model values of λ_e for brine-decane or brine-air saturated samples
in most cases is less than $\pm 15\%$. In general it should be noted that
part of these differences could be due to errors both in the experi-
mental data and in some of the input parameters leading to calculation
of the effective thermal conductivity. For example, there is uncer-
tainty regarding the mineral composition, and the effect is shown by
the two calculated curves in Figs. 32-38.

All the experimental data presented in Figs. 32 through 41 were
obtained by the steady state comparative method using the apparatus
described earlier in Chapter 1. It has been shown by Anand [31] that
using such an apparatus could result in an error of the order of $\pm 5\%$

in the value of thermal conductivity calculated from experimental data, based on precision of the measuring equipment. Other larger experimental errors could result from such problems as short or non-parallel test specimens, leaks in the fluid system, incomplete saturation of samples, etc.

Other than experimental errors, uncertainties in the estimation of thermal conductivity of the rock solids also contribute to the differences between the calculated and the experimental values of λ_e as shown earlier. Such uncertainties could arise from incorrect information on the mineral content within the rock, lack of adequate information about the thermal conductivity of minerals at different temperatures, and the fact that the method of calculation of the overall rock solid conductivity from mineral composition is still a questionable matter.

When the pore channels are filled with air, the predicted values of λ_e are generally higher than their experimental counterparts. Since subsurface reservoirs are never fully saturated with a gas, these errors are not considered important. However, this difference could be due to shortcomings in the model itself or possibly a thermal contact resistance between the grains at their area of contact, which is not considered in the model. Such a consideration would indeed result in reduction of the effective thermal conductivity, and consequently improvement of the model. This contact resistance would perhaps not exist, or would be of minor consequences for liquid saturated rocks. This matter is discussed by Ozbek [13].

Estimation of the dimensionless radius of top-bottom contacts, ρ_2, from porosity and the electrical formation resistivity factor,

could also be another source of error in the prediction of effective thermal conductivity by the model. Referring back to the earlier discussion on the calculated values of the electrical formation resistivity factor by the model, one may conclude that Fig. 24 in general overestimates ρ_2, especially when the porosities are of the order of unconsolidated sands. This can be seen very well from the high values of ρ_2 estimated for Ottawa sand, as it appears from Fig. 41. A smaller value of ρ_2 (for example $\rho_2 = 0.10$) would place the predicted values of λ_e much closer to the experimental ones, at least for the brine-air saturated case. Small grain-to-grain contact areas for unconsolidated sand packs could also be justified by the fact that they possess high values of thermal formation resistivity factor, as was discussed earlier in Chapter 2. It should be noted that the precise estimation of ρ_2 does not much affect the effective thermal conductivity when the pores are filled with a good conductor. For example, for fully brine saturated Ottawa sand a $\pm5\%$ diviation from $\rho_2 = 0.10$ would only cause a $\pm3\%$ change in the effective thermal conductivity. However, this change would be of the order of $\pm14\%$ and $\pm32\%$ when the pores are completely filled with decane and air, respectively.

To show that the present work is an improvement over the previous attempts of Gomaa and Ozbek, their models were used to predict the effective thermal conductivity of the tested samples. The λ_s values used were those calculated based on the mineral analysis of Clark. These predicted values, together with calculated values of λ_e by the present model and those measured experimentally, are given in Table 6. As it appears from this table, the predicted values of the effective thermal conductivity by the present model are closer to their experimental counterparts for most cases.

Table 6 Predicted values of the effective thermal conductivity
by Gomaa [23], Ozbek [13] and the present work for
tested samples and their experimental counterparts

Effective thermal conductivity W/m-K

Ozbek's samples

	Fully brine saturated				Fully decane saturated			
	A	B	C	D	A	B	C	D
Boise	2.05	2.37	2.54	2.56	0.77	1.48	1.68	1.72
Berea	2.53	3.10	3.37	3.92	0.94	2.16	2.64	3.00
Bandera	2.34	2.75	3.03	3.02	0.90	1.92	2.43	2.40
Ottawa sand	2.10	2.44	3.25 / 2.60*	3.4	0.73	1.34	2.64 / 1.25*	1.00

Gomaa's samples

	Fully brine saturated				Fully air saturated			
	A	B	C	D	A	B	C	D
Boise	2.01	2.31	2.48	2.62	.0 27	1.11	1.37	1.38
Berea	2.77	3.60	3.90	4.50	0.34	2.24	2.94	2.50
Bandera	2.58	3.05	3.37	3.12	0.36	1.87	2.71	1.88
Ottawa sand	2.33	2.91	4.07 / 3.00*	4.0†	0.26	.136	3.36 / 1.05*	0.60

Low porosity sample

Fully brine saturated				Fully air saturated			
A	B	C	D	A	B	C	D
3.82	4.37	4.60	5.10	0.70	3.38	4.15	2.85

A work of Gomaa, B work of Ozbek, C present work, D experimental results
*present work with ρ_2 = 0.10, † probably in error
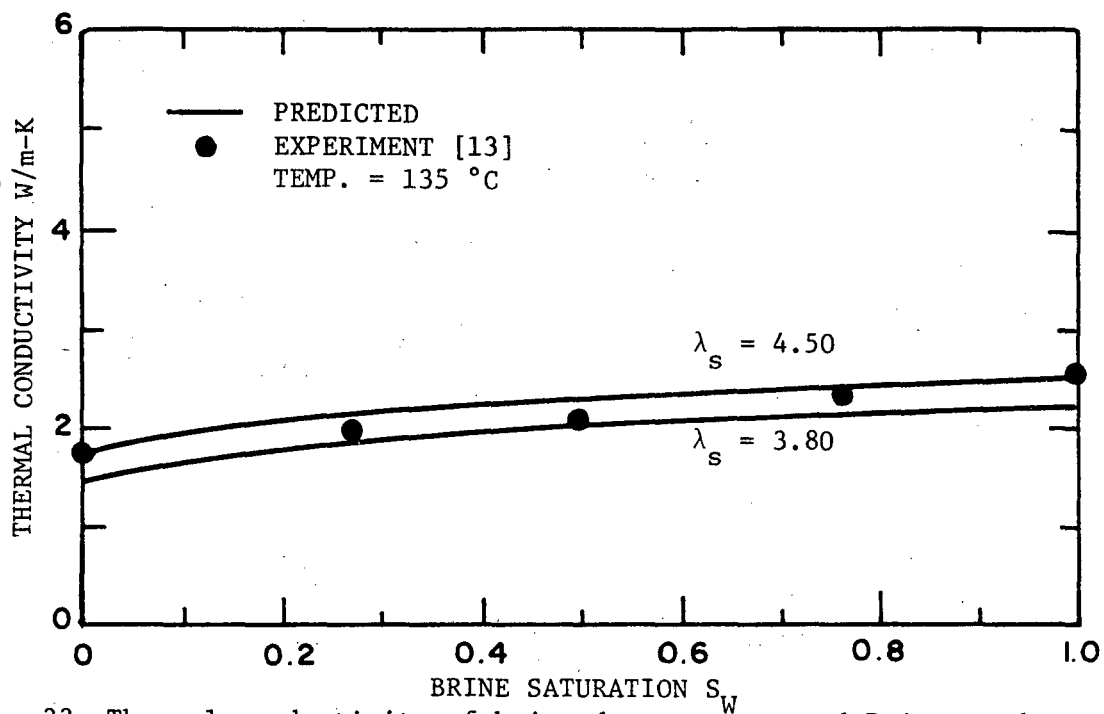
Fig. 33 Thermal conductivity of brine-decane saturated Boise sandstone
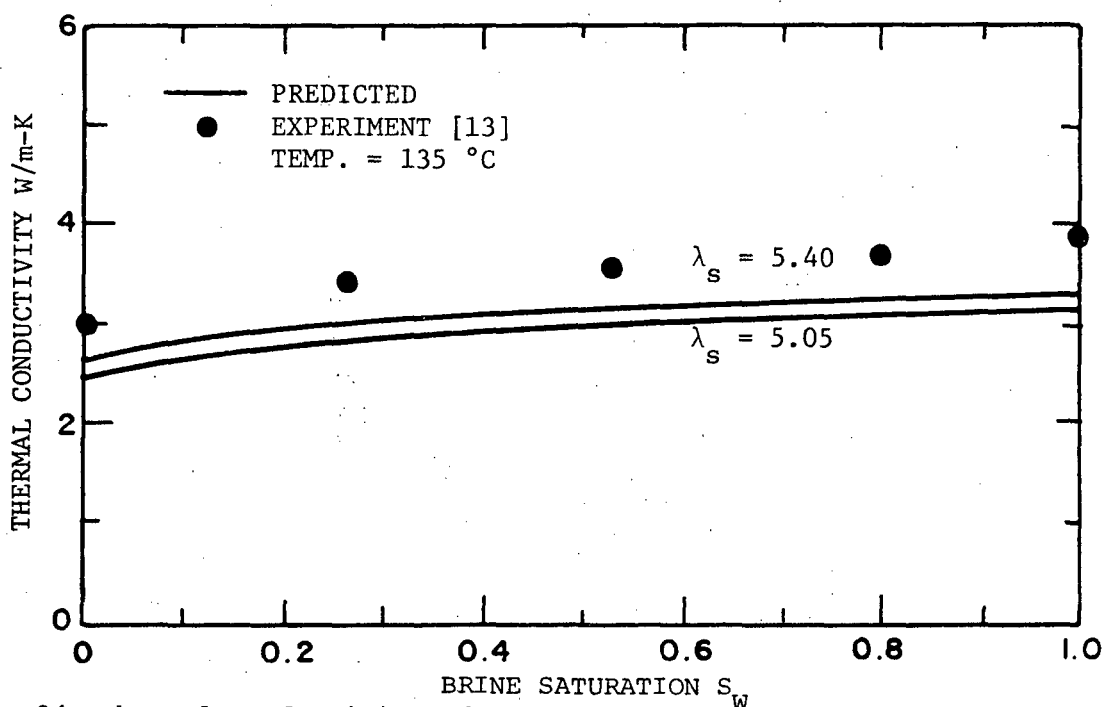
Fig. 34 Thermal conductivity of brine-decane saturated Berea sandstone
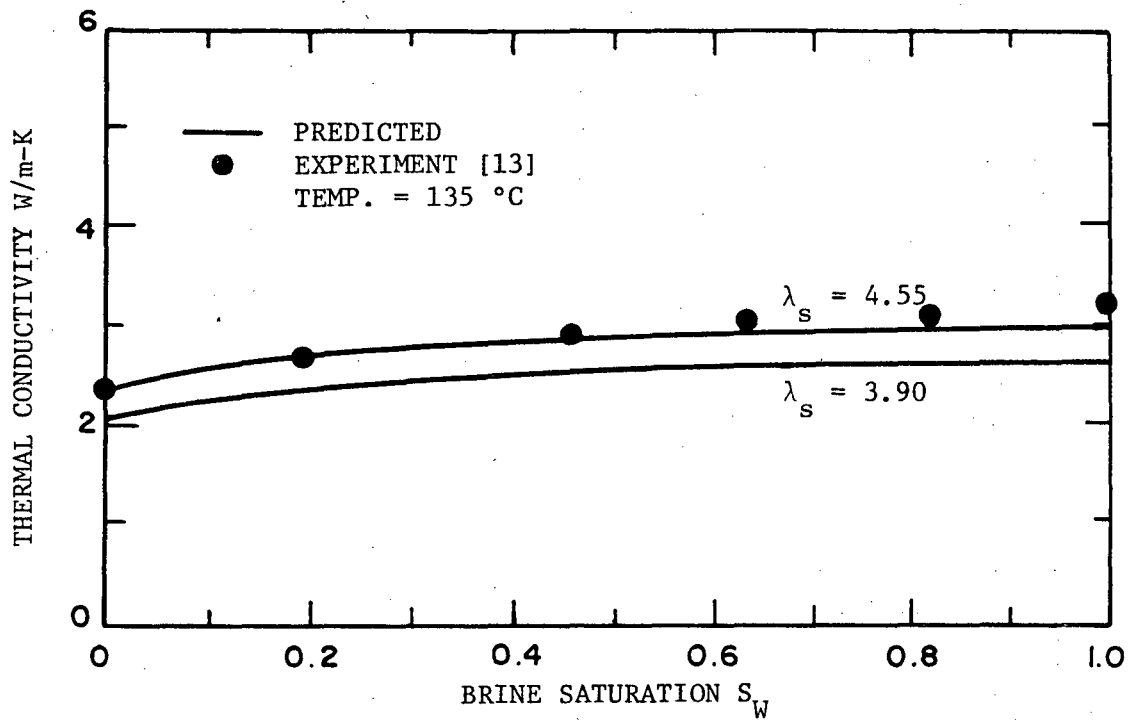
Fig. 35   Thermal conductivity of brine-decane saturated Bandera sandstone
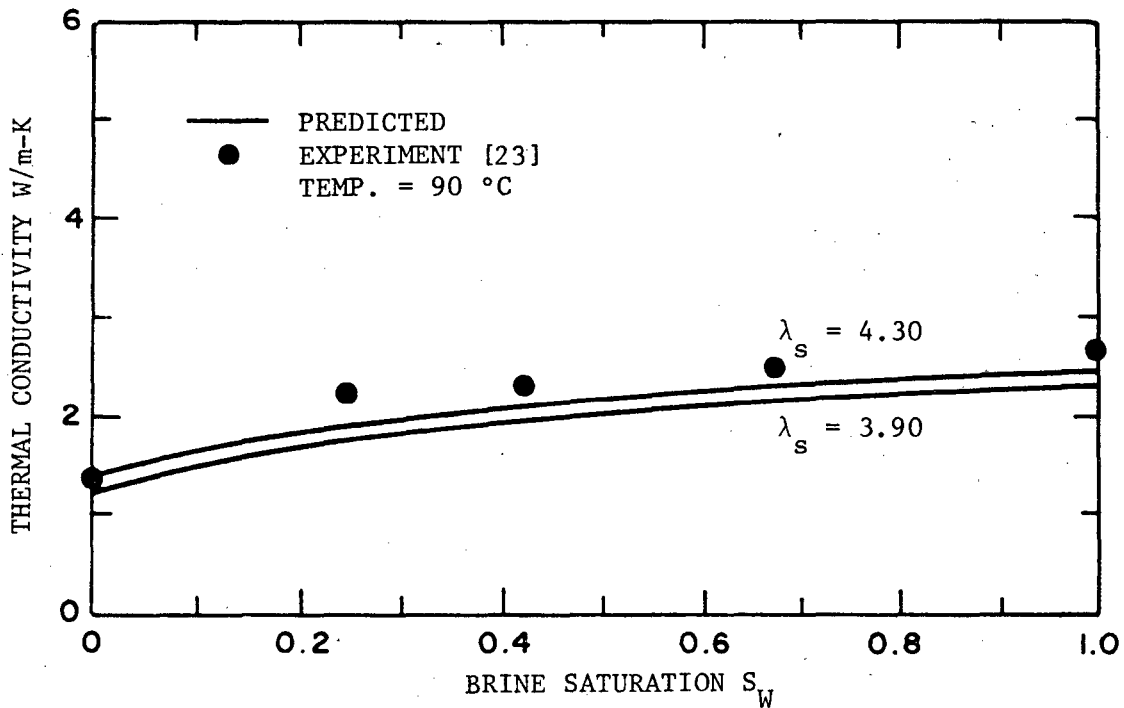
Fig. 36   Thermal conductivity of brine-air saturated Boise sandstone
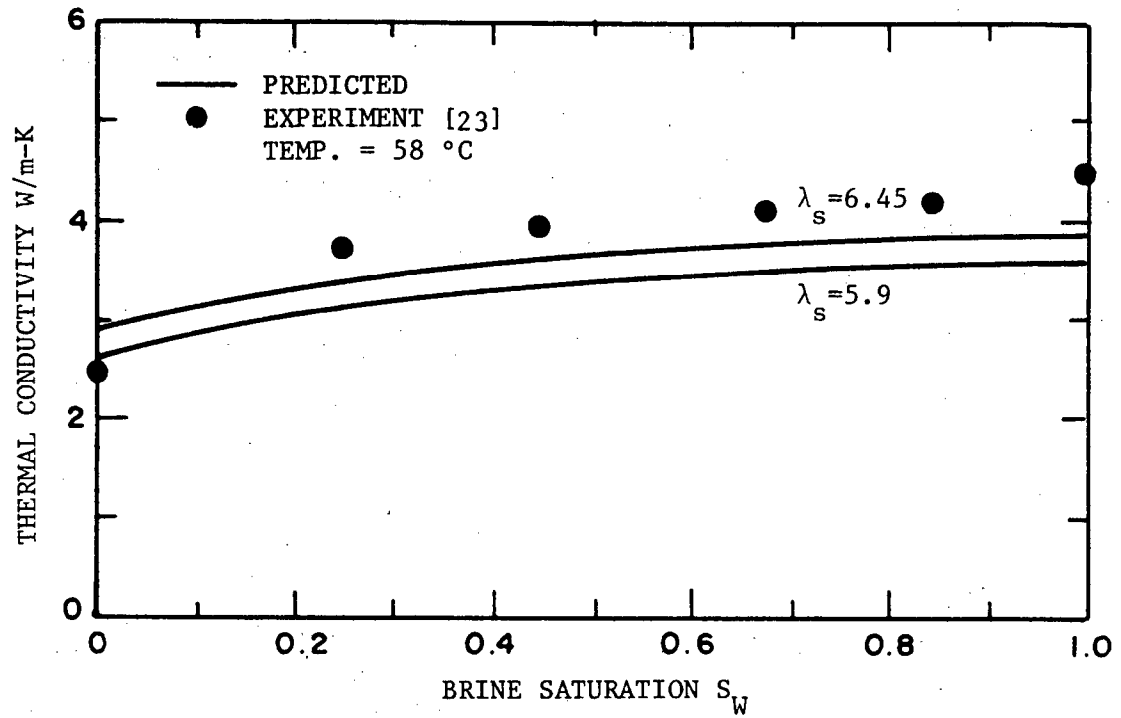
Fig. 37 Thermal conductivity of brine-air saturated Berea sandstone
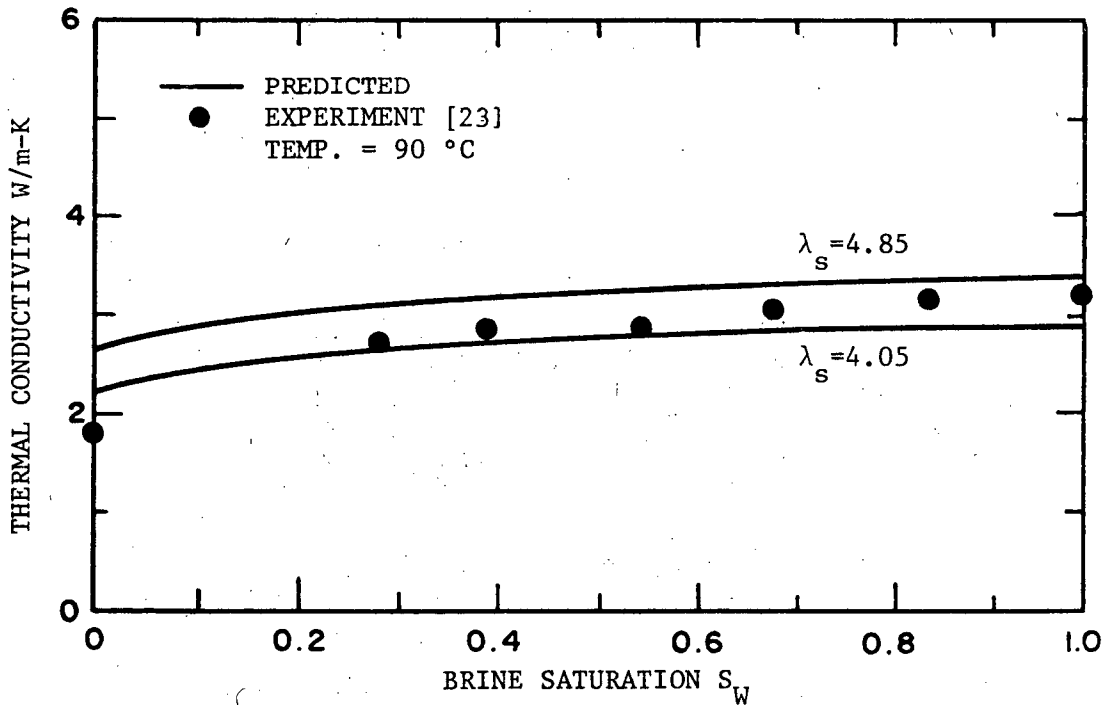
Fig. 38 Thermal conductivity of brine-air saturated Bandera sandstone
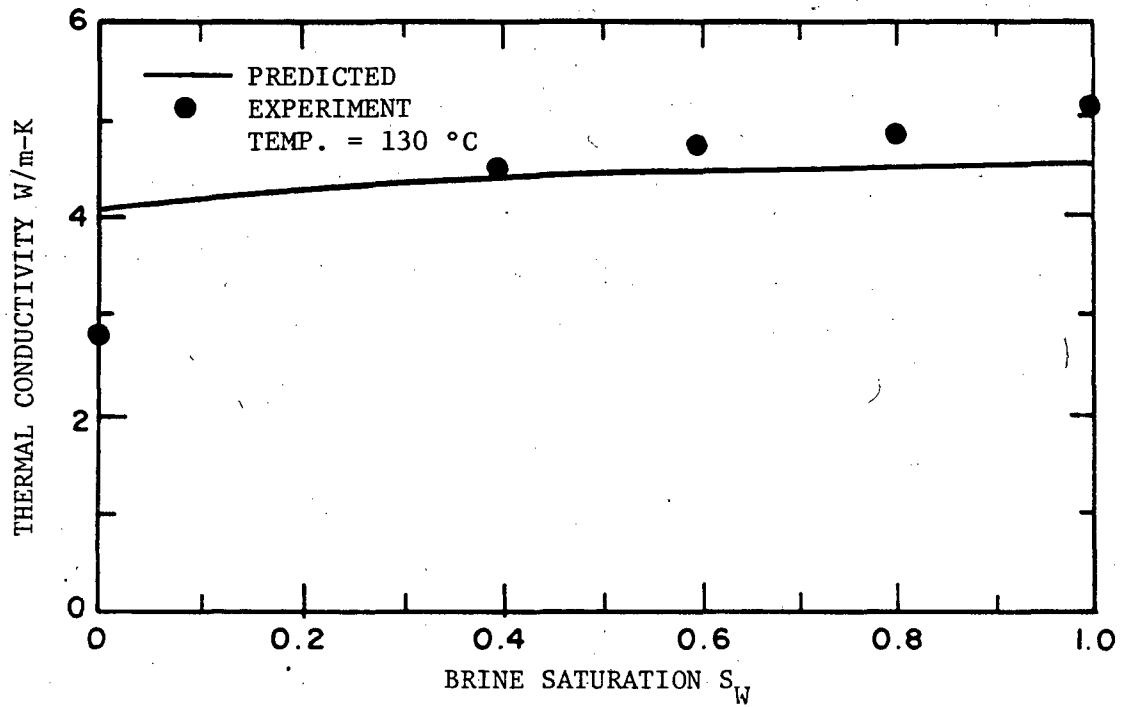
Fig. 39 Thermal conductivity of brine-air saturated low porosity consolidated sandstone
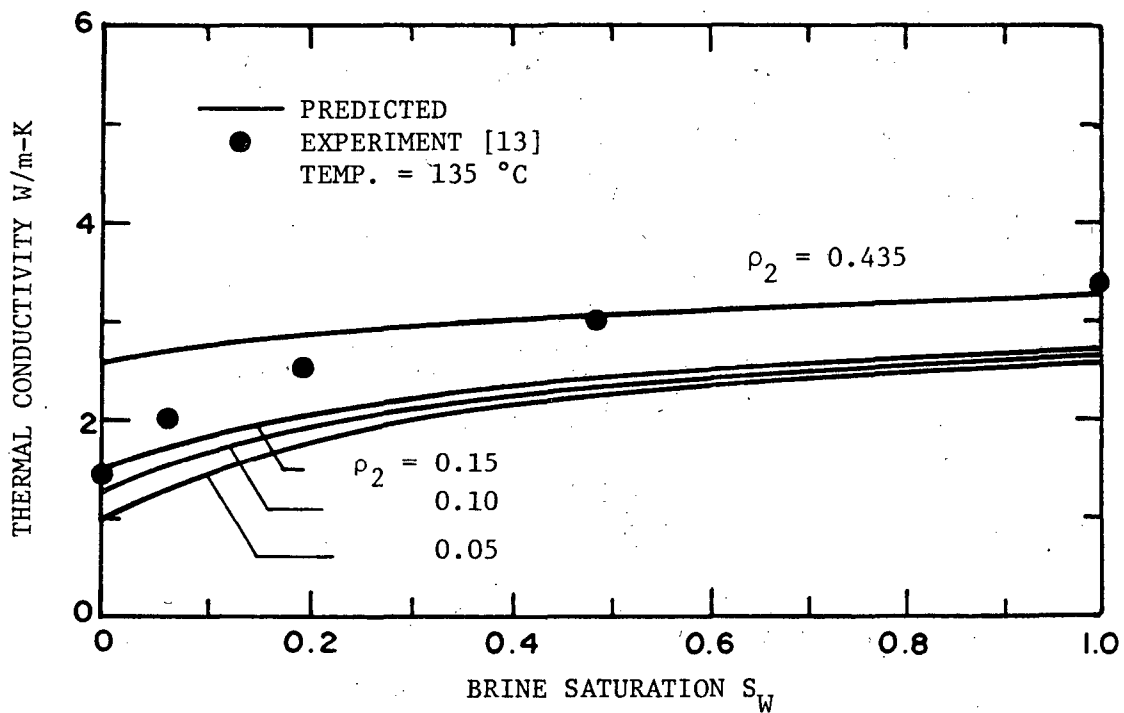
Fig. 40 Thermal conductivity of brine-decane saturated Ottawa sand
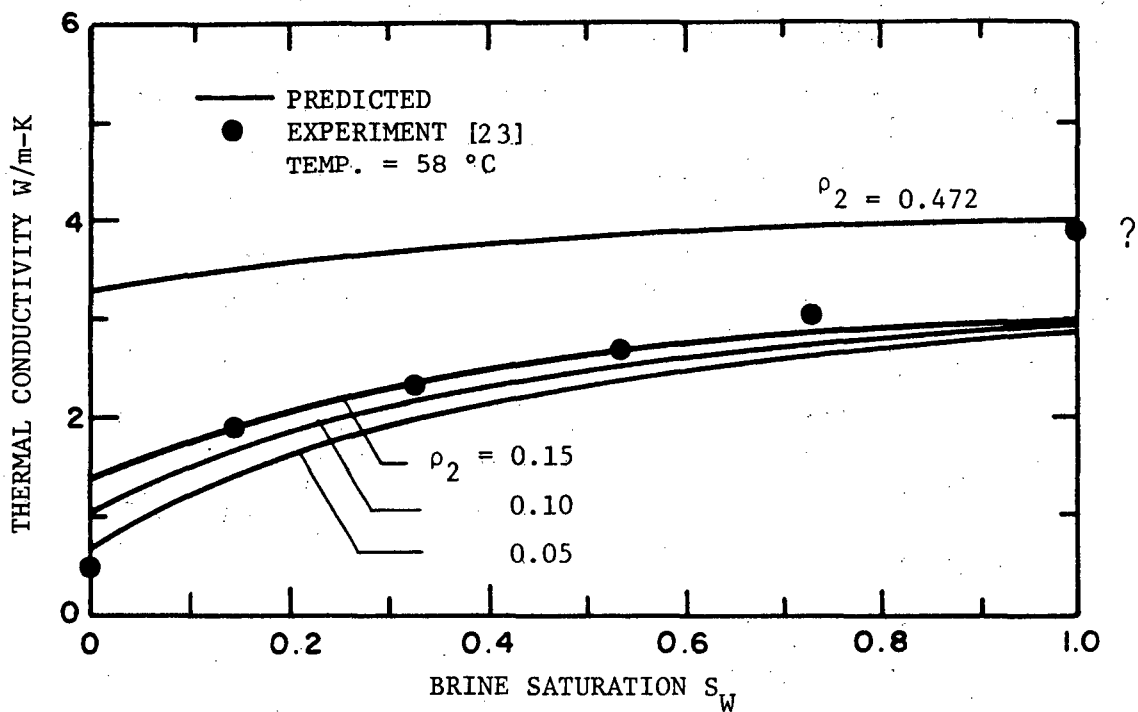
Fig. 41 Thermal conductivity of brine-air saturated Ottawa sand

CONCLUSIONS

1. A mathematical model has been developed which successfully predicts
the effective thermal conductivity of partially liquid saturated porous
rocks based on known values of porosity, electrical formation resistivity
factor, saturation of the wetting phase, and thermal conductivities of the
solid phase, wetting phase and non-wetting phase.

2. A distinction between unconsolidated sand packs and consolidated
sandstones is made by introducing either a thermal or electrical forma-
tion resistivity factor into the model.

3. The effective thermal conductivity predicted by the model increases
with increasing values of thermal conductivities of the solid, wetting
and non-wetting phase, and decreases with increase in porosity. When the
wetting phase has a higher thermal conductivity than the non-wetting
phase, the effective thermal conductivity also increases with increase
in saturation of the wetting phase.

4. The effective thermal conductivities predicted by the model for par-
tially liquid saturated porous rocks show reasonable agreement with experi-
mental data.

5. The effect of grain size could be studied by the present model if a
solid-solid or solid-fluid contact thermal resistance were considered in
the analysis. However, no proof has been given to show that this approach
is valid.

RECOMMENDATIONS

1. A more correct calculation for the electrical formation resistivity factor of the model should be performed by properly accounting for the distortion of the electricity flow lines passing through the pore channels. A full three-dimensional solution of the Laplace equation for conduction of electricity in the pore channels is needed.

2. An extensive and careful experimental study of the solid-solid and solid-fluid thermal contact resistances should be made for porous consolidated rocks and unconsolidated sand packs.

3. Other packing arrangements and grain size distributions should be studied both theoretically and experimentally to consider their effects on thermal conductivity.

REFERENCES

1. Combarnous, M.A., and Boris, S.A., "Hydrothermal Convection in Saturated Porous Media", Advances in Hydroscience, Vol. 10, 1975, P. 231.

2. Lapwood, E.A., "Convection of a Fluid in a Porous Media", Proceedings of the Cambridge Philosophical Society, Vol. 44, 1948, P. 508.

3. Katto, Y., and Masuoka, T., "Criterion for the Onset of Convective Flow in a Fluid in a Porous Media", International Journal of Heat and Mass Transfer, Vol. 10, 1967, P. 297.

4. Chan, C.K., and Tien, C. L.,"Radiative Transfer in Packed Spheres" Journal of Heat Transfer, Vol. 96, 1974, P. 52.

5. Schotte, W., "Thermal Conductivity of Packed Beds", A.I.Ch.E. Journal, Vol. 6, no. 1, 1960, P. 63.

6. Tien, C.L., and Vafai, K., "Statistical Bounds for Effective Thermal Conductivity of Microsphere and Fibrous", AIAA Progress in Astronautics and Aeronautics: Thermophysics and Thermal Control, Vol. 65, 1978, P. 135.

7. Maxwell, J.C., A Treatise on Electricity and Magnetism, Clarendon Press, Oxford, England, 1904, Vol. 1, P. 440.

8. Beck, A.E., "An Improved Method of Computing the Thermal Conductivity of Fluid-Filled Sedimentary Rocks", Geophysics, Vol. 41, no. 1, 1976, P. 133.

9. Kunii, D., and Smith, J.m., "Heat Transfer Characteristic of Porous Rocks", Journal of AIChE, Vol. 6, No. 1, 1960, P. 71.

10. Krupiczka, R., "Analysis of Thermal Conductivity in Granular Materials", International Chemical Engineering, Vol. 4, no. 1, 1967, P. 71.

11. Anand, J., Somerton, W.H., and Gomaa, E.E., "Prediction of Thermal Properties of Formations from Other Known Properties", SPE 4171, 1972.

12. Somerton, W.H., Kesse, J.A., and Chu, S.C., "Thermal Behavior of Unconsolidated Oil Sands", Soc. Pet. Eng. Journal, October, 1974.

13. Ozbek, H., "Thermal Conductivity of Multi-Fluid Saturated Porous Media", Ph.D. Dissertation, University of California, Berkeley, 1975.

14. Tikhominov, V.M., "Conductivity of Rocks and Their Relationship with Density, Saturation and Temperature", Neftianoe Khoziaistro (in Russian), Vol. 64, no. 4, 1968, P. 36.

15. Woodside, W., and Messmer, J.H., "Thermal Conductivity of porous Media II, Consolidated Rocks", Journal of Applied Physics, Vol. 32, no. 9, 1969, P. 1699.

16. Edmondson, T.A., "Thermal Diffusivity of Sedimentary Rocks Subjected to Simulated Overburden Pressure", M.S. Thesis, University of California, Berkeley, 1961.

17. Bridgman, B.W., The Physics of High Pressures, G. Bell and Sons, London, 1949, P. 307-326.

18. Tsederberg, N.V., Thermal Conductivity of Gases and Liquids, The MIT Press, 1965, P. 142.

19. Kruze, J.M., "Effect of Grain Size and Grain Size Distribution on the Thermal Conductivity of Saturated Porous Media", Research Report for M.S. Degree, University of California, Berkeley, 1979.

20. Tye, R.P., Thermal Conductivity, Academic Press, 1969, Vol. 1.

21. Anand, J., "Thermal Conductivity of Fluid Saturated Rocks at Elevated Pressures and Temperatures", M.S. Thesis, University of California, Berkeley, 1971.

22. Somerton, W.H., "Thermal Properties of Oil Sands", Final Report, University of California, Berkeley, Feb. 1974.

23. Gomaa, E.E., "Thermal Behavior of Partially Liquid Saturated Porous Media", Ph.D. Dissertation, University of California, Berkeley, 1973.

24. Carslaw, H., and Jaeger, J., Conduction of Heat in Solids, Clarendon, Oxford, 1959.

25. Forsythe, G.E., and, Wasow, W.R., Finite Difference Methods for Partial Differential Equations, John Wiley and Sons, New York, 1960.

26. Richtmeyer, R.D., and Morton, K.W., Difference Methods for Initial Value Problems, Interscience, New York, 1967.

27. Ames, W.F., Numerical Methods for Partial Differential Equations, Barens and Noble, Inc., New York, 1969.

28. Carre, B.A., "The Determination of the Optimum Acceleration Factor for Successive Over-relaxation", Computer Journal, Vol. 4, no. 1, 1961, P. 73.

29. Pettijohn, F.J., Sedimentary Rocks, Harper and Brothers Publisher, New York, 1949.

30. Blatt, H., Middleton, G., and Murray, R., Origin of Sedimentary Rocks, Prentice Hall Inc., 1972.

31. Tylor, J.M., "Pore Space Reduction in Sandstones", American Association of Petroleum Geologists, Bulletin, 34, 1950, P. 701.

32. Khan, J.S., "The Analysis and Distribution of Packing in Sand-Size Sediments", Journal of Geology, Vol. 64, 1956, P. 701.

33. Chan, C.K., and Tien, C.L., "Conductance of Packed Spheres in Vacuum", Journal of Heat Transfer, Vol. 95, 1973, P. 302.

34. Kaganer, B.M.G., "Thermal Insulation in Cryogenic Engineering", Translated from Russian by Moscona, Israel Program for Scientific Translation, Jerusalem, 1969.

35. Woodside, W., and Messner, J.H., "Thermal Conductivity of Porous Media, I, Unconsolidated Sandstones", Journal of Applied Physics, Vol. 32, no. 9, 1961, P. 1688.

36. Veziroglu, T.N., "Thermal Conductivity of Two Dimensional Constrictions", NASA Grant NGR 10-007 SUB3, Mech. Eng. Dep. University of Miami, Jan. 1971.

37. Archie, G.E., "The Electrical Resistivity Log as an Aid in Determining Some Reservoir Characteristics", Trans. AIME, Vol. 146, 1942, P. 45.

38. Kesse, J.A., "Thermal Conductivity of Unconsolidated Oil Sands", M.S. Thesis, University of California, Berkeley, 1971.

39. Sahnine, B., "Relationship Between Sonic Velocities and Thermal Conductivity of Fluid Saturated Rocks", M. Eng. Project Report, University of California, Berkeley, Sep. 1979.

40. Clark, K.K., "Reduction of Fracture Pressure of Rocks by Intensive Borehole Heating", M.S. Thesis, University of California, Berkeley, 1964.

41. Somerton, W.H., "Deformation Moduli of Water-Bearing Formations at Elevated Temperatures", Department of Water Resources Report, Jan. 1974.

42. Greenwald, R.F., "Volumetric Response of Porous Media to Pressure Variations", Ph.D. Dissertation, University of California, Berkeley, 1980.

43. Ki-Iti-Horai, "Thermal Conductivity of Rock-Forming Minerals" Journal of Geophysical Research, Vol. 76, no. 5, P. 1278.

44. Thermal Conductivity of Selected Materials, National Standard Reference Data Series, U.S. Department of Commerce, NBS 8.

45. Kreith, F., Principles of Heat Transfer, Dun-Donnelley, Publisher, New York, 1976.

46. Ramson, I., Hornberger, G.M., and Moltz, F.G., Numerical Methods in Subsurface Hydrology, Wiley-Interscience, New York, 1971.

47. Young, D., "Iterative Methods for Solving Partial Differential Equations of Elliptic Type", <u>Trans. AMS</u>, Vol. 76, 1954, P. 92.

APPENDIX A

DEVELOPMENT OF POROSITY AND SATURATION OF THE WETTING PHASE EQUATIONS

Because of the symmetry of the model, equations for porosity and saturation are developed for one eighth of a unit cell, which has been used as an elementary unit throughout this work.

A-1 Porosity Equation

Porosity is defined as the ratio of void to total volume. In terms of V_T the total volume, and V_s the volume of the solid phase of the elementary cell, porosity ϕ may be written as

$$\phi = \frac{V_T - V_s}{V_T} \quad . \qquad \text{(A-1-1)}$$

By referring to Fig. 5, the total volume is

$$V_T = (r_0^2 - r_{c1}^2)(r_0^2 - r_{c2}^2)^{\frac{1}{2}} \quad . \qquad \text{(A-1-2)}$$

For cases in which $r_{c2} \leqslant r_{c1} \leqslant \sqrt{\frac{2}{2}} \, r_0^2$, V_s is given by

$$V_s = \frac{1}{8} (\frac{4}{3}\pi r_0^3 - 4V_1 - 2V_2) \quad , \qquad \text{(A-1-3)}$$

where V_1 and V_2 are the volume of spherical caps having r_{c1} and r_{c2} as the radius of their bases, repsectively, and are calculated as:

$$V_i \Big|_{i=1,2} = \frac{\pi}{3}\Big[r_0 - (r_0^2 - r_{ci}^2)^{\frac{1}{2}}\Big]^2 \Big\{2r_0 + (r_0^2 - r_{ci}^2)^{\frac{1}{2}}\Big\} \quad . \qquad \text{(A-1-4)}$$

However, when $r_{c1} > \frac{\sqrt{2}}{2} r_0$, as long as $r_{c2} \leqslant r_{c1}$, Eq. (A-1-3) must be corrected as:

$$V_s = \frac{1}{8}(\frac{4}{3}\pi r_0^3 - 4V_1 - 2V_2) + V_3 \quad , \qquad \text{(A-1-6)}$$

where V_3 is the volume of spherical wedge OABC as shown in Fig. A1, and can be evaluated by the following integral:

$$V_3 = \int_0^{(2r_{c1}^2 - r_0^2)^{1/2}} S dz \quad , \tag{A-1-7}$$

where S is the area of segment $A'B'C'$ in Fig. A2, and is given by

$$S = (r_0^2 - r_{c1}^2)^{1/2} \left\{ (r_0^2 - r_{c1}^2)^{1/2} - (r_{c1}^2 - z^2)^{1/2} \right\} + (r_0^2 - z^2) \times$$

$$\left\{ \frac{\pi}{4} - \tan^{-1} \left(\frac{r_0^2 - r_{c1}^2}{r_{c1}^2 - z^2} \right)^{1/2} \right\} \quad . \tag{A-1-8}$$

Substituting the expression for S from Eq. (A-1-8) into Eq. (A-1-7) and carrying out the integration yields:

$$V_3 = \frac{1}{6} \left\{ 2(2r_{c1}^2 - r_0^2)^{1/2}(r_0^2 - r_{c1}^2) - 2(r_{c1}^2 + 2)(r_0^2 - r_{c1}^2) \sin^{-1}(\frac{2r_{c1}^2 - r_0^2}{r_{c1}^2})^{1/2} \right.$$

$$\left. + 4 \tan^{-1}(\frac{2r_{c1}^2 - 1}{r_0^2})^{1/2} \right\} \quad . \tag{A-1-9}$$

Using either Eq. (A-1-3) or Eq. (A-1-6) for V_s, and Eq. (A-1-2) for V_T, in Eq. (A-1-1) one can get the porosity as a function of dimensionless radii $\rho_1 = \frac{r_{c1}}{r_0}$ and $\rho_2 = \frac{r_{c2}}{r_0}$.

A-2   Saturation of the Wetting Phase Equation

The wetting phase saturation S_w is defined as the ratio of the volume of wetting phase V_w, to the pore volume V_p. Thus:

$$S_w = V_w / V_p \quad . \tag{A-2-1}$$

Knowing the total volume from Eq. (A-1-2), and porosity, V_p may be written as:

$$V_p = \phi \cdot V_T = \phi(r_0^2 - r_{c1}^2)(r_0^2 - r_{c2}^2)^{1/2} \quad . \tag{A-2-2}$$

By referring to Fig. 17, if the volume of the solid phase V_s is added to V_w, the resulting composite volume V would have a geometry similar to V_s. Therefore, Eqs. (A-1-3) and (A-1-6) may be used to evaluate V. Only it should be noted that r_0, r_{c1} and r_{c2} must be replaced by r_w, $(r_w^2 - r_0^2 + r_{c1}^2)^{\frac{1}{2}}$ and $(r_w^2 - r_0^2 + r_{c2}^2)^{\frac{1}{2}}$, respectively. Having calculated V, V_w can be obtained as follows:

$$V_w = V - V_s = V - (1 - \phi)V_T \quad ,$$

or

$$V_w = V - (1 - \phi)(r_0^2 - r_{c1}^2)(r_0^2 - r_{c2}^2)^{\frac{1}{2}} \quad . \qquad (A-2-3)$$

Substituting V_w from Eq. (A-2-3) and V_f from Eq. (A-2-2) into Eq. (A-2-1) provides the saturation of the wetting phase as a function of dimensionless radii $\rho_w = \dfrac{r_w}{r_0}$, $\rho_i = \dfrac{r_0}{r_0}$ and $\rho_2 = \dfrac{r_{c2}}{r_0}$.
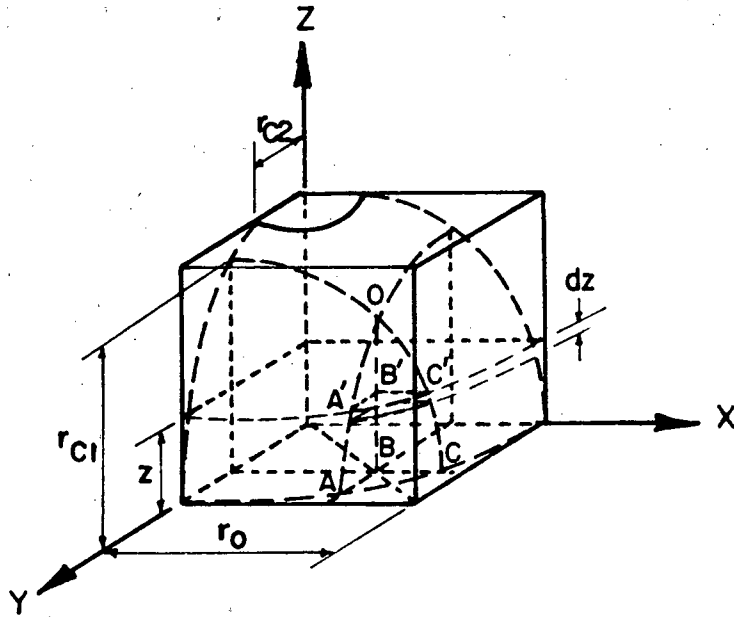
Fig. A1 One-eighth of a unit cell for $r_{cl} > \frac{\sqrt{2}}{2} r_o$
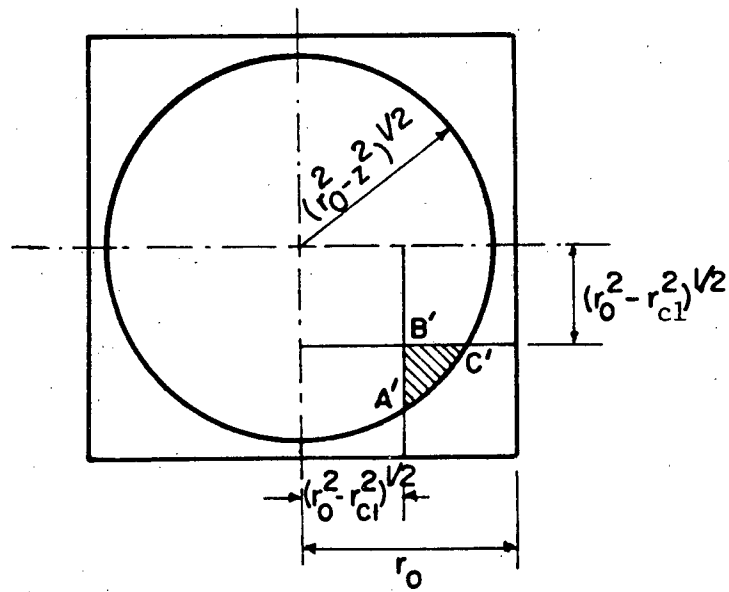
Fig A2 Horizontal cross-section of a unit cell with plane Z=z

APPENDIX B

FINITE DIFFERENCE REPRESENTATION OF THE GOVERNING EQUATION AND

BOUNDARY CONDITIONS

The governing equation for the steady state heat conduction in a homogeneous system of constant thermal conductivity, with no internal heat generation in cylindrical coordinates and for the case where temperature is independent of the coordinate θ, has the form:

$$\frac{\partial^2 T}{\partial r^2} + \frac{1}{r}\frac{\partial T}{\partial r} + \frac{\partial^2 T}{\partial z^2} = 0 \quad . \tag{B-1}$$

If function $T(r, z)$ is analytic within a region of interest R, then it may be expanded into a Taylor's series in this region about point (r_c, z_c), in the positive and negative r and z directions. Referring to Fig. (B-1), the above statement is written mathematically in the r direction as:

$$T_e = T_c + \alpha(\Delta r)(\frac{\partial T}{\partial r})_c + \frac{\alpha^2(\Delta r)^2}{2!}(\frac{\partial^2 T}{\partial r^2})_c + \frac{\alpha^3(\Delta r)^3}{3!}(\frac{\partial^3 T}{\partial r^3}) + \ldots , \tag{B-2}$$

$$T_w = T_c - (\Delta r)(\frac{\partial T}{\partial r})_c + \frac{(\Delta r)^2}{2!}(\frac{\partial^2 T}{\partial r^2})_c - \frac{(\Delta r)^3}{3!}(\frac{\partial^3 T}{\partial r^3})_c + \ldots \tag{B-3}$$

Note that for generality, the points W and E are considered to have different distances from point C. To obtain an approximation to the first and the second derivatives of temperature at the point (r_c, z_c), Eqs. (B-2) and (B-3) can be solved simultaneously, yielding:

$$(\frac{\partial T}{\partial r})_c = \frac{\alpha}{(1 + \alpha)(\Delta r)}\left\{\frac{1}{\alpha^2}(T_e - T_c) - (T_w - T_c)\right\} - 0\left[(\Delta r)^2\right] , \tag{B-4}$$
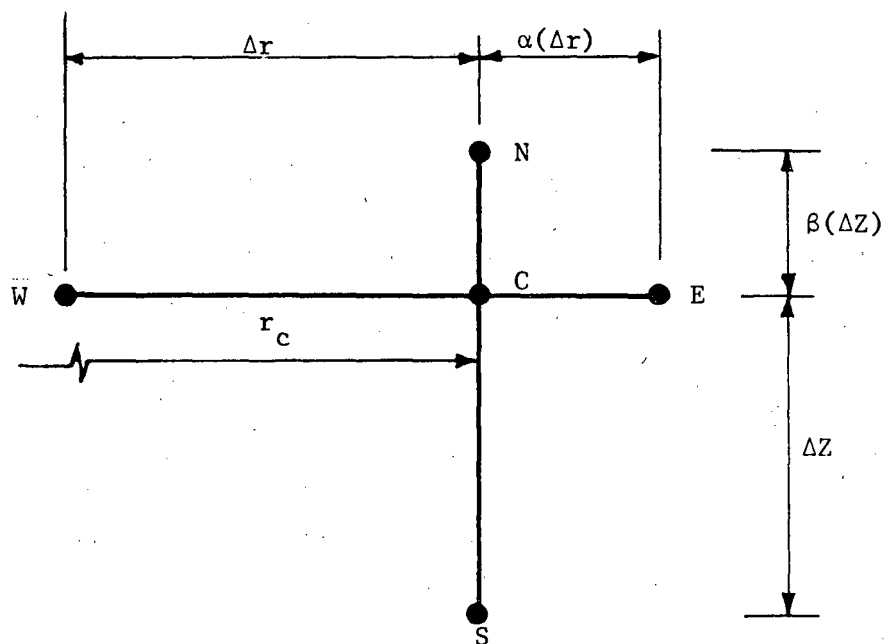
Fig. B1 Nodal points for a two-dimensional region

$$\left(\frac{\partial^2 T}{\partial r^2}\right)_c = \frac{2}{(1+\alpha)(\Delta r)^2}\left\{\frac{1}{\alpha}(T_e - T_c) + (T_w - T_c)\right\} - \frac{(\Delta r)(\alpha - 1)}{3}\left(\frac{\partial^3 T}{\partial r^3}\right)_c$$
$$+ 0\left[(\Delta r)^2\right] . \tag{B-5}$$

The term $0\ [(\Delta r)]^2$ means that all the terms containing expressions of the order of $(\Delta r)^2$ and smaller are dropped. By the same means a difference representation of $\left(\frac{\partial^2 T}{\partial z^2}\right)_c$ would be:

$$\left(\frac{\partial^2 T}{\partial z^2}\right)_c = \frac{2}{(1+\beta)(\Delta z)^2}\left\{\frac{1}{\beta}(T_n - T_c) + (T_s - T_c)\right\} + \frac{(\Delta z)(\beta - 1)}{3} \times$$
$$\left(\frac{\partial^3 T}{\partial z^3}\right)_c + 0\left[(\Delta z)^2\right] . \tag{B-6}$$

Truncating Eqs. (B-4), (B-5) and (B-6) after the first term, and substituting them into the governing equation (B-1) results in

$$\frac{\partial^2 T}{\partial r^2} + \frac{1}{r}\frac{\partial T}{\partial r} + \frac{\partial^2 T}{\partial z^2} = \frac{\left(\frac{2}{\Delta r} + \frac{1}{r_c}\right)}{\alpha(1+\alpha)(\Delta r)}(T_e - T_c) + \frac{\left(\frac{2}{\Delta r} - \frac{\alpha}{r_c}\right)}{(1+\alpha)(\Delta r)}(T_w - T_c) +$$
$$+ \frac{2}{(1+\beta)(\Delta z)^2}\left\{\frac{1}{\beta}(T_n - T_c) + (T_s - T_c)\right\} + 0\ (\Delta z). \tag{B-7}$$

Using Eq. (B-7), which is an approximation to the true partial differential equation, provides some truncational error associated with truncating the infinite series, representing the partial derivatives after a few finite terms. This error would be of the order of Δz (assuming $\Delta z > \Delta r$) in Eq. (B-7). However, for $\alpha = \beta = 1$, terms of the order of (Δr) and (Δz) drop out of Eqs. (B-5) and (B-6), and therefore the truncational error in Eq. (B-7) would be of the order of $(\Delta z)^2$. Cases in which α and β are not equal to 1 are useful if one wishes to change the distance between the nodal points, either to accommodate irregular boundaries or to increase the accuracy of the computation in some region of interest.

The difference equation (B-7) can also be obtained by another approach, that is, the method of making an energy balance for the node C. This can be written as:

$$\sum_{\substack{i = e,w \\ n,s}} K_{ic} (T_i - T_c) \quad ,$$

(B-8)

where K_{ic} is the thermal conductance between the node c and its adjacent nodes. In cylindrical coordinates the region between the adjacent nodes has the geometry of a cylindrical shell. Such an element with outer radius r, thickness t, height h and thermal conductivity λ has its thermal conductances in the r and z directions as:

$$K_r = \frac{2\pi\lambda h}{\ln\left(\frac{r}{r-t}\right)} = \frac{2\pi\lambda h}{t} (r - t/2) + 0(ht) \quad ,$$

(B-9)

$$K_z = \frac{[\pi r^2 - \pi(r-t)^2]\lambda}{h} = \frac{2\pi\lambda t}{h} (r - t/2) \quad .$$

(B-10)

Therefore, for the elements between the central node C and its four adjacent nodes E, W, N, S, Eqs. (B-9) and (B-10) can be used to calculate the thermal conductance. The results are tabulated in the following form:

outer radius	thickness	height	thermal conductance

Element CE

$r_c + \alpha(\Delta r)$	$\alpha(\Delta r)$	$(\beta + 1)(\frac{\Delta z}{2})$	$\frac{2\pi\lambda(\beta + 1)}{\alpha(\Delta r)} (\frac{\Delta z}{2})(r_c + \frac{\alpha\Delta r}{2})$

(B-9)

element CW

r_c	(Δr)	$(\beta + 1)(\frac{\Delta z}{2})$	$\frac{2\pi\lambda(\beta + 1)}{\Delta r} (\frac{\Delta z}{2}) (r_c - \frac{\Delta r}{2})$

(B-9)

element CN

$r_c + \alpha(\frac{\Delta r}{2})$	$(1 + \alpha)(\frac{\Delta r}{2})$	$\beta(\Delta z)$	$\frac{2\pi\lambda(\alpha + 1)}{\beta(\Delta z)} (\frac{\Delta r}{2})[r_c - (1 - \alpha)\frac{\Delta r}{4}]$

(B-10)

element CS

$r_c + \alpha(\frac{\Delta r}{2})$	$(1 + \alpha)(\frac{\Delta r}{2})$	(Δz)	$\frac{2\pi\lambda(\alpha + 1)}{(\Delta z)}(\frac{\Delta r}{2}) [r_c - (1 - \alpha)\frac{\Delta r}{4}]$

(B-10)

Substituting the above expressions for the thermal conductances in Eq. (B-8) yields the following difference equation for the node C:

$$\frac{2\pi\lambda(\beta + 1)(\frac{\Delta z}{2})}{(\Delta r)}\left\{(T_w - T_c)(r_c - \frac{\Delta r}{2}) + \frac{1}{\alpha}(T_e - T_c)(r_c + \frac{\alpha\Delta r}{2})\right\} +$$

$$\frac{2\pi\lambda(\alpha + 1)(\frac{\Delta r}{2})}{(\Delta z)}[r_c - (1 - \alpha)\frac{\Delta r}{4}]\left\{(T_s - T_c) + \frac{1}{\beta}(T_n - T_c)\right\} = 0 \quad .$$

$$(B-11)$$

The above difference equation does not look like Eq. (B-7), which was obtained by the method of finite difference. However, multiplying Eq. (B-7) by $\pi\lambda r_c(\alpha + 1)(\beta + 1)(\frac{\Delta z}{2})(\Delta r)$ results in the following form for this difference equation:

$$\frac{2\pi\lambda(\beta + 1)(\frac{\Delta z}{2})}{(\Delta r)}\left\{(T_w - T_c)(r_c - \frac{\alpha(\Delta r)}{2} + \frac{1}{\alpha}(T_e - T_c)(r_c + \frac{\Delta r}{2})\right\} +$$

$$\frac{2\pi\lambda r_c(1 + \alpha)(\frac{\Delta r}{2})}{(\Delta z)}\left\{(T_s - T_c) + \frac{1}{\beta}(T_n - T_c)\right\} = 0 \quad . \qquad (B-12)$$

For $\alpha = \beta = 1$ the above equation is the same as Eq. (B-11), and for $\alpha \neq 1$, $\beta \neq 1$ it is not very difficult to show that the difference between the two representations is of the order of (Δr) or (Δz), which ever is larger. This difference can be neglected because in the derivation of Eq. (B-7) errors of the order of (Δr) and (Δz) were already allowed.

Difference equations such as (B-7) may also be written for nodes on the insulated left and right boundaries (Fig. 9A). However, it should be noted that because of the condition $\frac{\partial T}{\partial r} = 0$ on the axis $(r = 0)$, the term $\frac{1}{r}\frac{\partial T}{\partial r}$ in Eq. (B-1) is indeterminate. Using

L'Hopital's rule, this term can be replaced by its limit as r tends to zero, i.e.

$$\lim_{r \to 0} \frac{1}{r} \frac{\partial T}{\partial r} = \lim_{r \to 0} \frac{\frac{\partial}{\partial r}(\frac{\partial T}{\partial r})}{\frac{\partial}{\partial r}(r)} = \frac{\partial^2 T}{\partial r^2})_{r = 0} \qquad (B\text{-}13)$$

Therefore Eq. (B-1) for the nodes on the left boundary becomes:

$$\frac{2\partial^2 T}{\partial r^2} + \frac{\partial^2 T}{\partial z^2} = 0 \qquad (B\text{-}14)$$

Now the difference equivalents of $\frac{\partial^2 T}{\partial r^2}$ and $\frac{\partial^2 T}{\partial z^2}$ from Eqs. (B-5) and (B-6) may be substituted into Eq. (B-14), which yields

$$\frac{2\partial^2 T}{\partial r^2} + \frac{\partial^2 T}{\partial z^2} = \frac{4}{(1 + \alpha)(\Delta r)^2} \left\{ \frac{1}{\alpha}(T_e - T_c) + (T_w - T_c) \right\} + \frac{2}{(\beta + 1)(\Delta z)^2} \times$$

$$\left\{ \frac{1}{\beta}(T_n - T_c) + (T_s - T_c) \right\} . \qquad (B\text{-}15)$$

Because node W is this case is imaginary, one could choose $\alpha = 1$, and use the boundary condition $\frac{\partial T}{\partial r} = 0$ to eliminate T_w in Eq. (B-15) as follows:

$$\frac{\partial T}{\partial r} = \frac{T_w - T_e}{2(\Delta r)} + 0(\Delta r)^2 = 0 ,$$

or

$$T_w = T_e .$$

Thus setting $\alpha = 1$, and $T_w = T_e$ in Eq. (B-15), provides the following difference equation for nodes on the left boundary.

$$\frac{4}{(\Delta r)^2} (T_e - T_c) + \frac{2}{(\beta + 1)(\Delta z)^2} \left\{ \frac{1}{\beta}(T_n - T_c) + (T_s - T_c) \right\} = 0 . \qquad (B\text{-}16)$$

With some algebraic manipulations, Eq. (B-16) may also be cast in the following form:

$$\frac{2\pi(\frac{\Delta r}{2})(\beta + 1)(\frac{\Delta z}{2})\lambda}{(\Delta r)} (T_e - T_c) + \frac{\pi(\frac{\Delta r}{2})^2\lambda}{\beta(\Delta z)}(T_n - T_c) + \frac{\pi(\frac{\Delta r}{2})^2}{(\Delta z)} (T_s - T_c) = 0 \ .$$

$$(B-17)$$

This representation would have been obtained, if one had used the method of energy balance for the node C on the axis. Only it should be noticed that:

$$\frac{2\pi(\frac{\Delta r}{2})(\beta + 1)(\frac{\Delta z}{2})\lambda}{(\Delta r)} = K_{ce} \ ,$$

$$\frac{\pi(\frac{\Delta r}{2})^2\lambda}{\beta(\Delta z)} = K_{cn}, \quad \frac{\pi(\frac{\Delta r}{2})^2\lambda}{(\Delta z)} = K_{cs} \ ,$$

where K_{ce}, K_{cn} and K_{cs} are the thermal conductances between the node C and its three adjacent nodes E, N, and S, respectively.

For nodes on the right boundary (Fig. 9A), the difference Eq. (B-7) can be used. However, because node E in this case is imaginary, it may be chosen so as to provide $\alpha = 1$. Furthermore, $T_e = T_w$ because of the condition $\frac{\partial T}{\partial r} = 0$ at this boundary. These conditions reduce Eq. (B-7) to the following form:

$$\frac{2}{(\Delta r)^2}(T_w - T_c) + \frac{2}{(1 + \beta)(\Delta z)^2}\left\{\frac{1}{\beta}(T_n - T_c) + (T_s - T_c)\right\} = 0 \ .$$

$$(B-18)$$

This equation may also be written as follows:

$$\frac{2\pi\lambda(\beta + 1)(\frac{\Delta z}{2})r_c}{(\Delta r)} (T_w - T_c) + \frac{2\pi\lambda r_c(\frac{\Delta r}{2})}{\beta(\Delta z)}(T_n - T_c) + \frac{2\pi\lambda r_c(\frac{\Delta r}{2})}{(\Delta z)}(T_s - T_c) = 0 \ ,$$

$$(B-19)$$

which is the difference representation of the governing equation, if the method of energy balance had been applied for a node on the right boundary.

The foregoing discussion on the difference representation of the governing equation (B-1) and its boundary conditions show that either a mathematical or a physical approach could be used to formulate the problem. These approaches give identical results and have truncational errors of the order of $(\Delta r)^2$ or $(\Delta z)^2$, whichever is larger, if the nodes in the r and the z directions are equally spaced (Δr and Δz are not necessarily equal). However, truncational error would be of the order of (Δr) or (Δz) if the distances between the nodes in the r or z directions are not equal.

APPENDIX C

DIRECT AND ITERATIVE METHODS OF SOLUTION OF THE DIFFERENCE EQUATIONS

In the numerical method of solution of partial differential equations, one has to solve a linear system of algebraic equations which may be written in matrix notation as:

$$AX = B , \qquad\qquad (C-1)$$

where A and B are square and column matrices of known quantities and X is a column matrix containing the unknowns.

The algebraic equations presented by Equa. (C-1) may be solved directly, either by successive elimination of the unknowns (Gaussian elimination), or by triangular decomposition of the matrix of coefficients. These techniques are most efficient whenever such equations are obtained by difference approximation of parabolic partial differential equations, or when the number of such equations is small. However, for systems involving a large set of equations generated by approximation of elliptic problems, the iterative methods are superior to the direct techniques. A comprehensive discussion on the direct and iterative methods may be found elsewhere [45]. Only the highlights of some iterative methods, especially the successive over-relaxation which is used in this work, are presented here.

In general, iterative methods for the solution of linear algebraic equations are those in which a first approximation for the unknowns is used to obtain a second approximation, which in turn is used to calculate a third, and so on. This idea may be applied to a set of equations generated by the difference approximation of $\nabla^2 T = 0$ in three different ways, which are considered in the following.

In Appendix B, it was shown that either a finite difference or an energy balance method of deriving a numerical solution of $\nabla^2 T = 0$ leads to the following equation for the temperature at a general node denoted by (i,j)

$$(K_w + K_e + K_s + K_n) \, T_{i,j} = K_w \, T_{i-1,j} + K_e \, T_{i+1,j} + K_s \, T_{i,j-1} + K_n \, T_{i,j+1} \, , \tag{C-2}$$

where K_w, K_e, K_s and K_n are the thermal conductances between the central node (i,j) and its four adjacent nodes $(i-1,j)$, $(i+1,j)$, $(i,j-1)$ and $(i,j+1)$, respectively.

Starting with a first approximation for the temperatures at each node, Eq. (C-2) suggests that a second approximation may be obtained as:

$$T_{i,j}^{(n+1)} = (K_w + K_e + K_s + K_n)^{-1} \left\{ K_w T_{i-1,j}^{(n)} + K_e T_{i+1,j}^{(n)} + K_s T_{i,j-1}^{(n)} + K_n T_{i,j+1}^{(n)} \right\} \, , \tag{C-3}$$

where the exponents (n) and $(n+1)$ denote the sequence of the approximations. This method is called the Jacobi iteration. Because the rate at which the successive iterations converge to the exact solution is very slow for this process, the Jacobi iteration is never used in practice.

There exists a slightly improved iteration method called Gauss-Siedel, in which one uses the latest iterative values as soon as they are available. This implies that if the nodes are scanned from left to right along the successive rows during the $(n+1)$ iteration, at any node (i,j), the values of $T_{i-1,j}^{(n+1)}$ and $T_{i,j-1}^{(n+1)}$ are already available from the previous calcuations, and may be used in Eq. (C-3) instead of $T_{i-1,j}^{(n)}$ and $T_{i,j-1}^{(n)}$. Therefore, the Gauss-Seidel

iteration formula is written as:

$$T_{i,j}^{(n+1)} = (K_w + K_e + K_s + K_n)^{-1} \left\{ K_w T_{i-1,j}^{(n+1)} + K_e T_{i+1,j}^{(n)} + K_s T_{i,j-1}^{(n+1)} \right.$$

$$\left. + K_n T_{i,j+1}^{(n)} \right\} \quad , \tag{C-4}$$

and the difference between the two successive iterates would be:

$$\Delta = T_{i,j}^{(n+1)} - T_{i,j}^{(n)} = (K_w + K_e + K_s + K_n)^{-1} \left\{ K_w T_{i-1,j}^{(n+1)} + K_e T_{i+1,j}^{(n)} + \right.$$

$$\left. K_s T_{i,j-1}^{(n+1)} + K_n T_{i,j+1}^{(n)} \right\} - T_{i,j}^{(n)} \quad . \tag{C-5}$$

A further improvement in the rate at which $T_{i,j}^{(n+1)}$ might converge

to the exact solution can be achieved by the method of relaxation in

which a larger change than Δ obtained from Eq. (C-5) is given to

$T_{i,j}^{(n)}$. This may be written as:

$$T_{i,j}^{(n+1)} = T_{i,j}^{(n)} + \omega \Delta \quad , \tag{C-6}$$

where ω is a parameter called the relaxation factor and may be given

a value between 0 and 2. Note that for $\omega = 1$, the relaxation method

is identical to the Gauss-Seidel technique. For $0<\omega<1$ the method is

called under-relaxation, and for $1<\omega<2$, over-relaxation. Substituting

Δ from Eq. (C-5) into Eq. (C-6) yields the following formula for

the successive relaxation method:

$$T_{i,j}^{(n+1)} = \omega(K_w + K_e + K_s + K_n)^{-1} \left\{ K_w T_{i-1,j}^{(n+1)} + K_e T_{i+1,j}^{(n)} + K_s T_{i,j-1}^{(n+1)} \right.$$

$$\left. + K_n T_{i,j+1}^{n} \right\} + (1 - \omega) T_{i,j}^{(n)} \quad . \tag{C-7}$$

The Jacobi, Gauss-Seidel, and relaxation methods may also be

written in matrix notation for the system of linear equations such as

Eq. (C-1). To do this the matrix A in Eq. (C-1) is decomposed into

three matrices, namely a lower triangular, a diagonal and an upper

triangular, as follows:

$$A = L + D + U \quad , \qquad (C-8)$$

where

$$A = \begin{bmatrix} a_{11} & a_{12} \cdots a_{1n} \\ a_{21} & a_{22} \cdots a_{2n} \\ \cdot & \cdot \cdot \cdot \cdot \cdot \\ a_{n1} & a_{n2} \cdots a_{nn} \end{bmatrix}, \quad L = \begin{bmatrix} 0 & 0 & . & . & 0 \\ a_{21} & 0 & & 0 \\ \cdot & \cdot & \cdot & \cdot & \cdot \\ a_{n1} & a_{n2} & . & . & 0 \end{bmatrix}, \quad D = \begin{bmatrix} a_{11} & 0 & . & . & 0 \\ 0 & a_{21} & . & 0 \\ \cdot & \cdot & \cdot & \cdot & \cdot \\ 0 & . & . & . & a_{nn} \end{bmatrix}, \quad U = \begin{bmatrix} 0 & a_{12} \cdots a_{1n} \\ 0 & 0 & . & . & a_{2n} \\ \cdot & \cdot & \cdot & \cdot & \cdot \\ 0 & . & . & . & 0 \end{bmatrix} .$$

Having done this, it would not be difficult to show that the Jacobi,

Gauss-Seidel and successive relaxation methods for solving the equa-

tions $AX = B$ have the following representation in matrix notation:

Jacobi:
$$X^{(n+1)} = D^{-1}B - D^{-1}(L + U) X^{(n)} \qquad (C-9)$$

Gauss-Seidel:
$$X^{(n+1)} = (D + L)^{-1}B - (D + L)^{-1}UX^{(n)} \qquad (C-10)$$

Successive relaxation:
$$X^{(n+1)} = \omega(D - \omega L)^{-1}B - (D + \omega L)^{-1}\left\{\omega U - (1 - \omega)D\right\}X^{(n)}$$

$$(C-11)$$

The matrices $J = -D^{-1}(L + U)$ in Eq. (C-9), $G = -(D + L)^{-1}U$ in Eq.

(C-10) and $S = -(D + \omega L)^{-1}\left\{\omega U - (1 - \omega)D\right\}$ in Eq. (C-11), which play

an essential role in the convergence of each method, are called, re-

spectively, the Jacobi, Gauss-Seidel, and the successive relaxation

iteration matrices. It has been shown [46] that the convergence of

these iteration methods, and the rate of convergence of the successive

relaxation technique, may be characterized in terms of their iteration

matrices as follows:

1) The iteration method converges whenever the spectral radius of

its corresponding iteration matrix is less than unity.

2)   The successive relaxation method has the fastest rate of con-
vergence when the spectral . radius of its iteration matrix is a
minimum.   Based on these requirements, Young [47] proves that the
successive relaxation method for solving the system of equations
AX = B converges for $0 < \omega \leq 2$, if A is a symmetric, positive definite
matrix.   Young also gives the following theoretical formula for the
optimum relaxation factor ω:

$$\omega_{opt.} = \frac{2}{1 + (1 - \rho^2(J))^{\frac{1}{2}}} \quad , \qquad (C-12)$$

where $\rho(J)$ is the spectra l radius of the Jacobi iteration matrix.
Equation (C-12) implies that knowledge of $\rho(j)$ is required for calcu-
lation of the optimum relaxation factor.   For a Drichlet problem
$(\nabla^2 T = 0$ where T is known on the boundaries), if the domain of interest
is a homogeneous rectangle with sides of length l_1 and l_2 subdivided
into a network of squares of side h, Young determines $\rho(J)$ explicitly
as follows:

$$\rho(J) = \frac{1}{2}\left\{ \cos\left(\frac{\pi h}{l_1}\right) + \cos\left(\frac{\pi h}{l_2}\right) \right\} \quad . \qquad (C-13)$$

Unfortunately, in a general problem where the domain of interest might
be heterogeneous with irregular boundaries, no simple formula can be
obtained for the calcuation of $\rho(j)$.   Therefore, its value is usually
estimated.   In this work a method described by Carré [2 8] is used to
estimate $\rho(j)$.   This technique, which is simple and convenient to use
in a computer, can be summarized as follows :

1)   Assigning a first approximation for the temperatures at each node,
the iteration process is started with iterating once, using a relaxa-
tion factor of unity.   Doing so provides better values for the temper-
atures, compared to the initial ones which might be very rough.

2) Several iterations are performed using a relaxation factor of $\omega < \omega_{opt.}$ (Carré suggests 12 iterations with $\omega = 1.375$).

3) An estimation for the spectral radius of the successive over-relaxation iteration matrix, i.e. matrix $S(\omega)$ which was defined earlier, is made by:

$$\rho(S(\omega)) = \frac{\sum (T^{(n + 1)} - T^{(n)})}{\sum (T^{(n)} - T^{(n - 1)})} \qquad (C-14)$$

where the summation signs cover all the nodes. It has been shown [46] that Eq. (C-14) is indeed an appropriate estimation for $\rho(S(\omega))$.

4) The spectral radius of the Jacobi iteration matrix is calculated from:

$$\rho(J) = \frac{[\rho(S(\omega)) + \omega - 1]^2}{\omega^2 \rho^2(S(\omega))} \qquad . \qquad (C-15)$$

Equation (C-15) was obtained by Young, and holds whenever the convergence requirements are satisfied.

5) The spectral radius of the Jacobi iteration matrix, calculated from Eq. (C-15), is substituted in Eq. (C-12) to obtain an estimation for $\omega_{opt.}$ This value of $\omega_{opt.}$ is then modified as:

$$\omega = 1.25 \; \omega_{opt.} - 0.5 \qquad (C-16)$$

Equation (C-16) was obtained empirically by Carré, and enhances the convergence.

6) Using the value of ω obtained from Eq. (C-16), the iteration process is repeated by going back to step 2.

The iteration procedure is stopped whenever the following convergence condition is satisfied for all the nodes:

$$\left| 1 - \frac{T^{(m)}}{T^{(m - 1)}} \right| \leqslant \varepsilon \; , \qquad (C-17)$$

where $T^{(m)}$ and $T^{(m-1)}$ are, respectively, the values of temperature at each node at the end of two successive processes defined by steps 2 through 6, and ε is a small number characterizing the required convergence.

APPENDIX D

LISTING OF THE COMPUTER PROGRAM

```
      PROGRAM MAIN(INPUT,OUTPUT)
C     ************** DIMENSIONS AND COMMON BLOCKS **********************
      COMMON/GENERAL/HK(100,100),VK(100,100),T(100,100),T1(100,100),X(10
     *0),Y(100),DX(100),DY(100),A(100),N,NN,NP1,TCS
C     -------
C     CHAPTER 111111111111111111111111111111111111111111111111111111111
C     PARAMETERS AND CONTROL INDICES
C     -------
      PRINT 100
  100 FORMAT(1H1,16X,97(1H*),/,17X,1H*,4X,1H*,10X,17H* SOLID THERMAL *,1
     *6H FLUID THERMAL *,11X,3(12H*             ),1H*,/,17X,5H* NO.,11H* P
     *OROSITY ,2(16H* CONDUCTIVITY  ),12H*  TCS/TCF  ,3(12H*   ETC/TCF  )
     *,1H*,/,17X,1H*,4X,1H*,10X,2(1H*,15X),1H*,11X,1H*,3X,5HMODEL,3X,2H*
     * ,9HEXPERIME.,3H *  ,9HKRUPICZKA,2H *,/,17X,97(1H*))
      PI=3.14159265
      N=40
C     N IS THE NUMBER OF NODAL POINTS IN THE R AND Z DIRECTIONS
      NN=N+N+1
      NP1=N+1
      NM1=N-1
      RCRIT=SQRT(2.)/2.
      KL=0
      NI=20
      T1=1.
      T2=.0
      TEST1=.01
      TEST2=.001
  105 READ 110,PHI,RC2,SW,TCS,TCF,TCNW,BI,EXP
  110 FORMAT(8F7.5)
C     PHI=POROSITY,RC2=DIMENSIONLESS RADII OF TOP-BOTTOM CONTACTS
C     SW=SATURATION OF THE WETTING PHASE,TCS=THERMAL CONDUCTIVITY OF
C     THE SOLID PHASE,TCF=THERMAL CONDUCTIVITY OF THE WETTING PHASE
C     TCNW=THERMAL CONDUCTIVITY OF THE NON-WETTING PHASE
C     BI=BIOT NUMBER,EXP=EXPERIMENTAL EFFECTIVE THERMAL CONDUCTIVITY
C     SET NCR=0 IF THERE IS NO SOLID-SOLID CONTACT RESISTANCE ,
C     OTHERWISE SET NCR=1
      NCR=0
      IF(PHI.EQ.1.) GO TO 760
      NC1=2
      NS=0
      IF(TCF.EQ..0) GO TO 120
      EXP=EXP/TCF
      RATIO=TCS/TCF
      RATIO1=TCS/TCNW
  120 CALL GEOPA(PHI,RC2,SW,RC1,RW)
      RY=SQRT(1.-RC2**2.)
      C1=1.-RC1**2.
      C2=SQRT(C1)
      C3=RY
      OMN=0
```

```
C -------
C     CHAPTER 22222222222222222222222222222222222222222222222222222222222
C     SPASING BETWEEN THE NODAL POINTS
C -------
      DO 200 I=1,N
      Y(I)=RY*(1.-(1.-FLOAT(I)/FLOAT(N))**NC1)
  200 CONTINUE
    , DO 202 I=1,NM1
      X(I)=(Y(N)-Y(N-I))*C2/RY
  202 CONTINUE
      X(N)=C2
      DY(1)=Y(1)
      DX(1)=X(1)
      A(1)=(X(1)-DX(1)/2.)**2.
      AOLD=A(1)
      DO 210 I=2,N
      DY(I)=Y(I)-Y(I-1)
      DX(I)=X(I)-X(I-1)
      ANEW=(X(I)-DX(I)/2.)**2.
      A(I)=ANEW-AOLD
      AOLD=ANEW
  210 CONTINUE
      DY(NP1)=.0
      A(NP1)=C1-AOLD
C--------
C     CHAPTER 3333333333333333333333333333333333333333333333333333333333
C     CALCULATION OF THE THERMAL CONDUCTANCES BETWEEN THE NODAL POINTS
C     HK(I,J)=THERMAL CONDUCTANCE BETWEEN THE NODAL POINTS IN THE
C     R DIRECTION
C     VK(I,J)=THERMAL CONDUCTANCE BETWEEN THE NODAL POINTS IN THE
C     Z DIRECTION
C--------
      IF(TCF.EQ..0) GO TO 300
      IF(RW.EQ.1.) RATIO1=RATIO
  300 DO 392 I=1,N
      KK=0
      KKK=0
      LL=1
      LLL=1
      IF(Y(I).GT.RC1) GO TO 314
      DO 310 J=1,N
      CALL CONDUCT (1,RW,I,J,TCS,TCF)
  310 CONTINUE
      VK(I,NP1)=A(NP1)/DY(I)
      GO TO 392
  314 RCW=SQRT(RC1*RC1+RW*RW-1.)
      XC=SQRT(1.-Y(I)*Y(I))
      IF(Y(I).GT.RCW) GO TO 348
      DO 338 J=1,N
      IF(X(J).GT.XC) GO TO 318
      CALL CONDUCT (1,RW,I,J,TCS,TCF)
      GO TO 338
  318 KK=KK+1
```

```
      IF(KK.GT.1) GO TO 324
      CALL CONDUCT (2,XC,I,J,TCS,TCF)
      GO TO 338
  324 IF(TCF.EQ..0) GO TO 326
      HK(I,J)=(X(J)-DX(J)/2.)*(DY(I)+DY(I+1))/2./RATIO/DX(J)*2.
      GO TO 329
  326 HK(I,J)=.0
  328 IF(LL.GT.1) GO TO 330
      YC=SQRT(1.-X(J-1)**2.)
      IF(YC.LT.Y(I-1)) GO TO 330
      CALL CONDUCT (3,YC,I,J,TCS,TCF)
      GO TO 338
  330 IF(TCF.EQ..0) GO TO 334
      VK(I,J)=A(J)/DY(I)/RATIO
      GO TO 336
  334 VK(I,J)=.0
  336 LL=LL+1
  338 CONTINUE
      IF(Y(I-1).GE.RC1) GO TO 342
      CALL CONDUCT (3,RC1,I,NP1,TCS,TCF)
      GO TO 392
  342 IF(TCF.EQ..0) GO TO 344
      VK(I,NP1)=A(NP1)/DY(I)/RATIO
      GO TO 346
  344 VK(I,NP1)=.0
  346 GO TO 392
  348 XW=SQRT(RW**2.-Y(I)**2.)
      KK=0
      LL=1
      DO 384 J=1,N
      IF(X(J).GT.XC) GO TO 354
      CALL CONDUCT (1,RW,I,J,TCS,TCF)
      GO TO 384
  354 IF(X(J).GT.XW) GO TO 374
      KK=KK+1
      IF(KK.GT.1) GO TO 362
      CALL CONDUCT (2,XC,I,J,TCS,TCF)
      GO TO 384
  362 IF(TCF.EQ..0) GO TO 364
      HK(I,J)=(X(J)-DX(J)/2.)*(DY(I)+DY(I+1))/2./RATIO/DX(J)*2.
      GO TO 366
  364 HK(I,J)=.0
  366 IF(LL.GT.1) GO TO 370
      YC=SQRT(1.-X(J-1)**2.)
      IF(YC.LT.Y(I-1)) GO TO 370
      CALL CONDUCT (3,YC,I,J,TCS,TCF)
      GO TO 384
  370 IF(TCF.EQ..0) GO TO 375
      VK(I,J)=A(J)/DY(I)/RATIO
      GO TO 371
  375 VK(I,J)=.0
  371 LL=LL+1
      GO TO 384
```

```
374 KKK=KKK+1
    IF(KKK.GT.1) GO TO 378
    IF(RW.EQ.1.) GO TO 376
    CALL CONDUCT (2,XW,I,J,TCF,TCNW)
    GO TO 384
376 CALL CONDUCT (2,XW,I,J,TCS,TCF)
    GO TO 384
378 IF(TCF.EQ..0) GO TO 379
    HK(I,J)=(X(J)-DX(J)/2.)*(DY(I)+DY(I+1))/2./RATIO1/DX(J)*2.
    GO TO 381
379 HK(I,J)=.0
381 IF(LLL.GT.1) GO TO 382
    YC=SQRT(RW**2.-X(J-1)**2.)
    IF(YC.LT.Y(I-1)) GO TO 382
    IF(RW.EQ.1.) GO TO 380
    CALL CONDUCT (3,YC,I,J,TCF,TCNW)
    GO TO 384
380 CALL CONDUCT (3,YC,I,J,TCS,TCF)
    GO TO 384
382 IF(TCF.EQ..0) GO TO 383
    VK(I,J)=A(J)/DY(I)/RATIO1
    GO TO 388
383 VK(I,J)=.0
388 LLL=LLL+1
384 CONTINUE
    IF((I-1).EQ.0) GO TO 385
    YLOW=Y(I-1)
    GO TO 387
385 YLOW=.0
387 IF(YLOW.GE.RCW) GO TO 390
    IF(RW.EQ.1.) GO TO 386
    CALL CONDUCT (3,RCW,I,NP1,TCF,TCNW)
    GO TO 392
386 CALL CONDUCT (3,RCW,I,NP1,TCS,TCF)
    GO TO 392
390 IF(TCF.EQ..0) GO TO 394
    VK(I,NP1)=A(NP1)/DY(I)/RATIO1
    GO TO 392
394 VK(I,NP1)=.0
392 CONTINUE
    IF(NCR.EQ.0) GO TO 400
    VK(NP1,1)=A(1)*BI/RATIO
    HK(NP1,1)=HK(N,1)
    DO 393 I=2,N
    IF(X(I-1).GT.RC2) GO TO 395
    VK(NP1,I)=A(I)*BI/RATIO
    GO TO 396
395 VK(NP1,I)=A(I)*(.1E+20)/RATIO
396 HK(NP1,I)=HK(N,I)
393 CONTINUE
    VK(NP1,NP1)=A(NP1)*(.1E+20)/RATIO
    DO 398 I=1,NM1
    DO 397 J=1,N
```

```
      VK(NP1+I,J)=VK(NP1-I,J)
      HK(NP1+I,J)=HK(N-I,J)
  397 CONTINUE
      VK(NP1+I,NP1)=VK(NP1-I,NP1)
  398 CONTINUE
      DO 399 J=1,NP1
  399 VK(NN,J)=VK(1,J)
      GO TO 402
C  ------
C     CHAPTER 444444444444444444444444444444444444444444444444444444444444
C     INITIAL TEMPERATURE DISTRIBUTION
C     ONE DIMENSIONAL HEAT FLOW ASSUMPTION
C  ------
  400 NN=N
  402 NN1=NN+1
      DO 406 J=1,NP1
      T(1,J)=TI
      T(NN1,J)=T2
  406 CONTINUE
      IF(TCF.EQ..0) GO TO 409
      DO 408 J=1,NP1
      R=.0
      DO 407 I=1,NN
  407 R=R+1./VK(I,J)
      HEAT=(T2-TI)/R
      DO 408 I=2,NN
      T(I,J)=T(I-1,J)+HEAT/VK(I-1,J)
  408 CONTINUE
      GO TO 411
  409 DO 410 I=2,NN
      T(I,1)=T(I-1,1)-(TI-T2)/FLOAT(NN)
      DO 410 J=2,NP1
      T(I,J)=T(I,1)
  410 CONTINUE
  411 DO 412 I=1,NN1
      DO 412 J=1,NP1
  412 T1(I,J)=T(I,J)
C  ------
C     CHAPTER 555555555555555555555555555555555555555555555555555555555
C     SUCCESSIVE OVER RELAXATION PROCESS
C  ------
      CALL RELAX(1.,14,OMN)
      OMO=OMN
      CALL RELAX(OMO,NI,OMN)
      NS=NS+NI
  500 HEATD=.0
      HEATU=0
      DO 510 I=1,NP1
      HEATD=HEATD+VK(1,I)*(1.-T(2,I))
      HEATU=HEATU+VK(NN,I)*T(NN,I)
  510 CONTINUE
      IF(ABS(1-HEATD/HEATU).GT.TEST1) GO TO 530
      DO 520 IO=2,NN
```

```
      DO 520 JO=1,NP1
      IF(ABS(1-T(IO,JO)/T1(IO,JO)).GT.TEST2) GO TO 530
  520 CONTINUE
      GO TO 600
  530 OMO=OMN
      NS=NS+NI
      CALL RELAX(OMO,NI,OMN)
      GO TO 500
C ------
C
C     CHAPTER 66666666666666666666666666666666666666666666666666666666666
C     HEAT FLOW CALCULATION
C ------
  600 HEAT=(HEATD+HEATU)*PI/2.
      RE1=4./HEAT
      IF(TCF.EQ..0) GO TO 640
      RE1=RE1/RATIO
      IF(SW.EQ.1.0) GO TO 608
      V1=C1*C3
      V2=(C3*(2.+RC2**2.)-3.*RC1+RC1**3.)*PI/12.
      V3=C1*RC1*PI/4
      VS=(1.-PHI)*V1-V2-V3
      V4=SQRT(RW**2.+RC1**2.-1.)
      VW=PHI*SW*V1+V2+V3-PI/4.*C1*V4-PI/12.*(3.*RW**2.*C3-3.*RW**2.*V4-C
     *3**3.+V4**3.)
      VT=(1.-PI/4.)*C1*C3
      VNW=VT-VS-VW
      TC2=TCS**(VS/VT)*TCF**(VW/VT)*TCNW**(VNW/VT)
      RT=C3/(1.-PI/4.)/C1/TC2*TCF
      GO TO 648
  608 RE2=(C3-RC1)/(1.-PI/4.)/C1
      IF(PHI.LT..476) GO TO 610
      RT=RE2
      GO TO 648
  610 IF(RC1-RCRIT) 616,640,640
  616 TETA=PI/2.-2.*ATAN(RC1/C2)
      RE3=(RATIO-1.)**2./(RATIO*ALOG(RATIO)-RATIO+1.)/RATIO/TETA/RC1
      RE4=RC1/(C1-TETA/2.-RC1*C2)
      CALL RESIS(RATIO,RC1,RE5)
      RT=RE2+1./(1./RE3+1./RE4+2./RE5)
      GO TO 648
  640 C4=2.*RC1**2.-1.
      C4=SQRT(C4)
      C5=(1.-PI/4.)*C1
      CALL RESIS(RATIO,RC1,RE5)
      RE6=C4/C5/RATIO
      RT=RE2+RE5/2.+RE6
  648 IF(NCR.EQ.1) RT=RT*2.
      RT=1./(1./RE1+1./RT)
      GO TO 650
  640 RT=RE1
  650 IF(NCR.EQ.1) C3=C3*2.
      ETC=C3/RT/C1
      IF(NCR.EQ.1) GO TO 655
```

```
      Q1=VK(N,1)*T(N,1)
      DO 652 I=2,N
      IF(X(I-1).GT.RC2) GO TO 652
      Q1=Q1+VK(N,I)*T(N,I)
  652 CONTINUE
      Q1=Q1/HEATU
      GO TO 657
  655 Q1=VK(NP1,1)*(T(NP1,1)-T(NP1+1,1))
      DO 656 I=2,N
      IF(X(I-1).GT.RC2) GO TO 656
      Q1=Q1+VK(NP1,I)*(T(NP1,I)-T(NP1+1,I))
  656 CONTINUE
      Q1=Q1/HEATU
  657 IF(TCF.EQ..0) GO TO 658
      B1=.28-.757*ALOG10(PHI)
      NCR=0
      PI=.15+20
      P2=-.757
      B3=B1+B2*ALOG10(RATIO)
      ETC2=RATIO**B3
      GO TO 700
  658 ETC2=.0
C ------
C     CHAPTER 77777777777777777777777777777777777777777777777777777777777
C                      OUT PUT
C ------
  700 KL=KL+1
      P=PHI
      PRINT 710,KL,P,TCS,TCF,RATIO,ETC,EXP,ETC2
  710 FORMAT(17X,2H* ,I2,2H *,3X,F5.4,2X,2(1H*,3X,E9.4,3X),3H*  ,F7.1,2X
     *,3(1H*,3X,F5.2,3X),1H*)
      PRINT 722,RC1,RC2
  722 FORMAT(10X,4HRC1=,F5.4,5X,4HRC2=,F5.4)
      PRINT 740,BI
  740 FORMAT(5X,3HBI=,E9.4)
      PRINT 742,SW,RW
  742 FORMAT(5X,3HSW=,F5.4,5X,3HRW=,F5.3)
      PRINT 744,Q1
  744 FORMAT(5X,6HQCT/Q=,F5.4)
      PRINT 746,OMH,NS
  746 FORMAT(5X,6HOMEGA=,F5.3,3X,13HNO. OF ITER.=,I3)
      DO 750 I=1,NN1
      IN=NN1+1-I
      PRINT 748,(T(IN,J),J=1,NP1)
  748 FORMAT(4(5X,15F7.4,/))
  750 CONTINUE
      GO TO 105
  760 PRINT 764
  764 FORMAT(17X,97(1H*))
      STOP
      END
```

```
      SUBROUTINE GEOPA(PHI,RC2,SW,RC1,RW)
C     THIS SUBROUTINE CALCULATES THE DIMENSIONLESS RADII OF LATERAL
C     CONTACTS,RC1,AND THE DIMENSIONLESS RADIUS TO THE WETTING-NON-
C     WETTING INTERFACE,RW,KNOWING THE POROSITY,PHI,DIMENSIONLESS
C     RADII OF TOP-BOTTOM CONTACTS,RC2,AND THE SATURATION OF THE
C     WETTING PHASE,SW.
      PI=3.141592654
      S2=SQRT(1.-RC2**2.)
      IF(PHI-.476) 110,104,104
  104 RC1=.0
      S1=SQRT(1.-RC1**2.)
      GO TO 155
  110 I=0
      IF(PHI.LT..196) GO TO 140
      IF(RC2.GT.0) GOTO 130
      A=(1.-PHI)*6./PI
      A1=3.+A**2./3.
      B1=2.*A**3./27.+A+1.
      GO TO 135
  130 A=(1.-PHI)*6.*S2/PI
      T=.5*(3.*S2-S2**3.-4.)
      A1=(9.+A**2.)/3.
      B1=2.*A**3./27.+A-T
  135 B2=SQRT(A1/3.)
      B=3.*B1/(2.*A1*B2)
      IF(B.GT.0) GO TO 136
      TETA=ACOS(-B)/3.
      GO TO 137
  136 TETA=(PI-ACOS(B))/3.
  137 X=2.*B2*COS(TETA)
      IF(PHI.LT..196) GO TO 150
  138 S1=X-A/3.
      IF(S1.LT.1.0) GO TO 139
      S1=1.0
  139 RC1=SQRT(1.-S1**2.)
      GO TO 155
  140 IF(RC2. GT.0) GO TO 145
      RC1=1.-3.*PHI/2.
      GO TO 155
  145 S2=SQRT(1.-RC2**2.)
      A11=(1.-PHI)*S2-1./3.
      B11=PI*(1.-S2)**2.*(2.+S2)/12.
      T=1.-(1.5*A11)**2.
      A1=T**2./3.-4.5*A11*B11
      B1=-2.*T**3./27+1.5*A11*B11*T+2.25*B11**2.
      GO TO 135
  150 IF(I.EQ.1) GO TO 138
      X=X+T/3.
      RC1=SQRT(1.-X)
      C1=SQRT(X)
      IF(RC1-.7071)152,152,155
  152 I=1
      GO TO 130
```

```
155 IF(SW-1.) 159,156,156
156 RW=1.0
    GO TO 160
159 A=6.*S1**2.*S2*PHI*(SW-1.+1./PHI)/PI
    A1=.75*(S1+.5*S2)**2.
    B1=.5*(S1**3.+.5*S2**3.+A)-.25*(S1+.5*S2)**3.
    TETA=ACOS(-.5*B1/(A1/3.)**1.5)/3.
    X=2.*SQRT(A1/3.)*COS(TETA+4.*PI/3.)
    RW=X+.5*(S1+.5*S2)
160 RETURN
    END
```

```
      SUBROUTINE CONDUCT (IS,X1,I,J,TC1,TC2)
C     THIS SUBROUTINE CALCULATES THE THERMAL CONDUCTANCES BETWEEN THE
C     NODAL POINTS.
      COMMON/GENERAL/HK(100,100),VK(100,100),T(100,100),T1(100,100),X(10
     *0),Y(100),DX(100),DY(100),A(100),N,NN,NP1,TCS
      GO TO (100,200,300),IS
100   HK(I,J)=2.*(X(J)-DX(J)/2.)*(DY(I)+DY(I+1))/2./DX(J)
      VK(I,J)=A(J)/DY(I)
      GO TO 400
200   XC=X1
      DX2=X(J)-XC
      DX1=DX(J)-DX2
      IF(TC1.EQ..0) GO TO 210
      R1=DX1/(XC-DX1/2.+.1E-10)/TC1*TCS
      IF(TC2.EQ..0) GO TO 210
      R2=DX2/(XC+DX2/2.)/TC2*TCS
      HK(I,J)=2.*(1./(R1+R2))*((DY(I)+DY(I+1))/2.)
      GO TO 220
210   HK(I,J)=.0
220   VK(I,J)=A(J)*TC1/DY(I)/TCS
      GO TO 400
300   YC=X1
      DY2=Y(I)-YC
      DY1=DY(I)-DY2
      IF(TC1.EQ..0) GO TO 310
      R1=DY1/A(J)/TC1*TCS
      IF(TC2.EQ..0) GO TO 310
      R2=DY2/A(J)/TC2*TCS
      VK(I,J)=1./(R1+R2)
      GO TO 400
310   VK(I,J)=.0
400   RETURN
      END
```

```
      SUBROUTINE RELAX(OMO,NI,OMN)
C     THIS SUBROUTINE CALCULATES THE OPTIMUM ACCELERATION FACTOR FOR
C     SUCCESSIVE OVER-RELAXATION AS DESCRIBED IN APPENDIX C.
      COMMON/GENERAL/HK(100,100),VK(100,100),T(100,100),T1(100,100),X(10
     *0),Y(100),DX(100),DY(100),A(100),N,NN,NP1,TCS
      OMEGA=OMO
      NIM1=NI-1
      NIM2=NI-2
      DO 109 II=1,NI
      DO 102 I=2,NN
      IP1=I+1
      IM1=I-1
      SUM1=T(IP1,1)*VK(I,1)+T(IM1,1)*VK(IM1,1)+T(I,2)*HK(IM1,1)
      SUM2=VK(I,1)+VK(IM1,1)+HK(IM1,1)
      IF(SUM2.EQ..0) GO TO 100
      T(I,1)=(1-OMEGA)*T(I,1)+OMEGA*(SUM1/SUM2)
  100 DO 101 J=2,N
      JP1=J+1
      JM1=J-1
      SUM1=T(IP1,J)*VK(I,J)+T(IM1,J)*VK(IM1,J)+T(I,JP1)*HK(IM1,J)+T(I,JM
     *1)*HK(IM1,JM1)
      SUM2=VK(I,J)+VK(IM1,J)+HK(IM1,J)+HK(IM1,JM1)
      IF(SUM2.EQ..0) GO TO 101
      T(I,J)=(1.-OMEGA)*T(I,J)+OMEGA*(SUM1/SUM2)
  101 CONTINUE
      SUM1=T(IP1,NP1)*VK(I,NP1)+T(IM1,NP1)*VK(IM1,NP1)+T(I,N)*HK(IM1,N)
      SUM2=VK(I,NP1)+VK(IM1,NP1)+HK(IM1,N)
      IF(SUM2.EQ..0) GO TO 102
      T(I,NP1)=(1-OMEGA)*T(I,NP1)+OMEGA*(SUM1/SUM2)
  102 CONTINUE
      IF(NIM1.EQ.0) GO TO 111
      IF(II.LT.NIM2) GO TO 109
      IS=NI-II+1
      GO TO (107,105,103),IS
  103 DO 104 I=2,NN
      DO 104 J=1,NP1
      T1(I,J)=T(I,J)
  104 CONTINUE
      GO TO 109
  105 EM=0
      DO 106 I=2,NN
      DO 106 J=1,NP1
      EM=EM+ABS(T(I,J)-T1(I,J))
      T1(I,J)=T(I,J)
  106 CONTINUE
      E1=EM
      GO TO 109
  107 EM=0
      DO 108 I=2,NN
      DO 108 J=1,NP1
      EM=EM+ABS(T(I,J)-T1(I,J))
  109 CONTINUE
```

```
      E2=EM
      ELANDA=E2/E1
109   CONTINUE
      OMEGA=OMO
      B=(ELANDA+OMEGA-1)/OMEGA
      C=1-(B*B/ELANDA)
      IF(C.GT.0) GO TO 110
      OMN=OMEGA
      GO TO 112
110   D=1.+SQRT(C)
      OMEGA=2./D
      OMEGA=OMEGA-(2-OMEGA)/4.
      OMN=OMEGA
      GO TO 112
111   OMN=1.375
112   RETURN
      END
```

```
      SUBROUTINE RESIS(RATIO,RC1,R)
C     THIS SUBROUTINE CALCULATES THE THERMAL RESISTANCE OF SECTION 4 .
      N=100
      NM1=N-1
      PI=3.141592654
      R=RATIO-1
      H1=SQRT(1.-RC1**2.)
      RCRIT=SQRT(2.)/2.
      IF(RC1-RCRIT) 100,110,110
100   H2=RC1
      XO=.0
      DX=RC1/FLOAT(N)
      ASI=((1.-H1**2.)*ATAN(H2/H1)-ACOS(H1)+H1*RC1)/2.
      ASF=.0
      GO TO 120
110   H2=H1
      XO=SQRT(2.*RC1**2.-1.)
      DX=(RC1-XO)/FLOAT(N)
      ASI=H1**2.*(ATAN(H2/H1)-PI/2.+1.)/2.
      ASF=.0
120   AT=(H1*H2-H1**2.*ATAN(H2/H1))/2.
      SUM=(1./(R*ASI+AT)+1./(R*ASF+AT))/2.
      A1=H1**2.
      A2=ATAN(H2/H1)
      DO 130 I=1,NM1
      X=XO+DX*FLOAT(I)
      A3=1.-X**2.
      H3=SQRT(A3)
      AS=((A3-A1)*A2-A3*ACOS(H1/H3)+H1*SQRT(A3-A1))/2.
      SUM=SUM+1./(R*AS+AT)
130   CONTINUE
      R=SUM*DX
      RETURN
      END
```